秋田県立大学大学院博士学位論文

Effect of the Microstructures on the Mechanical and Electrical Properties of Carbon Nanotube/Polymer Nanocomposites

（カーボンナノチューブ/高分子ナノ複合材料の力学特性と導電性に及ぼす内部構造の影響）

王　麗君

2016 年 3 月

Abstract

Since the beginning of the 21st-century, conductive polymer composites (CPCs) have been found a wide range of applications in electronic engineering fields and/or in automobile and aeronautical industries. To promote the rapid development of CPCs, it requires CPCs to have high conductive properties and good mechanical properties. The prospect of advanced CPCs with multifunctional features has attracted more attentions in both academia and industry. To attain excellent electrical and mechanical properties, the homogeneous dispersion of conductive filler in a polymer matrix and the strong interfacial interaction between the filler and the polymer are two major challenges in the preparation of CPC. In the present study, the different CPCs were produced by through extrusion molding and injection molding in industrial-scale, and achieved high electrical conductivity, as well as good mechanical properties. Moreover, to expand the application range of CPCs, the second stage processing (e.g., plastic processing) was performed by proposed approaches.

In Chapter 1, the research backgrounds, research significance, and the construction of this thesis were described.

In Chapter 2, the properties of experimental materials were presented. The experimental methods and characteristics were also presented in this chapter.

In Chapter 3, multi-walled carbon nanotube/polycarbonate (MWCNT/PC) composites with different MWCNT content (0–10 wt.%) were prepared by a two-step dispersion strategy (the twin-screw extrusion followed by injection molding process). As a result, the MWCNT/PC composites specimens with well-dispersed MWCNTs were successfully obtained. The effects of the MWCNT content and injection conditions on thermal, mechanical, and dynamic mechanical properties of the prepared composites were investigated and compared. Thermogravimetric analysis showed that a small MWCNT content (i.e., 1 wt.%) was more propitious for improving thermal stability of

the composites. Analysis of the mechanical properties demonstrated that the tensile properties of the composites with low MWCNT content could be comparable to that of PC. The tensile strength of the composites with 2.5 wt.% raw MWCNTs exhibited an increase of ~5 MPa (~8.6%) at a particular injection condition. However, as the MWCNT content increased to 10 wt.%, the tensile strength and bending strength decreased by 35% and 47%, respectively, from the values of PC. The impact strength and microhardness were improved with the increase in MWCNT content. Results of dynamic mechanical analysis showed that the storage modulus of PC was increased after the incorporation of MWCNTs, particularly at high temperature. The results also indicated that, MWCNT content, injection temperature and injection speed were all major factors that influence the properties of the prepared composites, in which the MWCNT content presented most efforts.

In Chapter 4, the effects of the MWCNT content and injection conditions on the MWCNTs dispersion and the electrical resistivity of the prepared MWCNT/PC composites (in chapter 3) were investigated. The optical micrograph showed that the MWCNTs were homogeneously dispersed in the PC matrix with minor agglomeration, confirming that the two-step dispersion method was effective for improving the dispersibility of the MWCNTs in the host polymer. Moreover, the electrical resistivity of the 5 wt.% raw MWCNTs composites was considerably decreased to 10^2 Ω/sq, a value approximately 15 orders of magnitude lower than that of PC. Furthermore, the effects of injection conditions on composite electrical properties were emphatically discussed. It was found that the electrical resistivity was sensitive to injection temperature and injection speed. Low electrical resistivity was achieved at high injection temperature and low injection speed. As well, the mold temperature and the surface roughness would affect the electrical resistivity. More importantly, since the formation mechanism of the internal microstructures of the prepared composites during injection molding, the distributions of the electrical resistivity had three stages of a rising distribution, a declining distribution and a constant distribution.

In Chapter 5, to expand the applications of composites, the second stage processing was performed to prepare a new-style CPC. The work demonstrated how rolling conditions during the rolling process as an industrially relevant plastic processing technique affected the microstructures, mechanical and electrical properties of PLA composites. Five different MWCNT/PLA composites were produced with variation of MWCNT contents. The crystal morphology, crystallinity, molecular orientation, mechanical properties and electrical properties of the rolled composites were investigated. The distribution and dispersion of MWCNTs in the PLA were observed by optical microscope. It was found that the size of MWCNT agglomeration was increased by the increase of MWCNT content. Besides, a proper incorporation of MWCNTs was a favorable method for maintaining good thermal properties of the PLA. The crystallinity of pure PLA was dropped as the rolling ratio increased, and whereas the crystallinity was greatly increased by the incorporation of MWCNTs. MWCNT played a role as a nucleating agent in PLA. Irrespective of the MWCNT content, the orientation was raised by the increase of rolling ratio, raised by approximately 1.5%–1.9%. When the rolling ratio reached 60%, the tensile strength and fracture strain in the rolling direction increased from 51.1 MPa to 86.0 MPa and from 5.3% to 103.1%, respectively. The incorporation of MWCNT was conducive to improving the electrical conductivity of PLA. When the carbon content was 5 wt.%, the surface resistivity was dropped to 10^1 Ω/sq. Moreover, the effect of rolling ratio on the electrical resistivity was not outstanding. Namely, the rolling process did almost not affect the improvement of the composite conductivity.

In chapter 6, general conclusions of the study were made.

Content

Abstract ..... **i**
Chapter 1 Introduction **1**
1.1 Background 1
1.2 Polymers 4
1.2.1 Introduction of polycarbonate 4
1.2.2 Introduction of polylactic acid 5
1.3 Electrical conductive filler 6
1.3.1 Structure of carbon nanotube 7
1.3.2 Properties of carbon nanotube 9
1.3.3 Carbon nanotubes' application 13
1.4 Conductive polymer composites 15
1.5 Purpose of this research 17
References 20
Chapter 2 Materials, Experiment and Evaluation Methods **32**
2.1 Materials 32
2.1.1 Multi-walled carbon nanotube (MWCNT) 32
2.1.2 Polycarbonate (PC) 33
2.1.3 Polylactic acid (PLA) 34
2.2 Preparation and processing of composites 36
2.2.1 Twin-screw extrusion 36
2.2.2 Injection molding process 37
2.2.3 Rolling molding process 39
2.3 Experiments and evaluation methods 40
2.3.1 Dynamic mechanical analysis (DMA) 40
2.3.2 Tensile test 41
2.3.3 Bending test 42
2.3.4 Impact test 43
2.3.5 Microhardness and its distribution test 44
2.3.6 Electrical resistivity and its distribution 46
2.3.7 X-ray diffraction (XRD) 48
2.3.8 Thermogravimetric analysis (TGA) 49
2.3.9 Differential scanning calorimetry (DSC) 49
2.3.10 Density determination 50
2.3.11 Optical microscope (OPM) 51
2.3.12 Scanning electron microscope (SEM) 51
References 53
Chapter 3 Preparation and Evaluation the Mechanical Properties of Carbon Nanotube-Reinforced Polycarbonate Conductive Composites **55**
3.1 Introduction 55

3.2 Experimental 56
3.3 Results and discussions 57
3.3.1 Thermal stability 57
3.3.2 Mechanical properties 61
3.3.3 Dynamic mechanical behavior 81
3.4 Conclusions 83
References 85
Chapter 4 Effects of Molding Conditions on Microstructures and Electrical Properties of Carbon Nanotube-Reinforced Polycarbonate Conductive Composites 89
4.1 Introduction 89
4.2 Experimental 91
4.2.1. Preparation composites specimens 91
4.2.2. Measurement of electrical resistivity 92
4.3 Results and discussions 92
4.3.1 Dispersion of MWCNTs 92
4.3.2 Electrical properties 93
4.4 Conclusions 112
References 114
Chapter 5 Polylactic acid-based Conductive Composites by a Cold Rolling Process 118
5.1 Introduction 118
5.2 Experimental 120
5.2.1 Preparation of MWCNT/PLA composites 120
5.2.2 Rolling process and specimen preparation 122
5.3 Results and discussions 124
5.3.1 Microstructures 124
5.3.2 Thermal behaviors 128
5.3.3 Effect of rolling ratio on the crystallization behaviors 130
5.3.4 Relationship between density and crystallinity 134
5.3.5 Effect of rolling ratio on the molecular orientation 137
5.3.6 Microhardness and its distribution for PLA 140
5.3.7 Dynamic mechanical behaviors 142
5.3.8 Effect of rolling ratios on the tensile properties 145
5.3.9 Effect of rolling ratios on the electrical properties 152
5.4 Conclusions 155
References 158
Chapter 6 Conclusions 164
Publications 167
Acknowledgements 171

Chapter 1 Introduction

1.1 Background

The polymers become indispensable in modern society and their applications are more and more widespread due to their lightweight, outstanding mechanical properties, excellent chemical resistance and good forming property [1]. The growth in their use has continued in the last few decades or more, despite the effects of several recessions in industrial activity (Fig. 1-1). In the same period the demand for traditional materials like metals, ceramics and glasses has remained static or even fallen. Since 21st-century, the growth in use of polymers is forecast to continue into the next millennium, with consumption approaching 4 million tonnes in the UK. In one of the most active areas, that of thermoplastic polymers, consumption is divided into packaging, building, and a wide range of other applications [2].

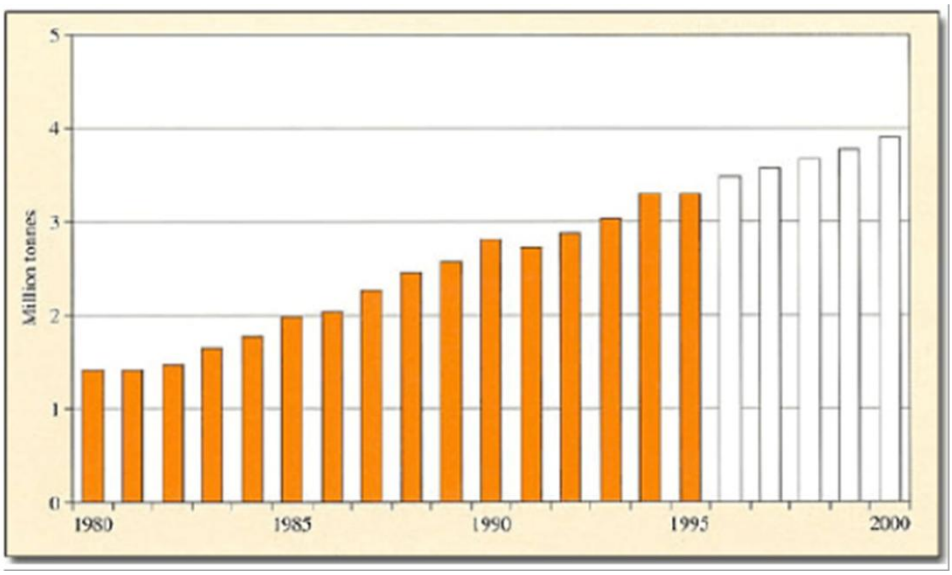

Fig. 1-1 The growth in demand for polymers in the UK (1980–2000) [2].

Especially, in recent years, the plastic products have been used in many fields. Fig. 1-2 shows the statistical report of plastic products from Japanese industry ministry in 2011 [3]. In 2011, the output of plastic products is approximately 5.68 million tonnes.

Therein, the plastic film and plastic sheets are approximately 42.2%, the plastic containers are approximately 15.2%, and the plastic products for machine tools and parts are approximately 10.7%. Besides, the statistical report indicates that the applications of plastic products are multifarious. In fact, due to their lightweight, cost reduction and environment friendly, the polymer materials used to be instead of metal materials has become the main development trend in 21st-century. For example, for automotive components, if the plastic products replace the metal products, the weight of automotive can be reduced by approximately 8%, the volume can be decreased by approximately 27% [4-10]. Therefore, in the future, the demand for plastic products is becoming higher and higher in industrial applications.

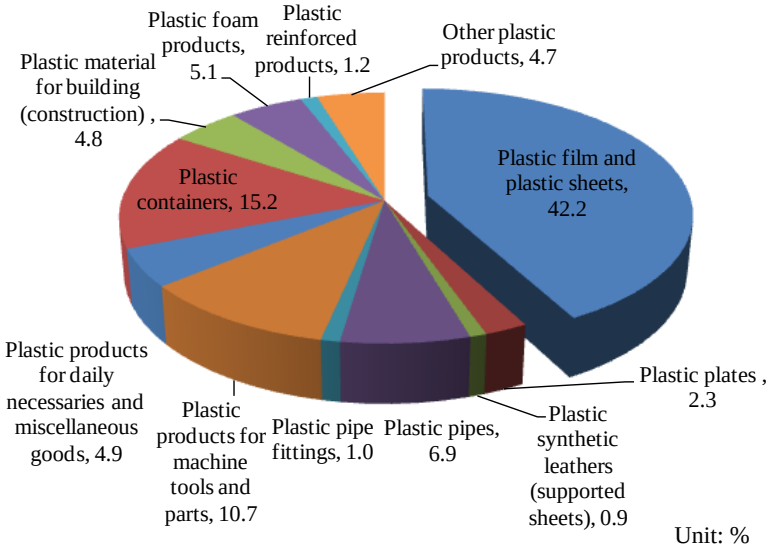

Fig. 1-2 The statistical report of plastic products in 2011 [3].

However, poor conductive properties of polymers have limited their applications. Therefore, conductive polymer composites (CPCs) have been developed rapidly. The CPCs have found a wide range of applications in electronic engineering fields and/or in automobile and aeronautical industries. Examples of such applications include dust-proof antistatic materials, electrostatic recording paper, over-current and over-temperature protection devices, electrostatic painting, electromagnetic shielding and electronic components [11, 12] (as shown in Table 1-1 and Fig. 1-3), whereas there

are still some problems to need solving in process and applications. The most prominent is the improvement of the dispersibility and compatibility of conductive filler, as well as the enhancement of the interfacial interaction between the polymer and filler [13-17]. Consequently, the type of polymers, the type and amount of conductive fillers, and processing methods are very important factors for CPCs.

Table 1-1 The applications of conductive polymer composites

Surface resistivity (Ω/sq)	purpose	application
10^{12}~10^{13}	Prevention of adverse effects in the static state	Dust proof
10^{10}~10^{12}	Prevention of adverse effects in the dynamic state	Manufacturing process of film and fiber
10^{8}~10^{9}	Antistatic	IC package
10^{7}~10^{8}	Low electrical conductivity	Electrostatic recording paper, electrostatic painting
10^{4}~10^{7}	electrical conductivity	Charge roll and so on
10^{0}~10^{4}	electrical conductivity	Electromagnetic shielding agent and so on
10^{-3}~10^{0}	High electrical conductivity	Electronic components

Fig. 1-3 The applications of conductive polymer composites in industry [18].

1.2 Polymers

Polymers are materials composed of long molecular chains that are well-accepted for a wide variety of applications. Traditionally, two main types of synthetic polymer, i.e., plastics and rubbers, have been produced in industry. The distinction is that plastics are, by and large, rigid materials at service temperatures while rubbers are flexible, low modulus materials which exhibit long-range elasticity [19]. Plastics are further subdivided into thermosets and thermoplastics. Due to the property of repeatable processing, the applications of thermoplastics are more widespread. Moreover, all of them, irrespective of their properties, can be reinforced by a very wide range of fillers to produce composites. The commonly used thermoplastic will be introduced as follows, i.e., PC and PLA, which are chosen as the matrix materials in our study.

1.2.1 Introduction of polycarbonate

Polycarbonate (PC) is a kind of engineering plastics, and is widely used in industry. It is a kind of non-crystalline thermoplastic polymer with excellent comprehensive properties, which has excellent electrical insulation, extension, size stability and chemical corrosion resistance, high strength, heat resistance, cold resistance and so on. The heat resistance temperature is from –100 ℃ to 135 ℃. Besides, PC is a quite strong plastic, and is used to make many different products. It is so hard to break that it is frequently used to produce bulletproof windows. In addition to being strong, it is also very lightweight. It weighs less than both acrylic and glass.

The most famous products of PC are CD and DVD. Another popular use for polycarbonate is making of eyeglass lenses. PC is showing up more often in the making of electronics. This material is a natural fit for mobile phone and computer shells, as it makes the products lighter, while at the same time providing stellar protection against damage. The original iMac case is just one example of this material being put to use in the computer world [20]. Though some toxic chemicals are used in the production of PC,

it is indeed recyclable. This fact makes this material preferable to polyvinyl chloride (PVC). It is not considered to be a completely "green" product, it does have at least some practical applications in the world of green solutions.

Furthermore, as a matrix, PC has been attached more and more attention. Pötschke et al. [21] prepared two PC composites with 2 and 5 wt.% multi-walled carbon nanotube (MWCNT) content, and proved that both composites variations in electrical resistivity of the injection-molded plates were up to 6 orders of magnitude. Besides, they found that a network-like structure occurred in the skin area at low injection velocity and high melt temperature. Moreover, Grady et al. [22] successfully prepared the MWCNT/PC composites, and evaluated the electrical, mechanical, and thermal properties of the composites.

1.2.2 Introduction of polylactic acid

In recent years, many biologically degradable polymers, e.g., polylactic acid (PLA), polybutylene succinate (PBS) and polycaprolactone (PCL), have been developed. Out of these polymers, PLA is considered as one of the most promising biodegradable, compostable, thermoplastic, and crystalline polymers. Additionally, PLA is a sustainable alternative to petrochemical-derived products and can be derived from renewable resources [23], such as corn starch (in the United States and Canada), tapioca roots, chips or starch (mostly in Asia), or sugarcane (in the rest of the world) [24]. In 2010, PLA had the second highest consumption volume of any bioplastic of the world [25]. As of June 2010, Nature Works was the primary producer of PLA (bioplastic) in the United States. Moreover, Galactic and Total Petrochemicals operate a joint venture, Futerro, which exclusively develops a second generation PLA product. This project includes the building of a PLA pilot plant in Belgium capable of producing 1500 tonnes/year [24].

PLA has a glass transition temperature of 60–65 ℃, a melting temperature of 173–178 ℃ and a tensile modulus of 2.7–16 GPa [26, 27]. Heat-resistant PLA can withstand temperatures of 110 ℃ [28]. Because PLA has many advantages, PLA can be

processed by extrusion, injection molding, film and sheet casting, 3D printing and spinning, providing access to a wide range of materials.

The applications of PLA are very wide in our daily life. PLA is used as medical implants in the form of anchors, screws, plates, pins, rods, and as a mesh. Besides, PLA can also be used as a decomposable packaging material, either cast, injection-molded, or spun [29], and used as a feedstock material in 3D printers [30, 31]. More importantly, PLA can be also filled with electrical conductive fillers to prepare new-style conductive polymer composites for solving environment friendly problem and replacing traditional polymers in potential industrial applications.

Many researchers are committed to produce conductive PLA-based composites. Chow et al. [32] reported that the polylactic acid/organo-montmorillonite (PLA/OMMT) nanocomposites toughened with maleated styrene-ethylene/butylene-styrene (SEBS-g-MAH) were prepared by melt-compounding using co-rotating twin-screw extruder followed by injection molding. They found that impact strength and elongation at break of the PLA nanocomposites was enhanced significantly by the addition of SEBS-g-MAH, and thermal stability of the PLA/OMMT nanocomposites was improved in the presence of SEBS-g-MAH. Subsequently, they successfully prepared the polylactic acid/halloysite nanotubes (PLA/HNTs) nanocomposites using melt compounding followed by compression molding [33].

1.3 Electrical conductive filler

Electrical conductive fillers are multifarious, including metal materials and carbon materials, such as stainless-steel fibers [34, 35], metallic nanowires [36], carbon nanotubes (CNTs) [37-39], carbon black (CB) [40, 41], carbon fibers (CF) [42, 43], graphite [44, 45] and so on. Carbon materials have been attached more and more interests in recent years, due to their many advantages.

Since fullerenes have been discovered by Kroto in 1985 [46] and carbon nanotubes have been discovered by Iijima in 1991 [47], the carbon allotrope scope has been

enlarged, and the studies of carbon materials have been more and more profound understanding. The discovery of the two kinds of carbon nano-materials has led contribution on human in the field of science and technology. Moreover, Novoselov successfully prepared another allotrope of carbon-graphene in 2004 [48], it has an ideal two-dimensional structure and peculiar electronic properties, because of this, the studies of carbon materials entered a new round of high tide [49]. Especially, the study of carbon nanotubes has been opened a prelude.

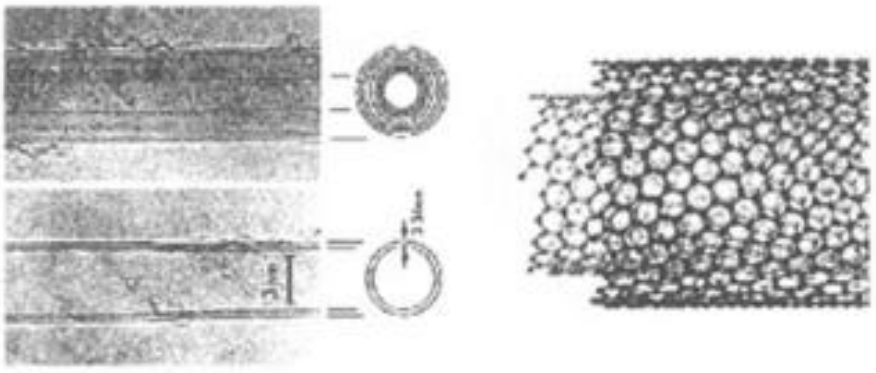

Fig. 1-4 Carbon nanotubes found by Iijima in 1991 [47].

1.3.1 Structure of carbon nanotube

Carbon nanotubes exist as a macro-molecule of carbon, analogous to a sheet of graphite rolled into a cylinder. Carbon nanotubes are built from sp^2 carbon units, with each atom joined to three neighbours as in graphite [50]. They are consist of honeycomb lattices and are a seamless structure. Carbon nanotubes divided into: multi-walled CNTs (MWCNTs) and single-walled CNTs (SWCNTs). This classification depends on the number of graphite walls: SWCNT is only one wall and MWCNT is several walls (as shown in Fig. 1-5) [51]. SWCNT is made of a single seamlessly rolled graphite sheet with a typical diameter of approximately 1.4 nm, and a length of 0.2–5 μm [52, 53]. MWCNT is closed graphite tubules rolled like a graphite sheet. Usually, its diameters is

in the range of 2–25 nm, and the distance between walls is approximately 0.34–0.35 nm (as shown in Fig. 1-6) [53, 54]. Whether SWCNTs or MWCNTs, they both have a high aspect ratio, generally it is 100–1000, even 1000–10000. Thus carbon nanotube is considered as a new type of one-dimensional nano-material.

However, due to large specific surface area, higher surface activation energy [55], and intrinsic Van der Waals attraction between CNTs, the CNTs agglomerate easily and the interfacial interaction between CNTs and polymers is weak, which hinder an efficient load transfer from the CNTs to the polymer matrix. Accordingly, a uniform dispersion of CNTs in a polymer matrix and a strong interfacial interaction [56, 57] between CNTs and polymers are necessary conditions to maximize the advantages of CNTs as effective reinforcing filler in polymer composites.

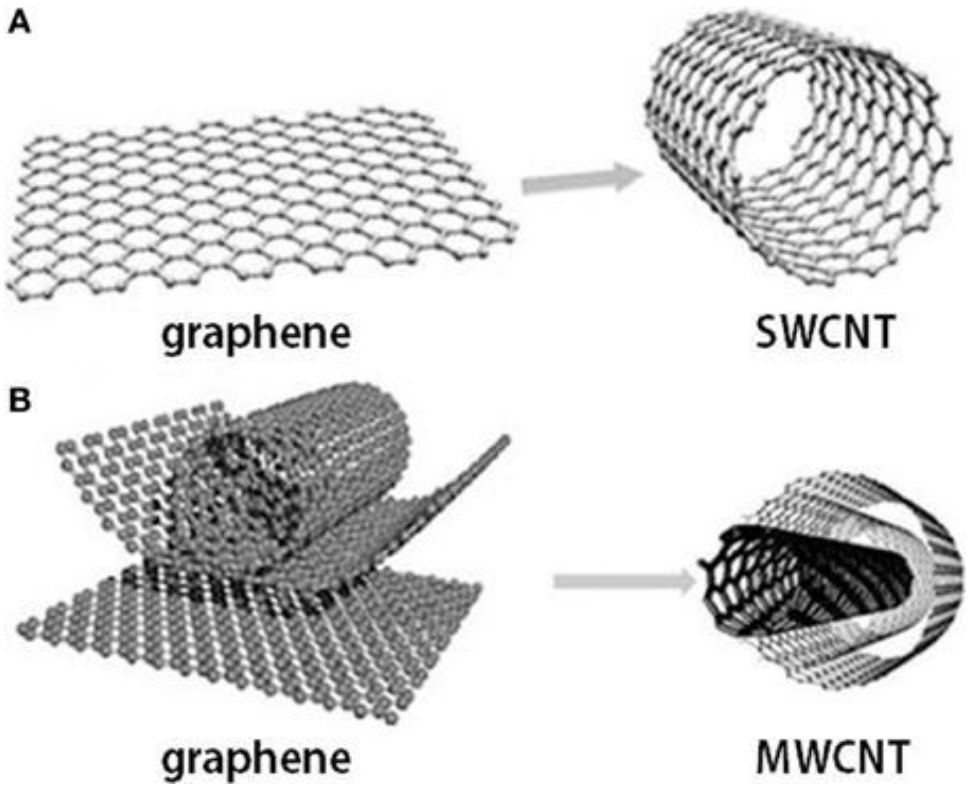

Fig. 1-5 Graphene and carbon nanotubes as (A) single-walled carbon nanotube (SWCNT) structure and (B) multi-walled carbon nanotube (MWCNT) structure [51].

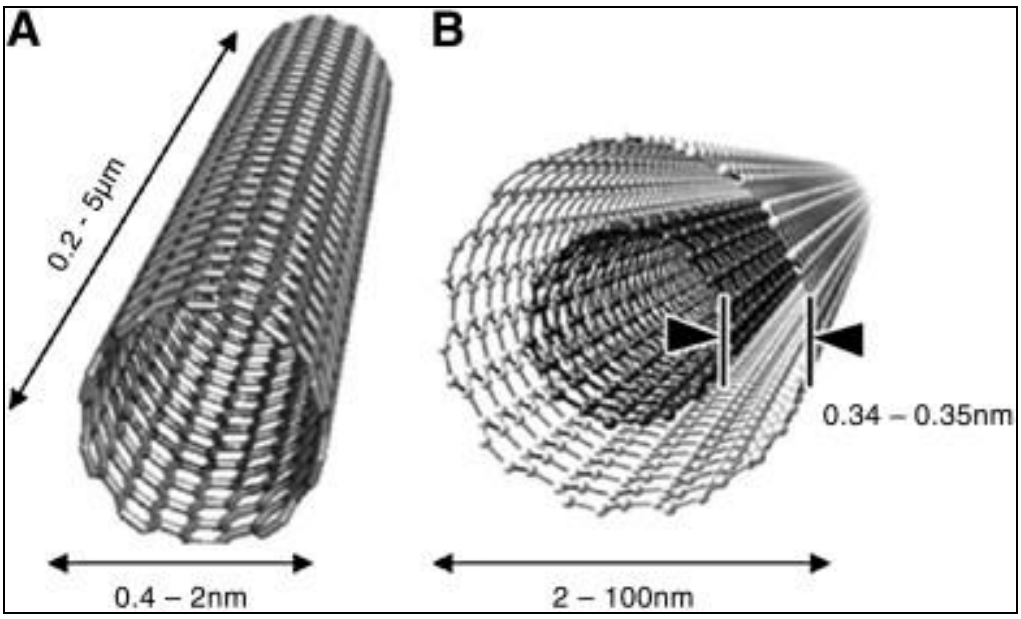

Fig. 1-6 The sizes of (A) SWCNT and (B) MWCNT [53].

1.3.2 Properties of carbon nanotube

Carbon nanotubes have generally been regarded as electrical conductive fillers with high potential to improve the polymers properties, owing to not only their unique nanostructure, but also excellent electrical, mechanical, thermal properties and so on [58-62].

(a) Electrical properties

There has been considerable practical interest in the conductivity of CNTs. CNTs with particular combinations of N and M, the structural parameters indicating how much the nanotube is twisted, can be highly conducting, and hence can be said to be metallic [63]. Their conductive property has been shown to be a function of their chirality, the helicity of the arrangement of graphitic rings in their walls, the degree of twist as well as their diameter [64, 65]. CNTs can be either semi-conducting or metallic in their electrical behaviors. Besides, the electrical properties of carbon nanotubes depend on how the hexagons are orientated along the axis of the tube [66]. The following figure shows the three orientations that are possible: armchair, zigzag, and chiral (shown in Fig. 1-7).

Researchers have developed the methods to explore and exploit the electrical properties of both SWCNTs and MWCNTs in many fields. Electrical properties of SWCNTs have been studied in a number of theoretical works [67, 68]. The intramolecular junctions of SWCNTs can be formed by interposing one or more 5–7 pairs in-between two nanotube sections with different (*n*, *m*) indices. Theoretical models have predicted that metal-semiconductor (M-S), metal-metal (M-M), or semi-conductor-semiconductor (S-S) junctions are possible in SWCNTs [69]. Fischer et al. found that the SWCNTs have outstanding electrical conductivity, and the electrical resistivity can be as low as 0.06 Ω·cm [67]. MWCNTs are composed of coaxial nanotube cylinders, of different helicities. These adjacent layers are generally non-commensurate (different chiralities) with a negligible inter-layer electronic coupling and could alternate randomly between semi-conducting and metallic varieties [70]. Moreover, MWCNTs display characteristics ranging from localization to metallic behavior at low temperature resulting in either a small or large phase coherence length. The electrical resistivity of MWCNTs is approximately 0.08 Ω·cm at room temperature [71]. The non-local interactions manifest in a disordered sample can cause difficulties in the interpretation of even four-terminal measurements [72].

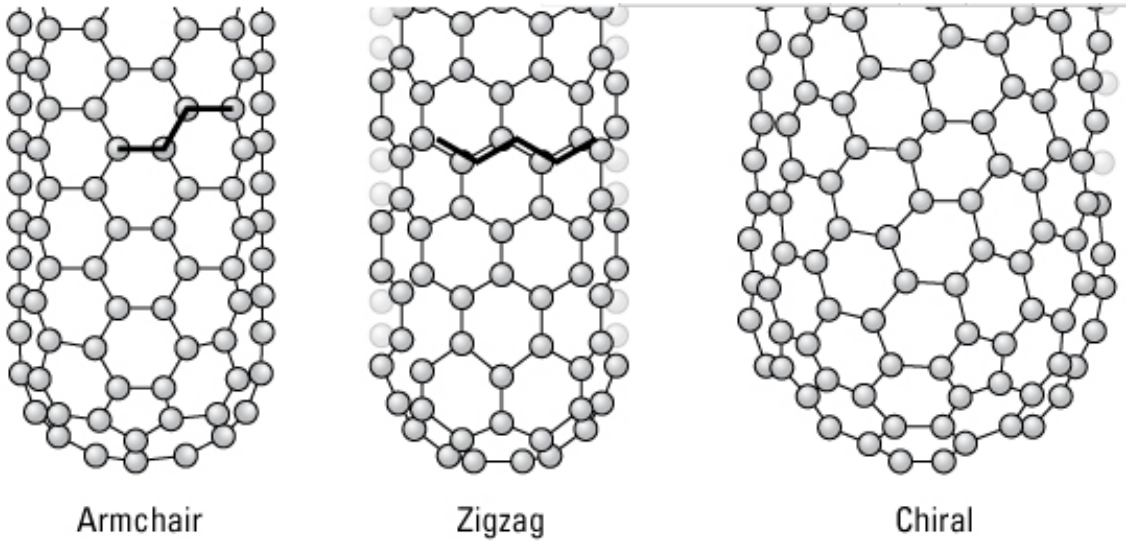

Fig. 1-7 Electrical properties depend on the orientation of the hexagons [66].

(b) Mechanical properties

Carbon nanotubes are composed of the C-C covalent bonds along the axial direction, so it has extremely high strength and huge toughness [73, 74]. Carbon nanotube is one of the strongest materials in nature. Carbon nanotubes (CNTs) are basically long hollow cylinders of graphite sheets. Although a graphite sheet has a 2D symmetry, carbon nanotubes by geometry have different properties in axial and radial directions. It has been shown that CNTs are very strong in the axial direction. According to the study of the mechanical properties of CNTs, it is found that young's modulus of carbon nanotubes is 200–950 GPa [75, 76], even 1–5 TPa [77], which is higher than the average carbon fiber by 1 order of magnitude, as similar as the young's modulus of diamond, and is one of the most hard materials currently. Moreover, the tensile strength of CNTs can be up to 11–150 GPa [75-77] (shown in Table 1-2). Carbon nanotubes demonstrate a high stiffness to an axial load or a bending of small amplitude, which translates to the record-high efficient linear-elastic modulus [78]. Furthermore, the bending strength has been reported approximately 14.2 GPa, and the strain energy can reach 100 Kev, which is approximately two times than the micron whisker [77].

Table 1-2 Mechanical properties of carbon nanotubes [75]

PROPERTIES

Mechanical

Materials	Young'modulus(Tpa)	Tensile strength(Gpa)	Elongation at break(%)
SWNT[E]	~1 (from 1 to 5)	13-53	16
Armchair SWNT[T]	0.94	126.2	23.1
Zigzag SWNT[T]	0.94	94.5	15.6-17.5
Chiral SWNT	0.92		
MWNT[E]	0.2-0.8-0.95	11-63-150	
Stainless steel[E]	0.186-0.214	0.38-1.55	15-50
Kevlar[E]	0.06-0.18	3.6-3.8	~2

[E]Experimental observation; [T]Theoretical prediction

7

For SWCNTs, young's module has been estimated in a range of 0.32–1.47 TPa and strengths between 10 GPa and 52 GPa with a toughness of ~770 J/g by Yu et al. [79]. Moreover, for MWCNTs, the young's modulus is dependent upon the degree of order within the tube walls, and proved that the young's modulus is decreased as the increase of disorder [80]. Besides, Pan et al. have directly measured the young's modulus and tensile strength of MWCNTs by pulling very long (~2 mm) aligned nanotube ropes with a specially designed stress-strain puller. The average young's modulus and tensile strength obtained were 0.45±0.23 TPa and 1.72±0.64 GPa, respectively [81].

(c) Thermal properties

Carbon nanotubes have a great aspect ratio, so a large amount of heat is transmitted along their length direction, and the rate of thermal energy transfer in one-dimensional direction can reach 10000 m/s [82]. The specific heat of individual nanotubes should be similar to that of 2D graphene at high temperatures, with the effects of phonon quantization becoming apparent at lower temperatures for SWCNTs of small diameter (less than 2 nm) [54]. The thermal conductivity, along with the specific heat, provides a sensitive tool for probing the interesting low-energy phonon structure of nanotubes, and also has the potential for practical applications that exploit the high thermal conductivity of these nanostructures [83]. Since the thermal conductivity along the tube axis is at least 2 orders of magnitude larger than that normal to the tube axis, the magnitude and temperature dependence of the thermal conductivity of a SWCNT bundle or an isolated MWCNT should be close to those of their constituent tubes, though some inter-tube thermal conduction could occur. The thermal conductivity of 'mat' samples, however, is expected to be dominated by inter-tube thermal conduction processes [84].

(d) Others

Carbon nanotubes have good nonlinear optical properties. Its three order nonlinear coefficient is 10^{-7}–10^{-10} esu. Besides, carbon nanotubes have a very good optical limiting property, and have gradually become a focus of the research of optical limiting

materials [85-88]. Moreover, because carbon nanotubes have a very high aspect ratio, it is required that the electric field applied on the carbon nanotube field is much lower than that of any conventional field emission material, when the same field current is generated [89, 90]. In 1997, Dillion found that the hydrogen storage capacity of SWCNTs was 5% at 0 ℃. Besides, because of the hollow structure of CNTs and the large layer spacing (0.34 nm), how can have a more excellent hydrogen storage properties, has become a focus of scientists [80, 91].

1.3.3 Carbon nanotubes' application

As the carbon nanotubes have excellent mechanical, electrical, thermal and other properties, so it has caused a worldwide attention. Professor Zettl of the California University made a very interesting analogy: If the application of fullerene can be written a page paper, the application of carbon nanotubes will be a book.

(a) Carbon nanotube reinforced composites

The most important application of carbon nanotubes based on their mechanical and electrical properties will be as reinforcements in composites. A major problem is in ensuring a strong interfacial interaction between nanotubes and the polymer matrix and attaining an efficient load transfer between the nanotubes and the polymer, during loading. Moreover, CNTs have large specific surface area, higher surface activation energy [55], and intrinsic Van der Waals attraction between CNTs, they agglomerate easily, and the interfacial interaction between CNTs and polymers is weak, preventing an efficient load transfer from the CNTs to the matrix. Accordingly, a uniform dispersion of CNTs in a polymer matrix and a strong interfacial interaction [56, 57] between CNTs and polymers are necessary conditions to maximize the advantages of CNTs as effective reinforcing filler in polymer composites. Nanotube reinforcements will increase the toughness of the composites by absorbing energy during their highly flexible elastic behavior. This will be especially important for nanotube-based ceramic matrix composites [92]. Use of the non-linear optical and optical limiting properties of

nanotubes has been reported for designing nanotube-polymer systems for optical applications, including photo-voltaic applications [93].

Moreover, since their high aspect ratio, only small amount of CNTs can introduce good level of conductivity in the composites. In the case of SWCNTs, the properties, especially the electrical properties, are highly related to the structure of the CNTs. The electron transport property of the MWCNTs is more complicated than SWCNTs. The network formation process in conductive polymer composites is very complicated. An ideal percolated network can be described by the percolation theory. However, actually, the conductivity of most conductive polymer composites is controlled by the tunnelling resistance, which can vary across many orders of magnitudes. This is defined as a continuum percolation network [94]. Carbon nanotube reinforced composites have been popular materials in the electric and electronic industries for a wide range of potential applications, such as nano-electronic devices, electrostatic recording paper, electromagnetic shielding, electromechanical actuators, electrochemical capacitors, nanowires, and superconductors [95-99].

(b) Synthesizing new materials

Due to its capillary properties, carbon nanotube was used to make certain elements integrate into the carbon nanotubes and prepare one-dimensional quantum wire with special properties (e.g., magnetic and superconducting properties). Besides, carbon nanotubes can be used as reaction media to transform into new-style one-dimensional nano-materials under certain conditions [100].

(c) Hydrogen storage

The area of hydrogen storage in carbon nanotubes remains active and controversial. Extraordinarily high and reversible hydrogen adsorption in SWCNTs-containing materials has been reported and has attracted considerable interest in both academia and industry [101, 102]. An even higher hydrogen uptake, up to 14–20 wt.%, at 20–400 ℃ under ambient pressure was reported [103] in alkali-metal intercalated carbon nanotubes. An electrochemical absorption and desorption of hydrogen experiment performed on

SWCNTs-containing materials reported a capacity of 110 mAh/g at low discharge currents [104].

(d) Others

Field emission characteristics of carbon nanotubes have been intensively studied using various methods [105]. The use of CNTs in cold cathode devices allows for [72] (i) instantaneous turn-on; (ii) high power; (iii) low control voltage operation, along with long life-times and miniaturization.

Besides, the small size and high sensitivity of carbon nanotubes makes them excellent sensors for biological and chemical systems. The first nanotube sensing experiment was performed by Kong et al. in Hongjie Dai's Stanford laboratory [106].

1.4 Conductive polymer composites

In recent years, conductive polymer composites (CPCs) are widely used in the electric, electronic, automobile and aeronautical industries because they meet requirements for miniaturized and light-weight industrial products. For the CPCs with high electrical conductivity, the main purpose of employing conductive polymer composites, however, is for their ability to prevent static electricity and heat generation, and they are extensively used for electronic functional components, such as sensors, capacitors and so on [107-110]. Ritchie et al. [107] presented the design principles which are currently employed to access polyoxometalate (POM)/conductive polymer (CP) composites; the applications of POM/CP composites in technologically relevant areas such as electrochemical and photoelectrochemical energy storage, sensors with ppb-sensitivity and electrochemical catalysis have been described. Besides, Acznik´s group [109] reported that the composite materials made of electrically conductive polymer–polypyrrole (PPy) and carbon materials have been prepared by oxidative chemical polymerization. Capacitance of the materials varied in the range of 90–135 F/g and has been retained during 5000 cycles of galvanostatic charging/ discharging, working in the acidic medium (i.e., 1 mol/L H_2SO_4 aqueous solutions). Moreover, the

measurements confirmed a very high electrochemical stability of polypyrrole supported by carbon materials with a current load of up to 50 A/g.

On the other hand, for the CPCs with low conductivity (e.g., the surface resistivity of 10^0–10^9 Ω/sq, shown in Table 1-1), the applications are more extensive in the industry, such as electromagnetic shielding agent, charge roll, electrostatic recording paper, computer shell, automobile components, etc. For these actual applications, the CPCs are needed to not only have a certain electrical conductivity, but also have a certain strength and toughness. In other words, it is necessary to prepare the CPCs as structural materials.

Most polymers have electrical conductivity values as low as 10^{-7}–10^{-14} S/cm [111]. Therefore, CPCs have not been yet very successful in large scale actual applications, which is attributable to the high conductive filler loading to achieve a sufficient level of conductivity. Besides, CNTs have some disadvantages that they are easily agglomerated and their dispersion is difficult to control, so several groups prepared the CPCs by chemical modifications and functionalize CNTs, not only to improve the solubility and dispersibility of CNTs, but also to enhance the interfacial interaction [112-118]. However, the main drawbacks of this method are time consuming and environmentally unfriendly. Another group is to prepare CPCs by different molding processes, such as melt mixing, extrusion molding, and injection molding. Many studies reported that the melt processing conditions must be optimized to achieve homogeneous MWCNT dispersion in the composites [32, 119-123]. For example, Villmow et al. [123] indicated that the extrusion conditions influenced the dispersion of MWCNTs in polylactic acid (PLA) matrix while using twin-screw extrusion whereas MWCNTs were added together with the polymer when using an extruder. Besides, they also prepared MWCNT/polycarbonate (MWCNT/PC) composites by injection molding, found that the resistivity of injection-molded MWCNT/PC composites can be influenced by selective variation of injection molding parameters at a fixed MWCNT content [21]. Moreover, Potschke et al. [122] stated that the feeding conditions of two different grades of

commercial MWCNTs influenced the dispersion of MWCNTs in polypropylene (PP), and they found that the individual optimization of the melt-mixing method is crucial to achieving uniform dispersion of MWCNTs to attain higher mechanical properties and lower electrical resistivity of PP-based composites.

Although varied methods are available to impart electrical conductivity to polymers, the simplest and easiest way is to directly incorporate conductive fillers into the polymer matrices by industrialized production methods such as extrusion molding process and injection molding process. Overall, in the present stage, the research on the production of the CPCs in industrial-scale is scarce.

1.5 Purpose of this research

As discussed above, currently, conductive polymer composites are mainly prepared in laboratory-scale. On the contrary, the industrialization of the production is very scarce. The overall aim of this thesis work is to produce conductive polymer composites in industrial-scale, through extrusion molding and injection molding, achieving high electrical conductivity, as well as good mechanical properties. On the other hand, since some properties have not achieved expected results, the application of the prepared CPCs has been limited. Thus, the second stage processing (e.g., plastic processing) was performed by proposed approaches to expand application range. Different matrix and different molding methods were chosen in this thesis work due to the following reasons:

(1) As a commonly used engineering material, PC has high strength and good toughness. To expand its application and make it have electrical property, the most easy and economical method is to add electrical fillers (i.e., MWCNTs) directly into PC through the molding process. However, MWCNT agglomerates easily and the interfacial interaction between PC and MWCNT is weak, preventing an efficient load transfer from the MWCNT to the PC. Accordingly, to prepare a new composite with excellent electrical properties and good mechanical properties, a uniform dispersion of MWCNTs and a strong interfacial interaction between MWCNTs and PC become the

major problems, which we have to solve firstly.

(2) Molding processing method is also a focus of our consideration. To realize the industrialized production of CPCs, the injection molding is preferred to prepare the MWCNT/PC composites. The dispersion and distribution of MWCNTs were controlled by through changing the injection conditions, resulting in controlling the electrical and mechanical properties. Finally, the preparation of the MWCNT/PC composites with excellent electrical conductivity and good mechanical property were achieved in industry-scale.

(3) The MWCNT/PC composites prepared by injection molding had good electrical and mechanical properties. To further expand the application of CPCs, we attempt to carry out the second stage processing (i.e., rolling process) to prepare a new-style composite with outstanding mechanical property (especially the ductility). However, our previous studies indicated that the MWCNT/PC composites were not suitable for rolling processing, due to the strong hygroscopicity of the PC. Therefore, the PLA was selected as the matrix polymer exemplarily for the next study. PLA was considered as an environmentally friendly polymer and be replaced traditional polymers in potential industrial applications. Besides, PLA was a crystalline thermoplastic polymer, we can attempt to change the microstructures (including crystalline structure, molecular orientation and crystallinity) to improve the mechanical properties through the rolling process.

The overall structure of the present study is presented in Fig. 1-8.

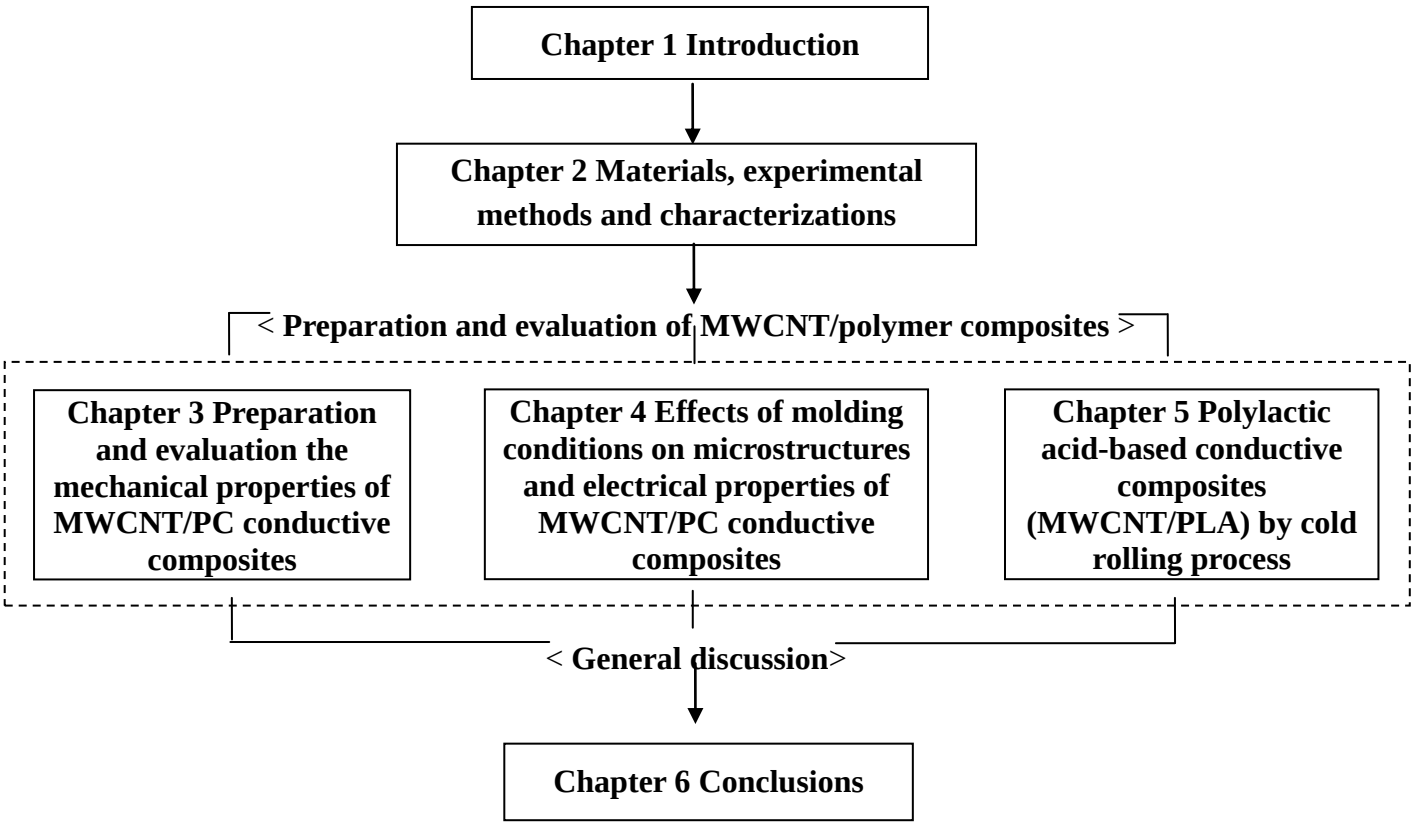

Fig. 1-8 The overall structure of the present study.

References

[1] K. Takano. Known the Plastic Technology, Japan. (2000).

[2] http://www.open.edu/openlearn/science-maths-technology/science/chemistry/ introduction -polymers/content-section-1.1. Retrieved in September 13th, 2015.

[3] Research and Statistics Department Minister's Secretariat Ministry of Economy, Trade and Industry (METI), (2011).

[4] Y. Miyamoto. Status of Plastics for Automobile (in Japanese). Kobunshi 54 (2005) 746-749.

[5] Y. Fujita. Development Trend of Polypropylene for Automobile (in Japanese). Expected Materials for the Future 5 (2005) 9-13.

[6] T. Yasuda. Resin Material for Automobile (in Japanese). Jamagazine (Japan) 40 (2006) 8-13.

[7] T. Oba. Polymers for Automobile and Environmental Problems (in Japanese). Journal of Network Polymer (Japan) 29 (2008) 25-28.

[8] K.J. Kim, C.W. Kim, B.I. Choi, C.W. Sung, H.Y. Kim, S.T. Won and H.Y. Ryou. Journal of Solid Mechanics and Materials Engineering 2 (2008) 574-581.

[9] K.J. Kim, M.H. Rhee, B.I. Choi, C.W. Kim, C.W. Sung, C.P. Han, K.W. Kang and S.T. Won. Development of Application Technique of Aluminum Sandwich Sheets for Automotive Hood. International Journal of Precision Engineering and Manufacturing 10 (2009) 71-75.

[10] T. Shimizu. Kobunshi. 59 (2011) 79-83.

[11] J. Amarasekera. J. Reinforced Plastics. 49 (2005) 38-41.

[12] Q. Yuan and D. Wu. Low Percolation Threshold and High Conductivity in Carbon Black Filled Polyethylene and Polypropylene Composites. Journal of Applied Polymer Science 115 (2010) 3527-3534.

[13] P. Liu. Modifications of Carbon Nanotubes with Polymers. European Polymer Journal 41 (2005) 2693-2703.

[14] H. H. So, J. W. Cho and N. G. Sahoo. Effect of Carbon Nanotubes on Mechanical and Electrical Properties of Polyimide/Carbon Nanotubes Nanocomposites. European Polymer Journal 43 (2007) 3750-3756.

[15] X. Wu, J. Qiu, P. Liu and E. Sakai. Synergistic Effect of MWCNTs and Graphite Powder on the Properties of Polymer Nanocomposites. Chemical Engineering Journal 246 (2014) 211-216.

[16] P. Costa, J. Silva, A. Anson-Casaos, M.T. Martinez, M.T. Abad, J. Viana and S. Lanceros-Mendez. Effect of Carbon Nanotube Type and Functionalization on the Electrical, Thermal, Mechanical and Electromechanical Properties of Carbon Nanotube/Styrene–Butadiene–Styrene Composites for Large Strain Sensor Applications. Composites: Part B 61 (2014) 136-146.

[17] N. Tekin, S.K. Beyaz, A. Kara, E. Simsek, F.D. Lamari, G. Cakmak and H.Y. Guney. The Synthesis of Covalent Bonded Single-walled Carbon Nanotube/ Polyvinylimidazole Composites by in Situ Polymerization and Their Physical Characterization. Polymer Composites 33 (2012) 1255-1262.

[18] http://www.mapeng.net/news/mechanical_English_article/2012/10/mapeng_ 12104932539005_2.html. Retrieved in September 16th, 2015.

[19] http://www.open.ac.uk/openlearn. Retrieved in September 16th, 2015.

[20] http://www.polycarbonate.org/. Retrieved in September 16th, 2015.

[21] T. Villmow, S. Pegel, P. Potschke and U. Wagenkncht. Influence of Injection Molding Parameters on the Electrical Resistivity of Polycarbonate Filled with Multi-walled Carbon Nanotubes. Composites Science and Technology 68 (2008) 777-789.

[22] J. Guo, Y. Liu, R. Prada-Silvy, Y. Tan, S. Azad, B. Krause, P. Pötschke and B. P. Grady. Aspect Ratio Effects of Multi-walled Carbon Nanotubes on Electrical, Mechanical, and Thermal Properties of Polycarbonates/MWCNT Composites. Journal of Polymer Science: Part B: Polymer Physics 52 (2014)73-83.

[23] M. Jonoobi, J. Harun, A.P. Mathew and K. Oksman. Mechanical Properties of

Cellulose Nanofiber (CNF) Reinforced Polylactic acid (PLA) Prepared by Twin Screw Extrusion. Composites Science and Technology 70 (2010) 1742-1747.

[24] https://en.wikipedia.org/wiki/Polylactic_acid. Retrieved in September 21st, 2015.

[25] Market Study Bioplastics, Ceresana, Dec. 2011.

[26] A. Södergård and M. Stolt. Properties of Lactic Acid Based Polymers and Their Correlation with Composition. Progress in Polymer Science 27 (2002) 1123-1163.

[27] J.C. Middelton and A.J. Tipton. Synthetic Biodegradable Polymers as Orthopedic Devices. Biomaterial 21 (2000) 2335-2346.

[28] G.L. Fiore, F. Jing, V.G. Young Jr, C.J. Cramer and M.A. Hillmyer. High Tg Aliphatic Polyesters by the Polymerization of Spirolactide Derivatives. Polymer Chemistry 1 (2010) 870-877.

[29] R.A. Auras, L.T. Lim, S.E.M. Selke and H. Tsuji. Poly (Lactic Acid): Synthesis, Structures, Properties, Processing, and Applications. 2011, DOI: 10.1002/ 9780470649848.

[30] "PLA". Reprap Wiki. Retrieved in September 25th, 2015.

[31] "PLA". MakerBot Industries. Retrieved in September 25th, 2015.

[32] Y.Y. Leu, Z.A. Mohd Ishak and W.S. Chow. Mechanical, Thermal, and Morphological Properties of Injection Molded Poly(lactic acid)/SEBS-g-MAH/ Organo-Montmorillonite Nanocomposites. J Appl Polym Sci. 124 (2012) 1200-1207.

[33] W.L. Tham, B.T. Poh, Z.A.M. Ishak and W.S. Chow. Thermal Behaviors and Mechanical Properties of Halloysite Nanotube-Reinforced Poly(lactic acid) Nanocomposites. J Therm Anal Calorim. 118 (2014) 1639-1647.

[34] H. Chang, M.J. Kao, K.D. Huang, C.G. Kuo and S.Y. Huang. Electromagnetic Shielding Effectiveness of Thin Film with Composite Carbon Nanotubes and Stainless Steel Fibers. J. Nanosci. Nanotechnol. 11 (2011) 1754-1757.

[35] A. Ameli, M. Nofar, S. Wang and C.B. Park. Lightweight Polypropylene/ Stainless-Steel Fiber Composite Foams with Low Percolation for Efficient

Electromagnetic Interference Shielding. ACS Appl. Mater. Interfaces 6 (2014) 11091-11100.

[36] M.H. Al-Saleh, G.A. Gelves and U. Sundararaj. Copper Nanowire/Polystyrene Nanocomposites: Lower Percolation Threshold and Higher EMI Shielding. Composites Part A: Applied Science and Manufacturing 42 (2011) 92-97.

[37] M. Liebscher, B. Krause, P. Pötschke, A. Barz, J. Bliedtner, M. Möhwald and A. Letzsch. Achieving Electrical Conductive Tracks by Laser Treatment of non-Conductive Polypropylene/Polycarbonate Blends Filled with MWCNTs. Macromolecular Materials and Engineering 299 (2014) 869-877.

[38] M. Arjmand, T. Apperley, M. Okoniewski and U. Sundararaj. Comparative Study of Electromagnetic Interference Shielding Properties of Injection Molded Versus Compression Molded Multi-walled Carbon Nanotube/Polystyrene Composites. Carbon 50 (2012) 5126-5134.

[39] G. Kasaliwal, A. Göldel and P. Pötschke. Influence of Processing Conditions in Small-scale Melt Mixing and Compression Molding on the Resistivity and Morphology of Polycarbonate–MWNT Composites. Journal of Applied Polymer Science 112 (2009) 3494-3509.

[40] Q. Cao, Y. Song, Z. Liu and Q. Zheng. Influence of Annealing on Rheological and Conductive Behaviors of High-density Polyethylene/Carbon Black Composites. Journal of Materials Science 44 (2009) 4241-4245.

[41] Q. Yuan, S.A. Bateman and D. Wu. Mechanical and Conductive Properties of Carbon Black-filled High-density Polyethylene, Low-density Polyethylene, and Linear Low-density Polyethylene. J. Thermoplastics Compos. Mater. 23 (2010) 459-471.

[42] A. Ameli, P.U. Jung and C.B. Park. Electrical Properties and Electromagnetic Interference Shielding Effectiveness of Polypropylene/Carbon Fiber Composite Foams. Carbon 60 (2013) 379-391.

[43] A. Ameli, P.U. Jung and C.B. Park. Through-plane Electrical Conductivity of

Injection-molded Polypropylene/Carbon-fiber Composite Foams. Composites Science and Technology 76 (2013) 37-44.

[44] L. Lei, J. Qiu, Y. Zhao, X. Wu and E. Sakai. Synthesizing Electrically Conductive Graphene-Poly(methyl methacrylate) (GNS-PMMA) Composites and Polylactic Acid (PLA)-Based Conductive Films. Science of Advanced Materials 4 (2012) 912-919.

[45] L. Lei, J. Qiu and E. Sakai. Preparing Conductive Poly(lactic acid) (PLA) with Poly(methyl methacrylate) (PMMA) Functionalized Graphene (PFG) by Admicellar Polymerization. Chemical Engineering Journal 209 (2012) 20-27.

[46] H.W. Kroto, J.R. Heath, S.C. O'Brien, R.F. Curl and R.E. Smalley. C60: Buckminsterfullerene. Nature 318 (1985) 162-163.

[47] S. Iijima. Helical Microtubules of Graphitic Carbon. Nature 354 (1991) 56-58.

[48] Intergovernmental Panel on Climate Change, Climate change 2007: The Physical Science Basis, IPCC WGI Fourth Assessment Report, Paris, February 5th (2007).

[49] A.K. Geim. Graphene: Status and Prospects. Science 324 (2009) 1530-1534.

[50] P.J.F Harris. Carbon Naotubes and Related Structures. London: Cambridge university press, 1999.

[51] R. Vidu, M. Rahman, M. Mahmoudi, M. Enachescu, T.D. Poteca and I. Opris. Nanostructures: a Platform for Brain Repair and Augmentation. Front Syst Neurosci. 8 (2014) 91-93.

[52] H. He, L.A. Pham-Huy, P. Dramou, D. Xiao, P. Zuo and C. Pham-Huy. Carbon Nanotubes: Applications in Pharmacy and Medicine, BioMed Research International (2013) DOI: org/10.1155/2013/578290.

[53] Z.W. Pan, S.S. Xie, B.H. Chang, C.Y. Wang, L. Lu, W. Liu, W.Y. Zhou, W. Z. Li and L.X. Qian. Very Long Carbon Nanotube. Nature 394 (1998) 631-632.

[54] M. Bockrath, D.H. Cobden, P.L. McEuen, N.G. Chopra, A. Zettl, A. Thess and R.E. Smalley. Single-Electron Transport in Ropes of Carbon Nanotubes. Science 275 (1997) 1922-1925.

[55] J.C. Kearns and R.L. Shambaugh. Polypropylene Fibers Reinforced with Carbon Nanotubes. J. Appl. Polym. Sci. 86 (2002) 2079-2084.

[56] A. Thionnet, H. Chou and B. Anthony. Fibre Break Failure Processes in Unidirectional Composites. Part 1: Failure and Critical Damage State Induced by Increasing Tensile Loading. Appl. Compos. Mater. 22 (2015) 119-140.

[57] M.A. Bily, Y.W. Kwon and R.D. Pollak. Study of Composite Interface Fracture and Crack Growth Monitoring Using Carbon Nanotubes. Appl. Compos. Mater. 17 (2010) 347-362.

[58] M.F. Yu, O. Lourie, M.J. Dyer, K. Moloni, T.F. Kelly and R.S. Ruoff. Strength and Breaking Mechanism of Multiwalled Carbon Nanotubes Under Tensile Load. Science 287 (2000) 637-640.

[59] E.T. Thostenson, Z. Ren and T.W. Chou. Advances in the Science and Technology of Carbon Nanotubes and Their Composites: A Review. Compos. Sci. Technol. 61 (2001) 1899-1912.

[60] C. Li and T.W. Chou. Elastic Moduli of Multi-walled Carbon Nanotubes and the Effect of Van Der Waals Forces. Compos. Sci. Technol. 63 (2003)1517-1524.

[61] D. Tasis, N. Tagmatarchis , A. Bianco and M. Prato. Chemistry of Carbon Nanotubes. Chem. Rev. 106 (2006) 1105-1136.

[62] T. Filleter, R. Bernal, S. Li and H.D. Espinosa. Ultrahigh Strength and Stiffness in Cross-Linked Hierarchical Carbon Nanotube Bundles. Adv. Mater. 23 (2011) 2855-2860.

[63] Carbon Nanotubes and the Electrical, Thermal, Mechanical and other Useful Properties of Carbon Nanotubes by Cheap Tubes. http://www. azonano. com/article. aspx?ArticleID=1564. Retrieved in September 26th, 2015.

[64] J.W. Mintmire, B.I. Dunlap and C.T. White. Are Fullerene Tubesmetallic? Physical Review Letters 68 (1992) 631-634.

[65] R. Saito, M. Fujita, G. Dresselhaus and M.S. Dresselhaus. Electronic Structure of Chiral Graphene Tubules. Applied Physics Letters 60 (1992) 2204-2206.

[66] http://www.understandingnano.com/electrical-properties-carbon-nanotubes.
Html. Retrieved in September 26th, 2015.

[67] J.E. Fischer, H. Dai, A. Thess, R. Lee, N. M. Hanjani, D. L. Dehaas and R. E. Smalley. Metallic Resistivity in Crystalline Ropes of Single-walled Carbon Nanotubes. Phys Rev B. 55 (1997) 4921-4924.

[68] T.W. Odom, J.-L. Huang, P. Kim and C.M. Lieber. Atomic Structure and Electronic Properties of Single-walled Carbon Nanotubes. Nature 391 (1998) 62-64.

[69] L. Chico, V.H. Crespi, L.X. Benedict, S.G. Louie and M.L. Cohen. Pure Carbon Nanoscale Devices: Nanotube Heterojunctions. Physical Review Letters 76 (1996) 971-974.

[70] R. Saito, G. Dresselhaus and M.S. Dresselhaus. Electronic Structure of Double-layer Graphene Tubules. Journal of Applied Physics 73 (1993) 494-500.

[71] H. Dai, E.W. Wong and C.M. Lieber. Probing Electrical Transport in Nanomaterials: Conductivity of Individual Carbon Nanotubes. Science 272 (1996) 523-526.

[72] P. Bandaru. Electrical Properties and Applications of Carbon Nanotube Structures. Journal of Nanoscience and Nanotechnology 7 (2007) 1-29.

[73] X. Zhou, J. Zhou, O.Y. Zhong-can. Strain Energy and Young's Modulus of Single-wall Carbon Nanotubes Calculated from Electronic Energy-band Theory. Physical Review B 62 (2000) 13692-13696.

[74] C. Bower, R. Rosen, L. Jin, J. Han and O. Zhou. Deformation of Carbon Nanotubes in Nanotube-Polymer Composites. Applied Physics Letters 74 (1999) 3317-3319.

[75] https://www.google.com.hk/search. Retrieved in September 26th, 2015.

[76] M.F. Yu, O. Lourie, M.J. Dyer, K. Moloni, T.F. Kelly and R.S. Ruoff. Strength and Breaking Mechanism of Multiwalled Carbon Nanotubes under Tensile Load. Science 287 (2000) 637-640.

[77] S. Li, X. Xu, Z. Li and M. Yang. Surface Modification of Carbon Nanotubes and Their Applications in Polymers. Engineering Plastics Application 10 (2004) 70-72.

[78] B.I. Yakobson and P. Avouris. Mechanical Properties of Carbon Nanotubes. Topics

in Applied Physics 80 (2001) 287-327.

[79] M.-F. Yu, B.S. Files, S. Arepalli and R.S. Ruoff. Tensile Loading of Ropes of Single Wall Carbon Nanotubes and their Mechanical Properties. Physical Review Letters 84 (2000) 5552-5555.

[80] J.P. Salvetat, J.M. Bonard, N.H. Thomson, A.J. Kulik, L. Forr ́o, W. Benoit and L. Zuppiroli. Mechanical Properties of Carbon Nanotubes. Applied Physics A 69 (1999) 255-260.

[81] Z.W. Pan, S.S. Xie, L. Lu, B.H. Chang, L.F. Sun, W.Y. Zhou, G. Wang and D.L. Zhang. Tensile Tests of Ropes of Very Long Aligned Multiwall Carbon Nanotubes. Applied Physics Letters 74 (1999) 3152-3154.

[82] J. Yuan. Surface Modification of Multi Wall Carbon Nanotubes and Study on the Thermoplastic Polymer Composites. Hunan University, Degree thesis (2009).

[83] R.S. Ruoff and D.C. Lorents. Mechanical and Thermal Properties of Carbon Nanotubes. Carbon 33 (1995) 925-930.

[84] J. Hone. Phonons and Thermal Properties of Carbon Nanotubes. Topics in Applied Physics 80 (2001) 273-286.

[85] M. Endo, K. Takeuchi, K. Kobori, Katsushi Takahashi, Harold W. Kroto and A. Sarkar. Pyrolytic Carbon Nanotubes from Vapor-grow Carbon Fibers. Carbon 33 (1995) 873-881.

[86] T. Guo, P. Nikolaev, A. Thess, D.T. Colbert and R.E. Smalley. Catalytic Growth of Single-walled Nanotubes by Laser Vaporization. Chemical Physics Letters 243 (1995) 49-54.

[87] G.Ya Sleypan, S.A. Maksimenko, A. Lakhtakia and O.M. Yevtushenko. Electromagnetic Response of Carbon Nanotubes and Nanotube Ropes. Synthetic Metals 124 (2001) 121-123.

[88] Z. F. Ren, Z. P. Huang, J. W. Xu, J. H. Wang, P. Bush, M. P. Siegal and P. N. Provencio. Synthesis of Large Arrays of Well-aligned Carbon Nanotubes on Glass. Science 282 (1998) 1105-1107.

[89] J.I. Sohn, S Lee, Y.H. Song, S.Y. Choi, K.I. Cho and K.S. Nam. Patterned Selective Growth of Carbon Nanotubes and Largrfield Emission from Vertically Well-aligned Carbon Nanotube Field Emitter Arrays. Appl. Phys. Lett. 78 (2001) 901-903.

[90] Z. Chen, D. den Engelsen, P. K. Bachmann, V. van Elsbergen, I. Koehler, J. Merikhi and D.U. Wiechert. High Emission Current Density Microwave-Plasma-Grown Carbon Nanotube Array by Postdepositional Radio-frequency Oxygen Plasma Treatment. Appl. Phys. Lett. 87 (2005) 1-3.

[91] Y. Lin, S. Taylor, H. Li, K. A. Shiral Fernando, L. Qu, W. Wang, L. Gu, B. Zhou and Y.P. Sun. Advances Toward Bioapplications of Carbon Nanotubes. J. Mater. Chem. 14 (2004) 527-541.

[92] S. Chang, R.H. Doremus, P.M. Ajayan and R.W. Siegel. Processing and Mechanical Properties of C-Nanotube Reinforced Alumina Composites. Ceramic Engineering and Science Proceedings 21 (2000) 653-658.

[93] H. Ago, K. Petritsch, M.S.P. Shaffer, A.H. Windle and R.H. Friend. Composites of Carbon Nanotubes and Conjugated Polymers for Photovoltaic Devices. Advanced Materials 11 (1999) 1281-1285.

[94] R. Zhang. Conductive TPU/CNT Composites for Strain Sensing. University of London, London (2009).

[95] B. Hornbostela, P. Potschke, J. Kotza and S. Roth. Mechanical Properties of Triple Composites of Polycarbonate, Single-walled Carbon Nanotubes and Carbon Fibres. Physica E: Low-dimensional Systems and Nanostructures 40 (2008) 2434-2439.

[96] R. Ramasubramaniam, J. Chen and H. Liu. Homogeneous Carbon Nanotube/ Polymer Composites for Electrical Applications. Appl. Phys. Lett. 83 (2003) 2928-2930.

[97] R. Andrews and M. Weisenberger. Carbon nanotube polymer composites. Curr. Opin. Solid State Mater. Sci. 8 (2004) 31-37.

[98] A. Bachtold, P. Hadley, T. Nakanishi and C. Dekker. Logic Circuits with Carbon

Nanotube Transistors. Science 294 (2001) 1317-1320.

[99] I. Amlani, R. Zhang, T. John, L. Nagahara and T. Raymond K. Directed Placement of Suspended Carbon Nanotubes for Nanometer-scale Assembly. Appl. Phys. Lett. 80 (2002) 3826-3828.

[100] H. Dai, E.W. Wong, Y.Z. Lu, S. Fan and C.M. Lieber. Synthesis and Characterization of Carbide Nanorods. Nature 375 (1995) 769-772.

[101] A.C. Dillon, K.M. Jones, T.A. Bekkedahl, C.H. Kiang, D.S. Bethune and M.J. Heben. Storage of Hydrogen in Single-walled Carbon Nanotubes. Nature 386 (1997) 377-379.

[102] C. Liu, Y.Y. Fan, M. Liu, H.T. Cong, H.M. Cheng and M.S. Dresselhaus. Hydrogen Storage in Single-walled Carbon Nanotubes at Room Temperature. Science 286 (1999) 1127-1129.

[103] P. Chen, X. Wu, J. Lin and K.L. Tan. High H2 Uptake by Alkali-Doped Carbon Nanotubes under Ambient Pressure and Moderate Temperatures. Science 285 (1999) 91-93.

[104] C. Nutenadel, A. Zuttel, D. Chartouni and L. Schlapbach. Electrochemical Storage of Hydrogen in Nanotube Materials. Solid State Letters 2 (1999) 30-32.

[105] Y.C. Choi, Y.M. Shin, Y.H. Lee, B.S. Lee, G.S. Park, W.B. Choi, N.S Lee and J.M. Kim. Controlling the Diameter, Growth Rate, and Density of Vertically Aligned Carbon Nanotubes Synthesized by Microwave Plasma-enhanced Chemical Vapor Deposition. Applied Physics Letters 76 (2000) 2367-2369.

[106] J. Kong, N.R. Franklin, C. Zhou, M.G. Chapline, S. Peng, K. Cho and H. Dai. Nanotube Molecular Wires as Chemical Sensors. Science 287 (2000) 622-625.

[107] S. Herrmann, C. Ritchie and C. Streb. Polyoxometalate–Conductive Polymer Composites for Energy Conversion, Energy Storage and Nanostructured Sensors. Dalton Trans. 44 (2015) 7092-7104.

[108] E. Frackowiak, V. Khomenko, K. Jurewicz, K. Lota and F. Beguin. Supercapacitors Based on Conducting Polymers/Nanotubes Composites. Journal of

Power Sources 153 (2006) 413-418.

[109] K. Lota, G. Lota, A. Sierczynska and I. Acznik. Carbon/Polypyrrole Composites for Electrochemical Capacitors. Synthetic Metals 203 (2015) 44-48.

[110] G.A. Snook, P. Kao and A.S. Best. Conducting-Polymer-Based Supercapacitor Devices and Electrodes. Journal of Power Sources 196 (2011) 1-12.

[111] S.K.H. Gulrez, M.E. Ali Mohsin, H. Shaikh, A. Anis, A.M. Pulose, M.K. Yadav, E.H.P. Qua and S.M. Al-Zahrani. A Review on Electrically Conductive Polypropylene and Polyethylene. Polymer Composites 35 (2014) 900-914.

[112] P. Liu. Modifications of Carbon Nanotubes with Polymers. European Polymer Journal 41 (2005) 2693-2703.

[113] D. Tasis, N. Tagmatarchis, A. Bianco and M. Prato. Chemistry of Carbon Nanotubes. Chem. Rev. 106 (2006) 1105-1136.

[114] H.H. So, J.W. Cho and N.G. Sahoo. Effect of Carbon Nanotubes on Mechanical and Electrical Properties of Polyimide/Carbon Nanotubes Nanocomposites. European Polymer Journal 43 (2007) 3750-3756.

[115] S. Wang, R. Liang, B. Wang and C. Zhang. Covalent Addition of Diethyltoluenediamines onto Carbon Nanotubes for Composite Application. Polym. Compos. 30 (2009)1050-1057.

[116] L. Meng, C. Fu and Q. Lu. Advanced Technology for Functionalization of Carbon Nanotubes. Progress in Natural Science 19 (2009) 801-810.

[117] X. Wu, J. Qiu, P. Liu and E. Sakai. Synergistic Effect of MWCNTs and Graphite Powder on the Properties of Polymer Nanocomposites. Chemical Engineering Journal 246 (2014) 211-216.

[118] S. Xu, A. Akchurin, T. Liu, W. Wood, X.W. Tangpong, I.S. Akhatov and W.H. Zhong. Mechanical Properties, Tribological Behavior, and Biocompatibility of High-density Polyethylene/Carbon Nanofibers Nanocomposites. Journal of Composite Materials 49 (2015) 1503-1512.

[119] R. Andrews, D. Jacques, M. Minot and T. Rantell. Fabrication of Carbon

Multiwall Nanotube/Polymer Composites by Shear Mixing. Mater. Eng. 287 (2002) 395-403.

[120] B. Krause, P. Potschke and L. Haussler. Influence of Small Scale Melt Mixing Conditions on Electrical Resistivity of Carbon Nanotube-Polyamide Composites. Compos. Sci. Technol. 69 (2009) 1505-1515.

[121] G.R. Kasaliwal, S. Pegel, A. Goldel, P. Potschke and G. Heinrich. Analysis of Agglomerate Dispersion Mechanisms of Multiwalled Carbon Nanotubes during Melt Mixing in Polycarbonate. Polymer 51 (2010) 2708-2720.

[122] M.T. Muller, B. Krause, B. Kretzschmar and P. Pötschke. Influence of Feeding Conditions in Twin-screw Extrusion of PP/MWCNT Composites on Electrical and Mechanical Properties. Composites Science and Technology 71 (2011) 1535-1542.

[123] T. Villmow, P. Potschke, S. Pegel, L. Haussler and B. Kretzschmar. Influence of Twin-screw Extrusion Conditions on the Dispersion of Multi-walled Carbon Nanotubes in a Poly (lactic acid) Matrix. Polymer 49 (2008) 3500-3509.

Chapter 2 Materials, Experiment and Evaluation Methods

2.1 Materials

2.1.1 Multi-walled carbon nanotube (MWCNT)

MWCNTs were provided by Showa Denko Company (Tokyo, Japan), and they are special carbon nanotubes for polymer composites. MWCNTs, the Vapor Grown Carbon Fiber (VGCF®-X), were synthesized by the method of catalytic chemical vapor deposition. The average diameter of MWCNTs is approximately 10–15 nm and the mean length of length is 3 μm (shown in Table 2-1), and the micro morphology is shown in Fig. 2-1.

Table 2-1 Physical parameters of VGCF-X type

Parameters	Unit	Value
Diameter [a]	nm	10–15
Average length [a]	μm	3
Bulk density [b]	g/cm^3	0.087
Consolidation resistivity [b]	Ω·cm	0.015

a: Catalog value

b: Production shipping list

Carbon nanotubes (CNTs) are regarded as a conductive filler having a high aspect ratio and excellent mechanical and electrical conductive properties, due to their tube diameter of a few dozens of nm and mean length of a few μm. If it can be ensured that the contact probability between the fillers is increased, a high effective conductivity can

be obtained even by adding only a small amount of filler into insulation polymers [1-3]. MWCNTs have drawn much attention for their potential application as conductive filler into polymers to produce conductive polymer composites [4-8].

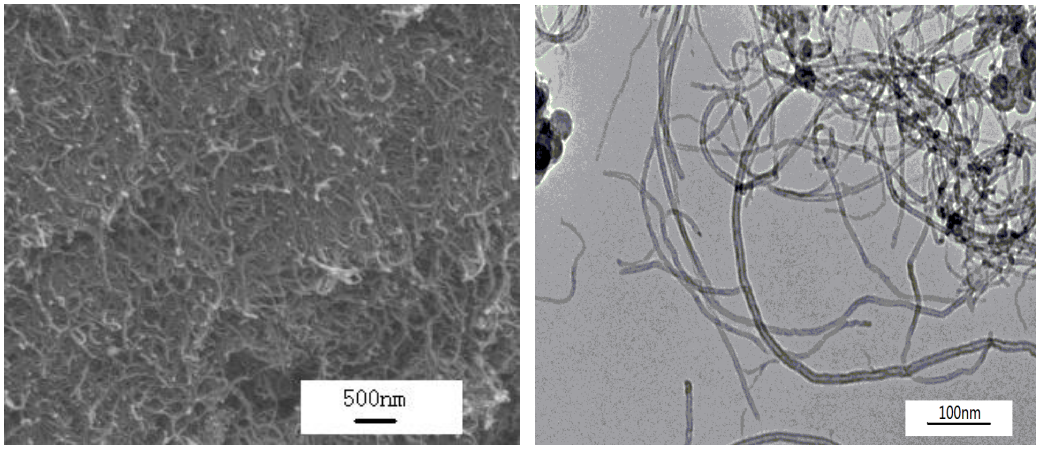

Fig. 2-1 SEM (a) and TEM (b) micrographs of MWCNTs.

2.1.2 Polycarbonate (PC)

Chemical structure of PC is shown in Fig. 2-2 [9]. PC has its own characteristics and many advantages. PC is a kind of non-crystalline thermoplastic polymer with excellent comprehensive properties, which has excellent electrical insulation, extension, size-stability and chemical corrosion resistance, high strength, heat resistance and cold resistance. Especially, its impact resistance is outstanding. The heat resistance temperature of PC is from –100 ℃ to 135 ℃. Besides, it is well known that PC is a kind of engineering plastics in wide applications, such as optical disc substrate, optical instrument, communication apparatus, automobile parts, medical apparatus and instruments, and so on [9-12].

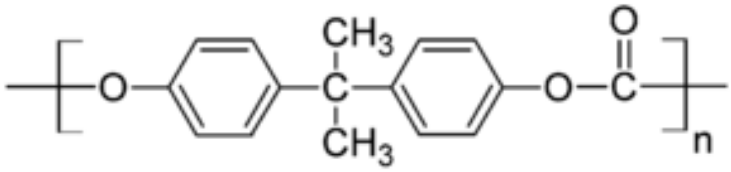

Fig. 2-2 Chemical structure of PC [9].

In this research, PC (L-1225L, Teijin Chemicals Co., Japan) was used as matrix, with a melt flow index of 1.8 cm^3/10min, and a density of 1.2 g/cm^3. The physical parameters are shown in Table 2-2.

Table 2-2 Physical parameters of PC

Parameters	Unit	Value
Density	g/cm^3	1.2
Melt flow index	cm^3/10min	1.8
Tensile strength	MPa	61
Fracture strain	%	>50
Flexural strength	MPa	93
Surface resistivity	Ω/sq	$>1\times10^{15}$
Volume resistivity	Ω・cm	$>1\times10^{13}$

2.1.3 Polylactic acid (PLA)

Polylactic acid (PLA) is aliphatic biodegradable polyester made up of lactic acid (2-hydroxy propionic acid). PLA is a biodegradable thermoplastic aliphatic polyester derived from renewable resources [14], such as corn starch (in the United States), tapioca roots, chips or starch (mostly in Asia), or sugarcane (in the rest of the world).

PLA can be produced by several techniques, including azeotropic dehydration condensation, direct condensation polymerization and polymerization through lactic acid formation which is pressed in Fig. 2-3. Owing to PLA's biodegradation under certain conditions, such as the presence of oxygen, it has been considered as one of the solutions to alleviate white waste disposal problems and to lessen the dependence on

petroleum-based plastics for packaging materials. Besides, PLA has many advantages, such as high-strength, high-modulus [15] and good stiffness [14].

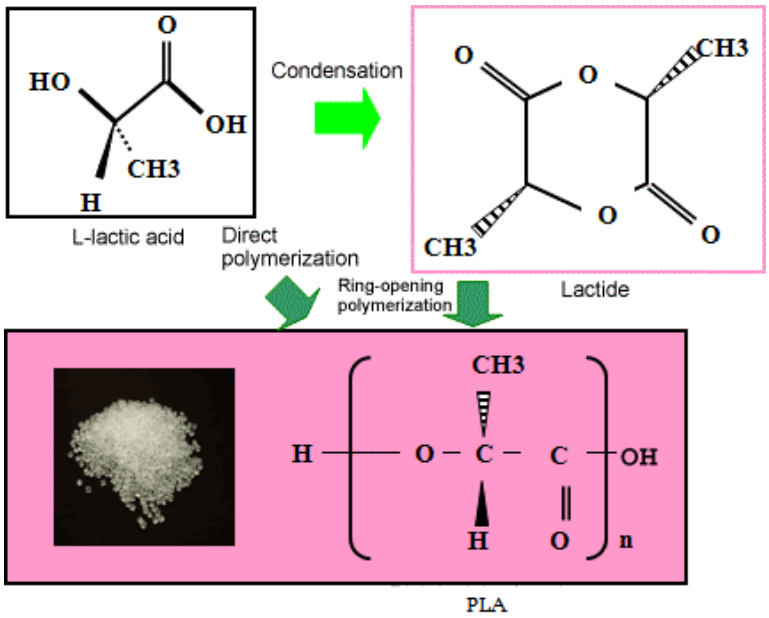

Fig. 2-3 Production process for PLA [13].

Table 2-3 Properties of PLA

Properties	Unit	Value
Specific gravity	g/cm^3	1.24
MFR	g/10min (210 ℃, 2.16 kg)	22
Clarity	Transparent	
Tensile yield strength	MPa	62
Tensile elongation	%	3.5
Notched izod impact	J/m	16
Flexural strength	MPa	108
Flexural modulus	MPa	3600
Heat distortion temperature	℃	55

PLA used for our experiments was purchased from Nature Works LLC (Ingeo

3001D, America), having a density of 1.24 g/cm^3 (ASTM D792) and a melt flow index of 22 g/10min (ASTM D1238). Its residual moisture content was less than 0.025% which was recommended to prevent viscosity degradation. The primary properties of PLA are shown in Table 2-3.

2.2 Preparation and processing of composites

2.2.1 Twin-screw extrusion

Prior to the preparation of composite master batches, both polymer (i.e., PC and PLA) and MWCNTs were dried at 120 ℃ (for PC) or 80 ℃ (for PLA) for more than 5 h. The compounding process of master batches began with preparation by a twin-screw extruder (KZX25TW-60MG-NH (-1200)-AKT, Technovel Co., Ltd, Osaka, Japan), which is shown in Fig. 2-4. For the complete compounding of master batches, polymer pellets and powdery MWCNTs with different contents were premixed, and then the mixed composite material was fed into the hopper of the extruder. All master batches were cooled in a water bath and pelletized after the extrusion process. The master batches of MWCNT/PC composites and MWCNT/PLA composites were prepared in this step.

Fig. 2-4 Twin-screw extruder.

After that, the prepared composites mater batches were dried again for 8 h, to ready for the preparation of the specimens in the next step.

On the other hand, the master batches of MWCNT/PLA composites were extruded to be the plates by using the same extruder, which was ready for the rolling process.

2.2.2 Injection molding process

The injection molding of extruded composites master batches was performed by using an injection molding machine (NP7-1F, Nissei Plastic industry Co., Ltd, Japan; shown in Fig. 2-5), subsequently obtaining the standard composite specimens. Dumbbell shaped specimens with dimensions of 75 mm × 10 mm × 2 mm (JIS K 7113 1(1/2), Fig. 2-6) and rectangle shaped specimens with dimensions of 80 mm × 10 mm × 4 mm (JIS K 7171 1(1/2), Fig. 2-7) were used for mechanical property tests and electrical property tests, respectively. Besides, the flat shaped specimens with a size of 60 mm × 60 mm × 3 mm (Fig. 2-8) were also prepared by the injection molding machine (ROBOSHTO-100C, FANUC Co., Ltd., Japan) for electrical property tests. The mold temperature was set to required temperature for different composites.

Fig. 2-5 Injection molding machine.

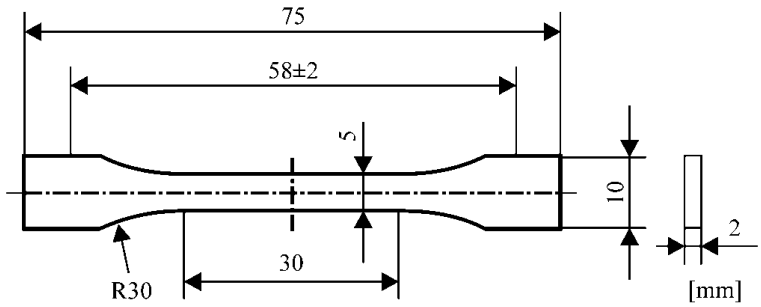

Fig. 2-6 Dumbbell shaped specimen (JIS K 7113 1(1/2)).

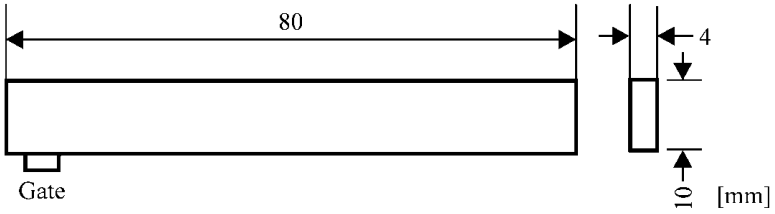

Fig. 2-7 Rectangle shaped specimen (JIS K 7171 1(1/2)).

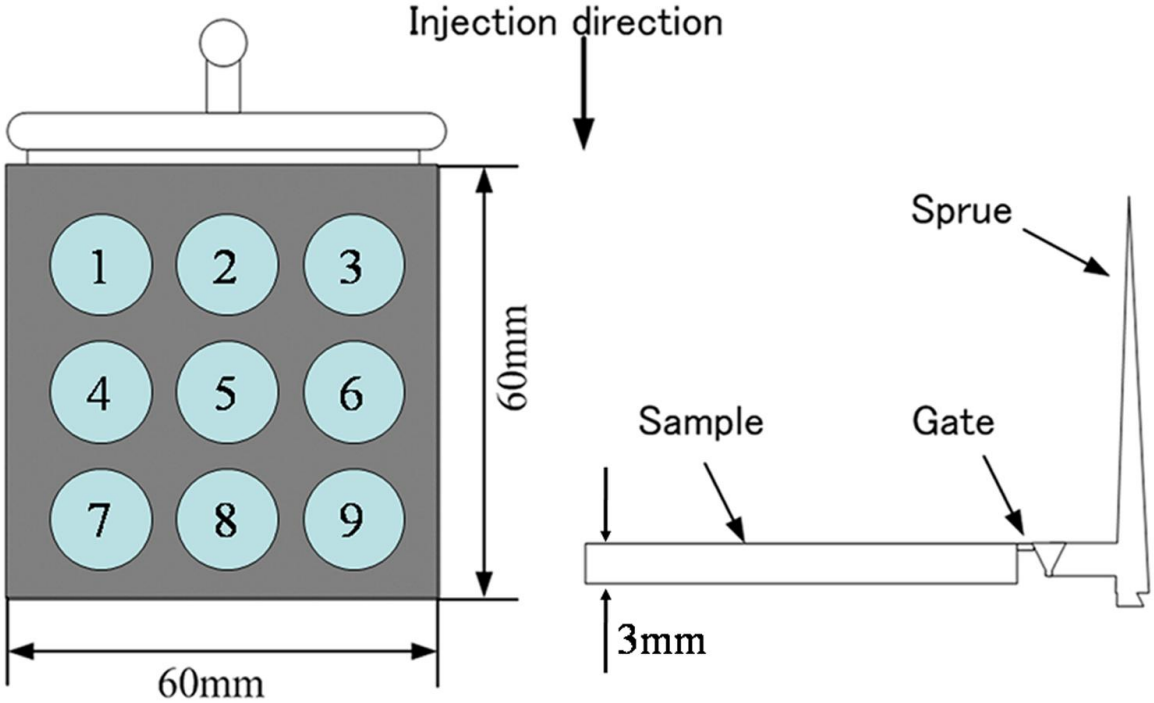

Fig. 2-8 Flat shaped specimen.

2.2.3 Rolling molding process

The extruded MWCNT/PLA plates were used for the rolling process. The rolling process was performed with different rolling ratios (ξ = 0%, 20%, 40%, 60, and 75%) to evaluate the effect of the rolling ratio on the properties and morphology of PLA. 2000 mm (length) × 100 mm (width) × 1.2 mm (thickness; the maximum thickness was 1.6 mm) extruded plates were machined into specimens with dimensions of 100 mm (length) × 80 mm (width) × 1.2 mm (thickness; the maximum thickness was 1.6 mm). The rolling processing was carried out by a rolling machine (TKE-0; Imoto Machinery Co., Ltd., Japan) at room temperature (23±2 ℃) with a rotation speed of 3 m/min (shown in Fig. 2-9). The rolling direction was matched to the extrusion direction, and the effective width and diameter of each roller were 150 and 100 mm, respectively. The rolling ratio ξ was calculated using the following equation:

$$\xi = [(H_0 - H_1) / H_0] \times 100\% \qquad (2\text{-}1)$$

where, H_0 – the initial thickness of the specimen (mm);

H_1 – the thickness of the rolled specimen (mm), which was measured by a micrometer after the rolling process.

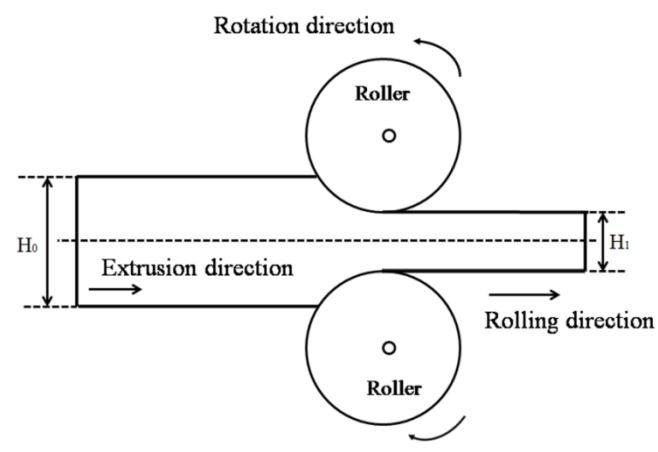

Fig. 2-9 Schematic diagram of the rolling process.

Finally, the rolled plates were cut using a dumbbell-shaped mold to obtain

specimens with dimensions of 75 mm (length) × 10 mm (width), but with different thicknesses based on the different rolling ratios. The different thicknesses of the rolled plates were achieved by adjusting the distance between the two rollers (Fig. 2-9). The specimens were used for evaluating the variations of crystallinity and molecular orientation of PLA, and the mechanical and electrical properties of the MWCNT/PLA composites were also investigated.

2.3 Experiments and evaluation methods

2.3.1 Dynamic mechanical analysis (DMA)

DMA of the MWCNT/PC composites was carried out with a dynamic mechanical analyzer (RSA-G2, TA Instruments, Wilmington, USA, shown in Fig. 2-10), and the storage modulus E', loss modulus E'', and tan δ (δ is defined as the phase lag between the stress and the strain) were determined by the average value of three measurement results. The clamping mode of the specimen was three-point bending and the span of the girder was 10 mm. The parallel part of the dumbbell shaped specimen was used for the measurements. The specimens were heated from 30 ℃ to 180 ℃, and each specimen was subjected to the temperature scan mode at a programmed heating rate of 3 ℃/min and a frequency of 1.0 Hz; the amplitude of strain was 0.1%.

Moreover, for the MWCNT/PLA composites, the dynamic mechanical analysis was also carried out with the same dynamic mechanical analyzer in tension mode, and the storage modulus E′, loss modulus E″, and tan δ were determined by the average value of three measurement results. The span of the girder was 20 mm. Strip test pieces were cut from the middle of the dumbbell shaped specimen with a size of 30 mm (length) × 5 mm (width). The test was performed in the temperature scan mode, heating from 30 to 120 ℃ at a programmed heating rate of 2 ℃/min. The amplitude of the strain was 0.1%, and the frequency was set at 1.0 Hz.

Fig. 2-10 Dynamic mechanical analyzer [16].

2.3.2 Tensile test

The tensile properties involving the tensile strength and the fracture strain of the composites were measured using a universal testing machine (3360, INSTRON Co., Ltd, Kanagawa, Japan). The specimens used were the dumbbell-shaped specimen. The specimen is presented in Fig. 2-6 and the schematic of tensile test is presented in Fig. 2-11. The specimens were placed for over 48 h before testing (similarly hereinafter). The measurements were carried out at a room temperature of 23±2 ℃ and a tensile speed of 10 mm/min (according to JIS for tensile properties testing method). Besides, the relative humidity of atmospheric was 50±5%. The outputs of the testing machine were the load [N] and the displacement [mm], and then the relationship of stress–strain was calculated from the obtained load and displacement. The tensile strength and fracture strain were calculated by equation 2-2 and equation 2-3, respectively. Besides, at least five specimens were tested and the average value was determined as the tensile

strength and fracture strain of composites (similarly hereinafter, for other mechanical property tests and electrical property tests).

$$\sigma = F/A \qquad (2\text{-}2)$$

$$\xi = [(L - L_0) / L_0] \times 100\% \qquad (2\text{-}3)$$

where, F – the maximum load (N);

A – the cross-section area (mm^2);

L – the distance at tensile fractured (mm);

L_0 – the original distance (mm), which is confirmed as 30 mm.

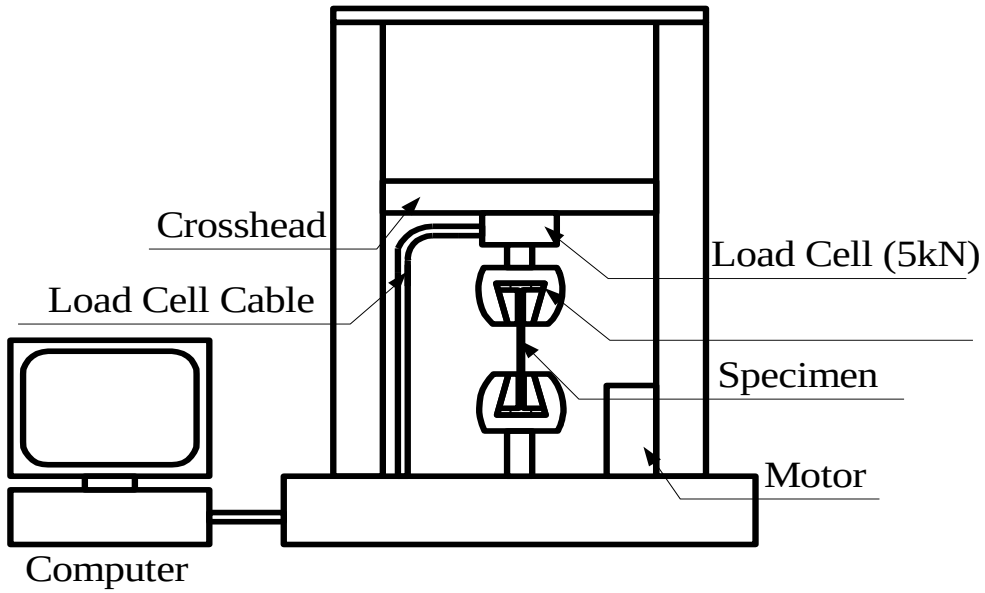

Fig. 2-11 Schematic diagram of the tensile test.

2.3.3 Bending test

The bending strength and bending strain were measured by the same universal testing machine (3360, Instron Co., Ltd, Kanagawa, Japan). The specimen for bending test is present in Fig. 2-7 and the schematic of bending test is presented in Fig. 2-12. The tests were performed at a bend speed of 2 mm/min at room temperature (23±2 ℃) and atmospheric conditions (relative humidity of 50±5%).

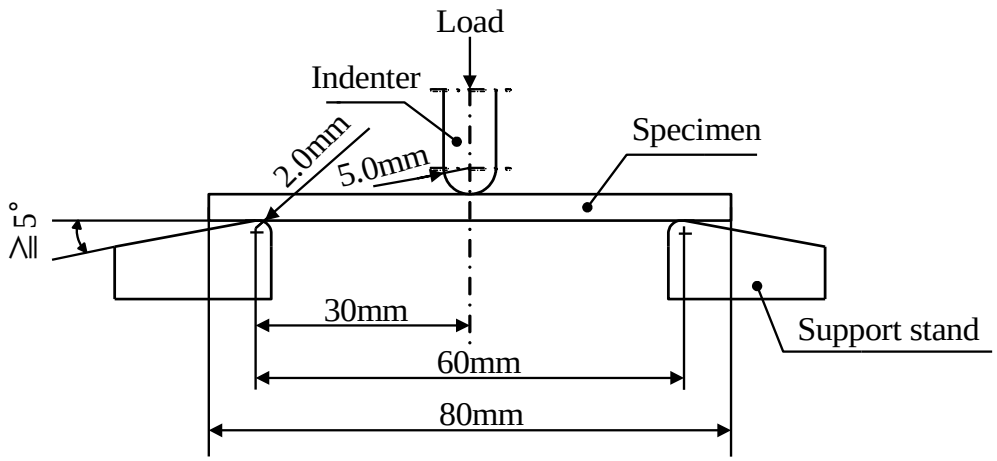

Fig. 2-12 Schematic diagram of the bending test.

Also, the bending strength and bending strain were calculated by using equation 2-4, and equation 2-5, respectively.

$$\sigma = \frac{3FL}{2bh^2} \quad (2\text{-}4)$$

$$\varepsilon = \frac{6hS}{L^2} \quad (2\text{-}5)$$

where, F – the load (N);

L – the fulcrum distance (mm);

b – the width of the specimen (mm);

h – the thickness of the specimen (mm);

S – the deflection (mm).

2.3.4 Impact test

The impact properties of the MWCNT/PC composites were tested by a pendulum impact tester (Shangai jiming measuring equipment Co., Ltd, China, shown in Fig. 2-13). The specimens were rectangular shape specimens (JIS K 7171 1(1/2), Fig. 2-7), and a 2 mm deep standard V-notch was carved on each sample (Fig. 2-14). The maximum impact energy was set to be 7.5 J and the impact speed was 3.5 m/s.

Fig. 2-13 Pendulum impact tester.

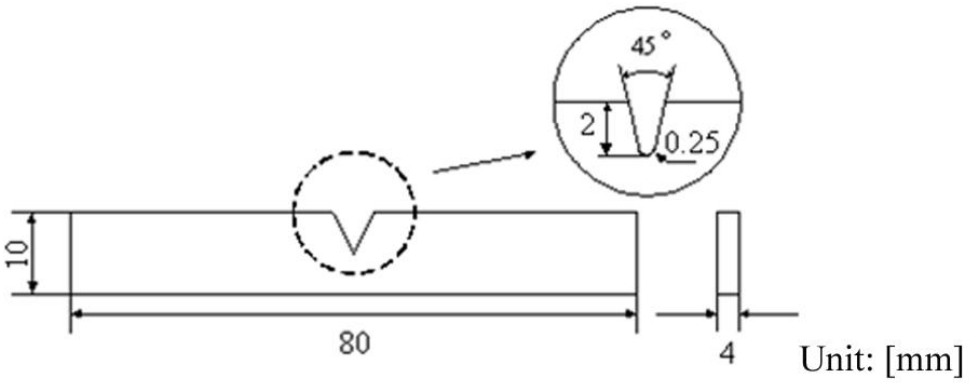

Fig. 2-14 Rectangle shaped specimen with a V-notch for the impact test.

2.3.5 Microhardness and its distribution test

Microhardness measurements were performed using a manual turret microhardness tester (HMV-2000, Shimadzu Co., Ltd, Kyoto, Japan) to determine the surface microhardness and the microhardness distribution. The microhardness tester consisted of a computer display and a Vickers square-based pyramidal diamond (with an angle of 136 ° between the opposite faces). The specimen used was the dumbbell-shaped specimen. Moreover, for the microhardness distribution measurement, a specimen was

cut from the center line of the rectangular specimen with a width of 10 mm (Fig. 2-15) and then the surface to be measured was polished and buffed. The measurements were carried out with a load of 10 gf for the recommended load-holding time of 15 s (JIS B 7774). Continuous measurements on the specimens were made at equally spaced (50 μm) points. The microhardness (H_V) was calculated with the following equation:

$$H_V = \frac{2F\sin(136°/2)}{d^2} \qquad (2\text{-}6)$$

where, F – the force applied to the diamond in kilograms-force (gf);

d – the average length of the diagonal left by the indenter in millimeters (μm).

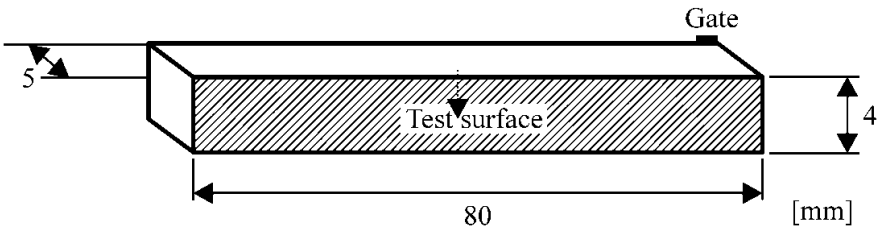

Fig. 2-15 Schematic diagram of rectangular specimen for the microhardness test.

On the other hand, for the rolled MWCNT/PLA composites, the specimen used was the dumbbell-shaped specimen, and the microhardness distribution was determined by the microhardness of the middle part in the longitudinal sections (Fig. 2-16). The measurements were also carried out with a load of 10 gf for the recommended load-holding time of 15 s (JIS B 7774). Continuous measurements on the specimens were made at equally spaced (50 μm) points. The microhardness (H_V) was calculated with the equation 2-6.

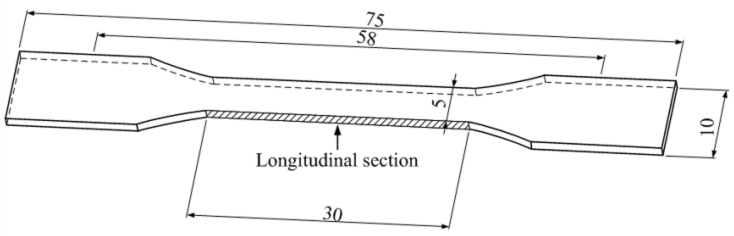

Fig. 2-16 Schematic diagram for the microhardness distribution test.

2.3.6 Electrical resistivity and its distribution

The electrical resistivities (i.e., surface resistivity and volume resistivity) were determined by using different shaped specimens. The specimens were the rectangle shaped specimen (Fig. 2-7) and flat shaped specimen (Fig. 2-8). A double loop resistance meter (UPMCP-HT450, Mitsubishi Chemical Co., Ltd, Japan) was used for the measurement of electrical resistivity in the range of 10^4–10^{14} Ω/sq, and the measurement principle was given in Fig. 2-17. The surface resistivity and volume resistivity were obtained according the 2-7 and 2-8 equations, respectively.

$$\rho s = R \times RCF\,(S) \qquad (2\text{-}7)$$

$$\rho s = R \times RCF\,(V) \times 1/t \qquad (2\text{-}8)$$

where, R – the resistivity;

$RCF(S)$ – the amendatory coefficient of the surface resistivity;

$RCF(V)$ – the amendatory coefficient of the volume resistivity;

t –the thickness of the specimen (cm).

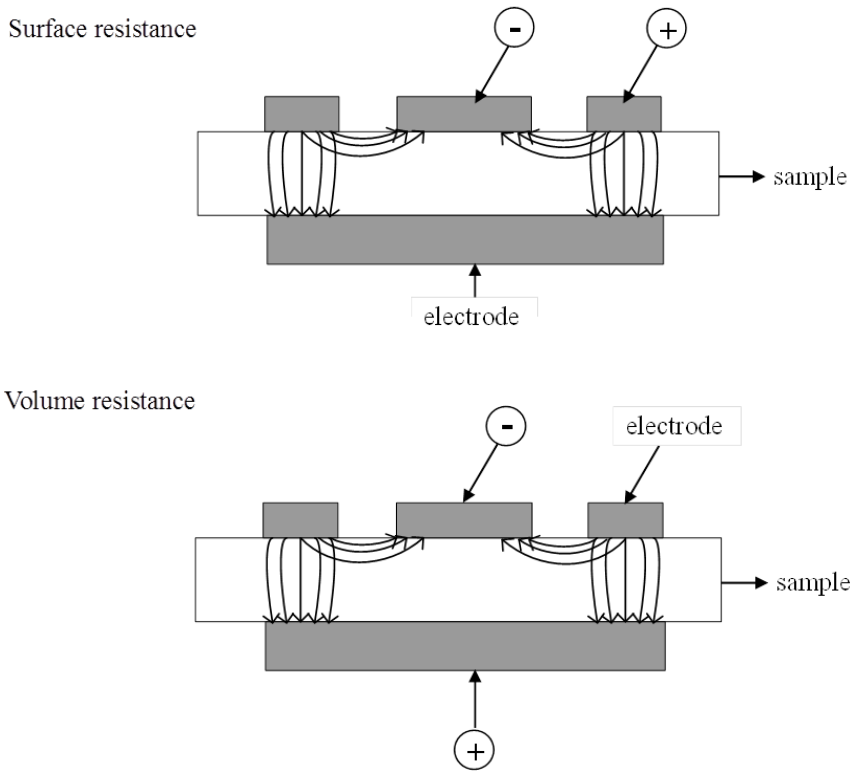

Fig. 2-17 The principle of measurement for high resistance meter.

Moreover, a four-probe resistivity tester (SDY-4, Guangzhou Semiconductor Material Academy Co., Ltd., China) was employed for measuring the electrical resistivity below 10^4 Ω/sq according to "Four Point Probes (FPP) technique" [17]. To ensure the reproducibility of the result, the measurement of the electrical resistivity of each specimen was repeated more than five times and the average value was quoted as the electrical resistivity of the composite specimen. The measurement principle is shown in Fig. 2-18.

The electrical conductivity of the sample was obtained according the following equation:

$$R_{\square} = \frac{V}{I} \times F(D/S) \times F(W/S) \times Fsp \ (\Omega/\square) \qquad (2\text{-}9)$$

where, V – the voltage (mV);

I – the current (mA);

D – the diameter of the specimen (cm);

S – the average distance of the probes (cm);

W – the thickness of the specimen (cm);

F(D/S) – the amendatory coefficient of the diameter of the pallets;

F(W/S) – the amendatory coefficient of the thickness of the pallets;

Fsp – the amendatory coefficient of the space between the probes, which is confirmed as 1.000.

Furthermore, the distributions of electrical resistivity were measured by using double loop resistance meter and four-probe resistivity tester according to different electrical resistivity. The surfaces of composite specimens to be tested were repeatedly ground in the same direction using the different type sandpapers (e.g., #240, #600, #800, #1000, etc.), and the electrical resistivity of each ground specimen was measured to examine the distribution of electrical resistivity from the surface to the core. The grinding load was kept at 2.5 kg and the grinding distance was fixed at approximately 250 mm (shown in Fig. 2-19).

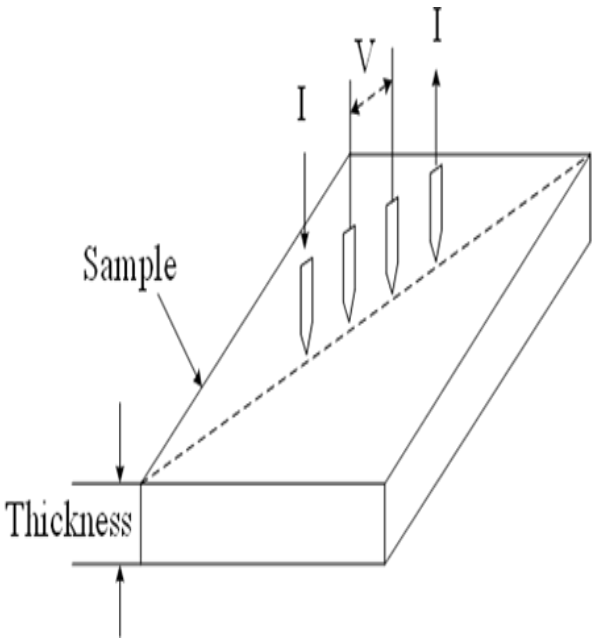

Fig. 2-18 The principle of measurement for four-probe resistivity tester.

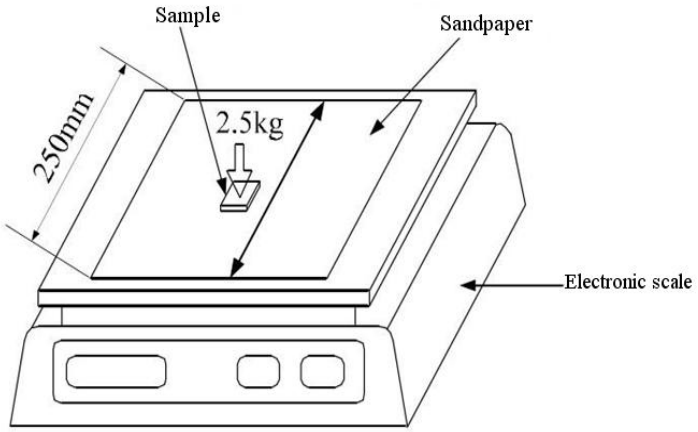

Fig. 2-19 The grinding method of the composite specimen.

2.3.7 X-ray diffraction (XRD)

The molecular orientation of the rolled PLA was determined by X-ray diffraction (XRD). The XRD patterns of PLA were recorded using Panalytical X´Pert Pro (Cambridge, UK）with nickel-filtered Cu Kα radiation (λ=0.15418 nm, XRD-6000, Shimadzu Co., Kyoto, Ltd.), operated at a generator voltage of 45 kV and a tube current

of 40 mA. The specimen used was the dumbbell-shaped sample. The scattering angle was in the range of 2θ=5–50 ° at a scan speed of 2.13 °/min. To ensure accuracy and repeatability, XRD investigations of each specimen groups were repeated three times. The molecular orientation was calculated by the following equation [18].

$$H\,[\%] = [(180 - W) / 180] \times 100\% \qquad (2\text{-}10)$$

where, W – the half-width of the diffraction peak.

2.3.8 Thermogravimetric analysis (TGA)

Thermogravimetric analysis (TGA) was performed on a thermal analyzer (DTG-60, Shimadzu Co., Ltd, Kyoto, Japan) by recording the weight loss as a function of temperature. And the derivative thermogravimetric analysis (DTG) and the differential thermal analysis (DTA) were also determined. Experiments were performed at a linear heating rate of 10 ℃/min within the temperature range of 30–800 ℃ in a steady stream of nitrogen with a flow rate of 50 mL/min.

2.3.9 Differential scanning calorimetry (DSC)

Differential scanning calorimetry (DSC) was performed using a DSC instrument (X-DSC7000, SII Nano Technology Inc., Tokyo, Japan, Fig. 2-20). The specimens (approximately 10 mg) for the test were cut from the cross-section of the middle part of the dumbbell-shaped specimens in the whole cross-sectional direction, and were scanned from 30 ℃ to 200 ℃ at a scan rate of 10 ℃/min under a nitrogen flow of 50 mL/min. Only the heating process was carried out to investigate the effect of the rolling ratio on the crystallization behavior of the rolled PLA. The DSC result was obtained from by three measurements of each specimen group. Again, the degree of crystallization χ_c of PLA was determined from the DSC heating traces by the following equation:

$$\chi_c = [(\Delta H_m - \Delta H_c) / \Delta H_m^{\,0}] \times 100\% \qquad (2\text{-}11)$$

where, ΔH_m – the melting enthalpy during the heating process (J/g);

ΔH_c – the enthalpy of crystallization (J/g);

$\Delta H_m^{\ 0}$ – the enthalpy for 100% crystallization of PLA, which is approximately 93.6 J/g [19].

Fig. 2-20 DSC instrument.

2.3.10 Density determination

A water displacement method (JIS K7112, method A) was employed to measure the density of the rolled PLA and composites by using an electronic gravity meter (SD-200L, Alfa Mirage Co., Ltd., Osaka, Japan). The measurements were performed on the dumbbell-shaped specimens at room temperature (23±2 ℃), and the water used was purified. The density of PLA was calculated by equation (2-12).

$$\rho = (m_{S,A} \times \rho_{IL}) / (m_{S,A} - m_{S,IL}) \qquad (2\text{-}12)$$

where, $m_{S,A}$ – the quality of PLA in the air (g);

$m_{S,IL}$ – the quality of PLA in the water (g);

ρ_{IL} – the density of PLA in the water (g/cm^3).

Moreover, the degree of crystallization χ_c of PLA was also determined by the density using the following equation.

$$\chi_c = [(\rho_{PLA} - \rho_a) / (\rho_c - \rho_a)] \times 100\% \qquad (2\text{-}13)$$

where, ρ_{PLA} – the actual density of the PLA (g/ml);

ρ_a – the density of amorphous PLA, which is 1.248 g/ml;

ρ_c– the density of 100% crystalline PLA, which is 1.290 g/ml, which are reported by Nampoothiri et al. [20] and Wei et al. [21].

Besides, the actual density of the PLA (ρ_{PLA}) was calculated by equation (2-14).

$$\rho_{PLA} = m_A(1 - w) / [v - (m_A \times w) / \rho_{CNT}] \quad (2\text{-}14)$$

where, m_A – the quality of PLA in the air (g);

w – the MWCNT content (wt.%);

v – the volume of the measured specimen (cm^3);

ρ_{CNT}– the actual MWCNT density (g/cm^3).

The actual density of MWCNT was also measured by using density method. Because PLA is a crystalline polymer, the actual MWCNT density can't be obtained by measuring the MWCNT/PLA composite specimen. Thus the density of MWCNT/PC composites was measured and the actual density of MWCNT is 1.8574 g/cm^3.

2.3.11 Optical microscope (OPM)

The microstructure was investigated by a polarized optical microscopy (OPM, Eclipse model ME600D, Nikon, Tokyo, Japan). To achieve visibility, the composite specimens (Fig. 2-7) were cut into 5 μm slices in longitudinal sections by a microtome (RM2145, Leica Microsystems, Tokyo, Japan). Moreover, for the crystalline polymer, to investigate the variation of the crystal structures, the middle part of dumbbell shaped specimens (Fig. 2-6) was cut into 10 μm slices in longitudinal sections by the microtome; but for the composites, the specimen was cut to 2–5 μm to achieve visibility.

2.3.12 Scanning electron microscope (SEM)

The microstructures of the tensile fractured surface were observed by scanning electron microscope (SEM, S-4300, Hitachi Co., Ltd., Tokyo, Japan). Dispersion of MWCNTs in PC and interfacial adhesion between carbon materials and polymer matrix

were examined. Before examination, the fractured surfaces were sputter-coated with gold using an ion sputtering apparatus (E-1030, Hitachi Science Systems Co., Ltd., Yokohama, Japan) to avoid charging. For the MWCNT/PC composites, the fractured surfaces were observed under an acceleration voltage of 15 kV and electric current of 10 μA at room temperature of 23±2 ℃; and for the MWCNT/PLA composites, the acceleration voltage was 3 kV.

References

[1] K. Enomoto, T. Yasuhara, K. Kato and N. Ohtake. Injection Molding of Polystyrene Matrix Composites Filled with Vapor Grown Carbon Fiber (in Japanese). Transactions of the Japan Society of Mechanical Engineers Series A 69 (2003) 1145-1152.

[2] T. Fukuyo and S. Iinou. Fabrication and Application of Vapor Grown Carbon Fiber (in Japanese). TANSO 243 (2010) 130-134.

[3] S. Shinagawa. Electromagnetic Interference Shielding with Conductive Papers. Journal of the Japanese Technical Association of the Pulp and Paper Industry 42 (1988) 131-137.

[4] B. Hornbostela, P. Potschke, J. Kotza and S. Roth. Mechanical Properties of Triple Composites of Polycarbonate, Single-walled Carbon Nanotubes and Carbon Fibres. Physica E 40 (2008) 2434-2439.

[5] R. Ramasubramaniam, J. Chen and H. Liu. Homogeneous Carbon Nanotube/ Polymer Composites for Electrical Applications. Appl. Phys. Lett. 83 (2003) 2928-2930.

[6] R. Andrews and M.C. Weisenberger. Carbon Nanotube Polymer Composites. Current Opinion in Solid State and Materials Science 8 (2004) 31-37.

[7] A. Bachtold, P. Hadley, T. Nakanishi and C. Dekker. Logic Circuits with Carbon Nanotube Transistors. Science 294 (2001) 1317-1320.

[8] L.A. Nagahara, I. Amlani, J. Lewenstein and R.K. Tsui. Directed Placement of Suspended Carbon Nanotubes for Nanometer-Scale Assembly. Appl. Phys. Lett. 80 (2002) 3826-3828.

[9] Polycarbonate. https://en.wikipedia.org/wiki/Polycarbonate, retrieved in September 30th, 2015.

[10] D.G. Legrand and J.T. Bendler. Handbook of Polycarbonate Science and Technology, 1999.

[11] O.S. Carneiro, J.A. Covas, C.A. Bernardo, G. Caldeira, F.W.J. Van Hattuma, J.M. Ting, R.L. Alig and M.L. Lake. Production and Assessment of Polycarbonate Composites Reinforced with Vapour-Grown Carbon Fibres. Composites Science and Technology 58 (1998) 401-407.

[12] J.A. King, W.A. Pisani, D.R. Klimek-McDonald, W.F. Perger and G.M. Odegard. Shielding Effectiveness of Carbon-Filled Polycarbonate Composites. Journal of Applied Polymer Science 132 (2015), DOI: 10.1002/app. 42719.

[13] Production Process for Polylactic acid (PLA). http://www.hitachi.com/businesses/ infrastructure/product_site/ip/process/pla.html, Retrieved in September 30th, 2015.

[14] M. Jonoobi, J. Harun, A.P. Mathew and K. Oksman. Mechanical Properties of Cellulose Nanofiber (CNF) Reinforced Polylactic acid (PLA) Prepared by Twin Screw Extrusion. Compos. Sci. Technol. 70 (2010) 1742-1747.

[15] D. Garlotta. A Literature Review of Poly(lactic acid). Journal of Polymers and the Environment 9 (2001) 63-84.

[16] http://www.tainstruments.com/product.aspx?id=24&n=1&siteid=11, retrieved in September 30th, 2015.

[17] F.M. Smits. Measurement of Sheet Resistivities with the Four-Point Probe. Bell System Technical Journal 37 (1958) 711-718.

[18] M. Kakudo and Kasai N. X-ray Diffraction by Macromolecules. Maruzen, Japan, 1968, pp. 187-200.

[19] B. Kalb and A.J. Pennings. General Crystallization Behavior of Poly(l-lactic acid). Polymer 21 (1980) 607-612.

[20] K.M. Nampoothiri, N.R. Nair and R.P. John. An Overview of the Recent Developments in Polylactide (PLA) Research. Bioresource Technol. 101 (2010) 8493-8501.

[21] G. Wei and P.X. Ma. Structure and Properties of Nano-Hydroxyapatite/Polymer Composite Scaffolds for Bone Tissue Engineering. Biomaterials 25 (2004) 4749-4757.

Chapter 3 Preparation and Evaluation the Mechanical Properties of Carbon Nanotube-Reinforced Polycarbonate Conductive Composites

3.1 Introduction

As mentioned in Chapter 1, the low electrical conductivity of polymers limits their applications in related fields. Therefore, the development of novel CPCs with high electrical conductivity and good mechanical properties has become an attractive new subject in materials science.

Although several methods are available to impart electrical conductivity to polymers, the simplest and easiest way is to directly incorporate conductive fillers into the polymer matrices by melt mixing using different preparation methods such as extrusion molding and injection molding. However, because of the conductive filler, i.e., CNTs, having some disadvantageous, e.g., inherent large specific surface area [1], higher surface activation energy, and ease in forming agglomerations [2, 3]; there is still a big challenge in achieving the desired dispersibility and compatibility of CNTs in a polymer matrix. In addition, the relatively weak interfacial interaction between CNTs and many polymers has prevented its application in the electrical components that demand high mechanical strength and stability. Therefore, for the preparation of CNT-reinforced composites, the homogeneous dispersion of CNTs in a polymer matrix and the strong interfacial interaction between CNTs and the polymer are two major challenges that must be overcome to attain excellent mechanical and electrical properties.

Nowadays, CNT-reinforced composites are commonly prepared by laboratory-scale melt mixing of CNTs in thermoplastic polymers using extrusion molding. Most of the related studies have been carried out to clarify the influence of extrusion conditions on

CNT dispersion or the mechanical and electrical properties of the prepared composites [4-8]. Nevertheless, although a few related researchers have reported on the effects of injection conditions on the dispersion of CNTs and the electrical properties of CNT-reinforced composites [9-11], there is scarcely any report on the effect of injection conditions on thermal, mechanical, and dynamic mechanical properties.

According to a review of the literature, it is essential to optimize the conditions in the two common molding processes, i.e., extrusion molding and injection molding, for preparing CNT-reinforced composites to obtain homogeneous dispersion of CNTs as well as better thermal and higher mechanical properties [12]. Moreover, for industrial application of CNT/polymer composites, a two-step dispersion strategy, i.e., extrusion process followed by injection molding, is the preferred method for preparing CNT-reinforced composites. This method is very efficient in minimizing the formation of CNT agglomerations, enhancing the dispersion of CNTs, and improving the mechanical properties of polymer matrices.

In this work, the MWCNT/PC composites with different MWCNT contents (0–10 wt.%) were prepared by using the two-step dispersion strategy (the twin-screw extruding and injection molding processes). The effects of MWCNT content and injection conditions on the thermal, mechanical, and dynamic mechanical properties of the prepared composites were then systematically assessed by various characterization techniques. The effect of injection conditions on the mechanical reinforcement of the prepared composites was also evaluated. The dynamic mechanical behavior was investigated by dynamic mechanical analysis (DMA). Moreover, the MWCNT dispersibility, orientation, skin-core microstructure, and morphology were further characterized by scanning electron microscopy (SEM).

3.2 Experimental

Preparation of MWCNT/PC composites

To improve the dispersion of MWCNTs, a two-step dispersion strategy (i.e.,

twin-screw extrusion and injection molding processes) was adopted. Prior to the preparation of MWCNT/PC master batches, both MWCNTs and PC were dried at 120 ℃ for more than 5 h. The compounding process of master batches began with preparation by a twin-screw extruder (shown in Fig. 2-4) at an extrusion temperature of 290 ℃ and a rotational speed of 100 rpm. For the complete compounding of master batches, PC pellets and powdery MWCNTs (at a content of 0, 1, 2.5, 5, and 10 wt.%) were premixed, and then the mixed MWCNT/PC materials were fed into the hopper of the extruder. All master batches were cooled in a water bath and pelletized after the extrusion process.

Thereafter, the MWCNT/PC master batches were dried again, and the injection molding was performed using an injection molding machine (shown in Fig. 2-5). The injection speeds were set to 10, 40, and 80 mm/s, and the injection temperatures were 280 ℃, 305 ℃, and 330 ℃, respectively. The mold temperature was 80 ℃. Five different injection-molded specimens were produced under different injection conditions to evaluate the influence of injection conditions on the properties of the prepared MWCNT/PC composites. The injection-molded products were dumbbell-shaped specimens (JIS K 7113 1(1/2)) with dimensions of 75 mm × 10 mm × 2 mm (Fig. 2-6) and rectangular specimens (JIS K 7171 1(1/2)) with dimensions of 80 mm × 10 mm × 4 mm (Fig. 2-7).

3.3 Results and discussions

3.3.1 Thermal stability

The thermal decomposition of CPCs is of fundamental importance in the study of the effect of MWCNTs on the polymers' thermal properties. Besides, MWCNT as a reinforced filler has been reported to enhance the thermal stability of the host polymer matrices [13, 14]. The thermal stability of pure PC, pure MWCNTs, and the MWCNT/PC composites were assessed by TGA and DTG. Fig. 3-1 shows the obtained

TGA curves of the composites with different MWCNT contents prepared at an injection temperature of 80 ℃ and an injection speed of 80 mm/s. The TGA curves of pure PC and pure MWCNTs are also included in the same figure for comparison. Evidently, both pure PC and the composites showed single-stage decomposition. In addition, once the temperature reached a certain value (referred to as onset decomposition temperature hereafter), rapid mass loss began, indicating that thermal decomposition was occurring dramatically. The mass then settled at a steady value (referred to as residue mass hereafter) when the temperature rose to another value (referred to as closure decomposition temperature hereafter). It was further found that both the onset and closure temperatures and the residue mass were different for the composites with different MWCNT contents. For pure PC, the onset and closure temperatures were around 320 and 410 ℃, respectively, and the residue mass was completely decomposed (i.e., 0% of residue mass), whereas for the composite with just 1 wt.% MWCNTs, the two temperatures rose to around 420 ℃ and 520 ℃, respectively, an increase of more than 100 ℃, and the residue mass remained at around 20%. It was also determined that with the increase in MWCNT content, the onset and closure temperatures decreased but the residue mass increased slightly; for example, for the composite with 10 wt.% MWCNTs, its onset temperature and residue mass were approximately 380 ℃ and 25%, respectively, which are 40 ℃ lower and 5% higher, respectively, than those for the composite with 1 wt.% MWCNTs. Similar behavior was also reported by Guo′s group, and it was considered that the decomposition of PC at $T_{5\%}$ (onset decomposition temperature of 5% mass loss) might have been related to the random chain scission of PC immobile chains, and the decrease in molecular weight of PC during melt mixing with high MWCNT content [15]. Overall, the incorporation of MWCNTs at a proper proportion could considerably improve the thermal stability of PC. Similar behavior of CNTs as a reinforced filler to improve the thermal stability of the polymer matrix was reported by Yuen and Mkhabela [16, 17].

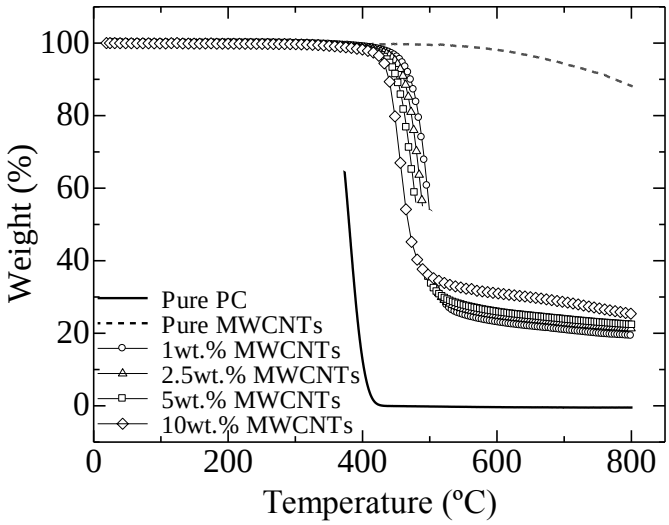

Fig. 3-1 TGA curves of pure PC, pure MWCNTs, and the MWCNT/PC composites prepared at an injection temperature of 280 ℃ and an injection speed of 80 mm/s.

To investigate in detail the effect of MWCNT content on the thermal stability of the MWCNT/PC composites, the onset decomposition temperatures $T_{5\%}$, $T_{10\%}$, $T_{20\%}$, and $T_{50\%}$ at the respective weight losses of 5, 10, 20, and 50%, and the residue weight fraction at 800 ℃ are obtained from the data of Fig. 3-1; and the results are summarized in Table 3-1. Evidently, the onset temperatures $T_{5\%}$, $T_{10\%}$, $T_{20\%}$, and $T_{50\%}$ of all the MWCNT/PC composites were higher than those of pure PC, and the residue weight fractions at 800 ℃ of all the composites were over 19%, while the pure PC specimen was decomposed completely to 0% of the residue weight, indicating the incorporation of MWCNTs considerably improved the thermal stability of PC. Similar behavior of other polymers has also been reported [18]. However, it was also noticed that the onset temperature and the residue weight fractions of the composites depended on the MWCNT content: as the MWCNT content increased, the onset temperature tended to drop, whereas the residue weight fraction tended to rise. The residue weight was considered to consist of dominant contribution from the residues of elemental carbon not only from MWCNTs but also from PC since its decomposition at high temperature produced much elemental carbon, which was adsorbed on the MWCNTs.

Table 3-1 Thermal stability data of pure PC, pure MWCNTs, and the MWCNT/PC composites ($T_{n\%}$ denotes the onset decomposition temperature of 5%, 10%, 20%, and 50% weight loss).

Sample	$T_{5\%}$(℃)	$T_{10\%}$ (℃)	$T_{20\%}$ (℃)	$T_{50\%}$ (℃)	Residue weight at 800℃ (%)
PC	345.76	354.99	364.41	379.94	0
MWCNT	688.08	774.98	>800	>800	88.07
1wt.% MWCNT/PC	458.00	471.63	483.38	501.64	19.30
2.5wt.% MWCNT/PC	449.04	461.72	472.94	492.12	21.30
5wt.% MWCNT/PC	438.99	451.74	462.73	483.33	22.26
10wt.% MWCNT/PC	430.80	439.56	448.12	467.77	25.31

To study the rate of weight loss, the DTG curves of pure PC, pure MWCNTs, and MWCNT/PC composites were plotted, and are shown in Fig. 3-2. The DTG peaks of the composites became smaller and smaller as the MWCNT content increased, and they were all lower than the DTG peak of pure PC. Moreover, the temperature at which the DTG peak appeared was slightly decreased with the increase in MWCNT content, demonstrating that the incorporation of MWCNTs could slow down the decomposition of PC, hence resulting in improved thermal stability of PC. The enhanced thermal stability might have contributed to the homogeneous dispersion of MWCNTs in the PC matrix and the improvement in compatibility between MWCNTs and PC. It was considered that C_{60} retarded the thermal stability of pure PC owing to interactions between C_{60} and macroradicals generated during decomposition [13].

Overall, these results demonstrated that MWCNTs are favorable for improving the thermal properties of the MWCNT/PC composites, and enhanced thermal stability of the composites might testify to homogeneous dispersion of MWCNTs in the PC matrix. However, excessive MWCNTs would lead to the quick decomposition of the

MWCNT/PC composites, eventually resulting in the slight attenuation of the decomposition temperature. In addition, these results confirmed that the compatibility between MWCNTs and PC was very good.

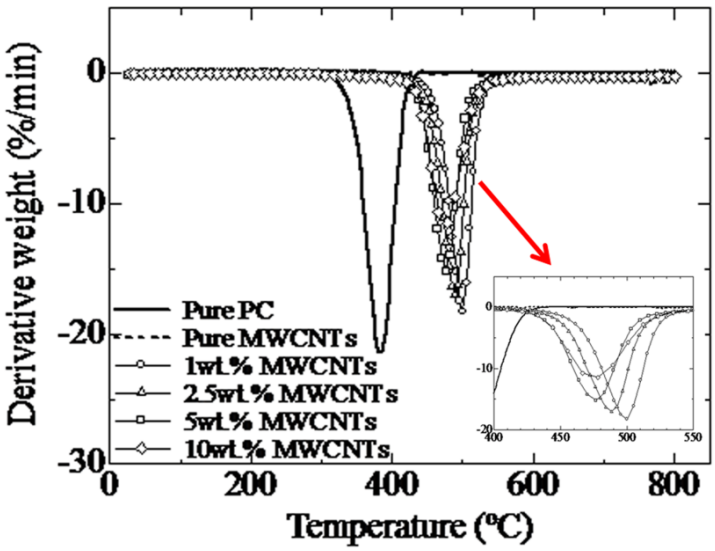

Fig. 3-2 DTG curves of pure PC, pure MWCNTs, and the MWCNT/PC composites prepared at an injection temperature of 280 ℃ and an injection speed of 80 mm/s.

3.3.2 Mechanical properties

(a) Tensile properties

Effect of MWCNT content

The tensile tests were performed to examine the effects of MWCNT content on the mechanical properties of the MWCNT/PC composites and the results are shown in Fig. 3-3 (prepared at the injection temperature of 305 ℃ and injection speed of 10 mm/s). The pure PC specimen showed that when its tensile strength reached 58 MPa, the yield phenomenon occurred, and the specimen was fractured at the strain of 160%. This is a typical characteristic of ductile materials. When MWCNTs were added, although the tensile strength and the number of incipient elastic modules were increased, the crack strains were below 20%, and the composite specimens were fractured before the yield

phenomenon occurred. That is to say, the addition of MWCNTs could slightly improve the strength of the polymer itself, but it also result in greater brittleness of the MWCNT/PC composites. It was considered that the increase of MWCNT content beyond a certain point (i.e., 5 wt.%) may cause a defect-inducing agglomeration of MWCNT in the PC matrix and increase brittleness.

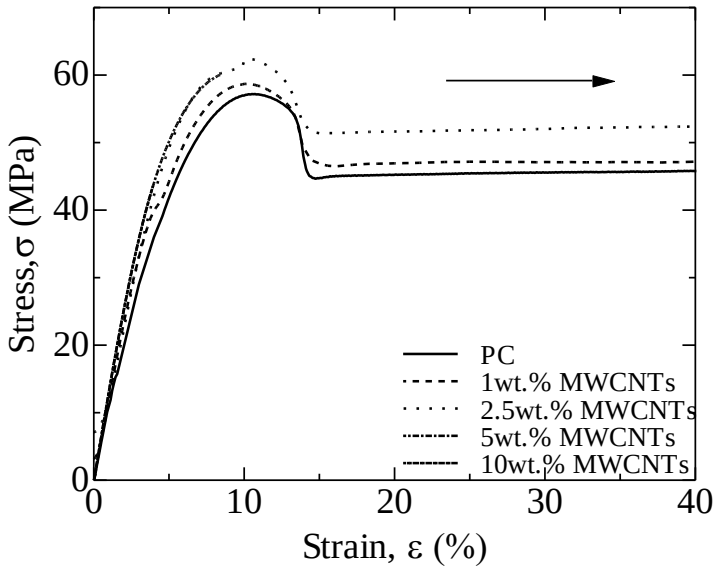

Fig. 3-3 Strain-stress curves of the MWCNT/PC composites prepared at an injection temperature of 305 ℃ and injection speed of 10 mm/s.

The morphology of pure PC and the MWCNT/PC composites was examined by SEM. Fig. 3-4 displays the SEM micrographs of the fractured surfaces of pure PC and the composites with 5 wt.% MWCNTs. The fractured surfaces of pure PC showed typical ductile fracture in Fig. 3-4 (a). There was a homogeneous dispersion of the MWCNTs in the PC matrix for the composites (Fig. 3-4 (b)). No agglomeration of MWCNTs was observed on the composite specimen fractured surface for the image at high magnification, which provided evidence of satisfactory compatibility and interface interaction between the MWCNTs and host PC matrix. In addition, plastic deformation was not observed on the fractured surface, namely, brittle fracture had occurred. This

might be because the introduction of MWCNT hindered the plastic deformation of PC. Overall, it was concluded that the MWCNT/PC composites with uniformly dispersed MWCNTs as fillers were successfully prepared by injection molding.

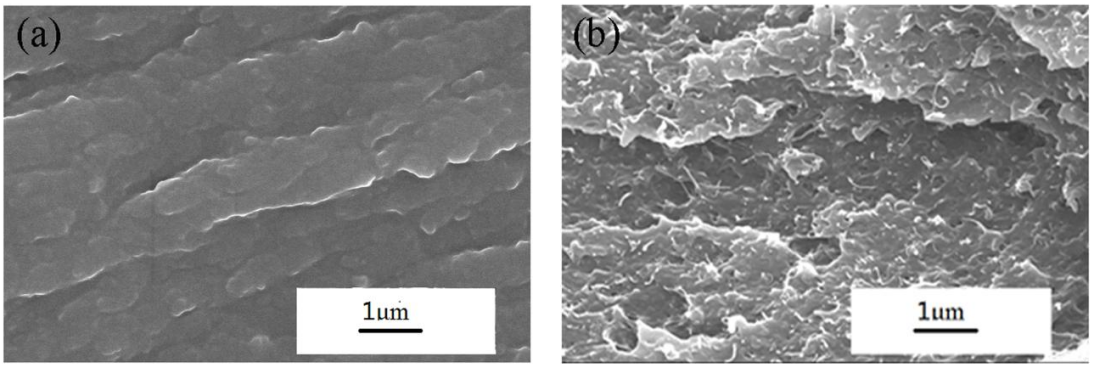

Fig. 3-4 SEM micrographs of tensile-fractured surfaces of (a) pure PC and (b) the MWCNT/PC composites with 5 wt.% MWCNTs.

Moreover, the tensile properties of pure PC and the MWCNT/PC composites were determined, and the results are plotted in Fig. 3-5. Irrespective of the injection conditions, the tensile strengths of the composites were basically at the same level as that of pure PC when the MWCNT content was less than 5 wt.% (above 55 MPa). On the other hand, once the MWCNT content reached 10 wt.%, the tensile strength decreased drastically by 23.94–38.22%, possibly because the dispersion of MWCNTs was deteriorated owing to agglomerations of MWCNTs in the PC matrix when the MWCNT content had reached beyond a certain level. It is evident that if MWCNTs were incorporated in PC, even at a small content of 1 wt.%, the fracture strains dropped significantly regardless of the injection conditions. Then, as the MWCNT content increased, the fracture strains decreased gradually. It is, however, worthy to note from Fig. 3-5 (c) that at a higher injection temperature of 330 ℃ with lower injection speed of 10 mm/s, the fracture strain of the composite with 1 wt.% MWCNTs reached 96.82%, which was 9 times the value for the composite with 10 wt.% MWCNTs. This meant that the injection conditions easily affected the fracture strain of the composites.

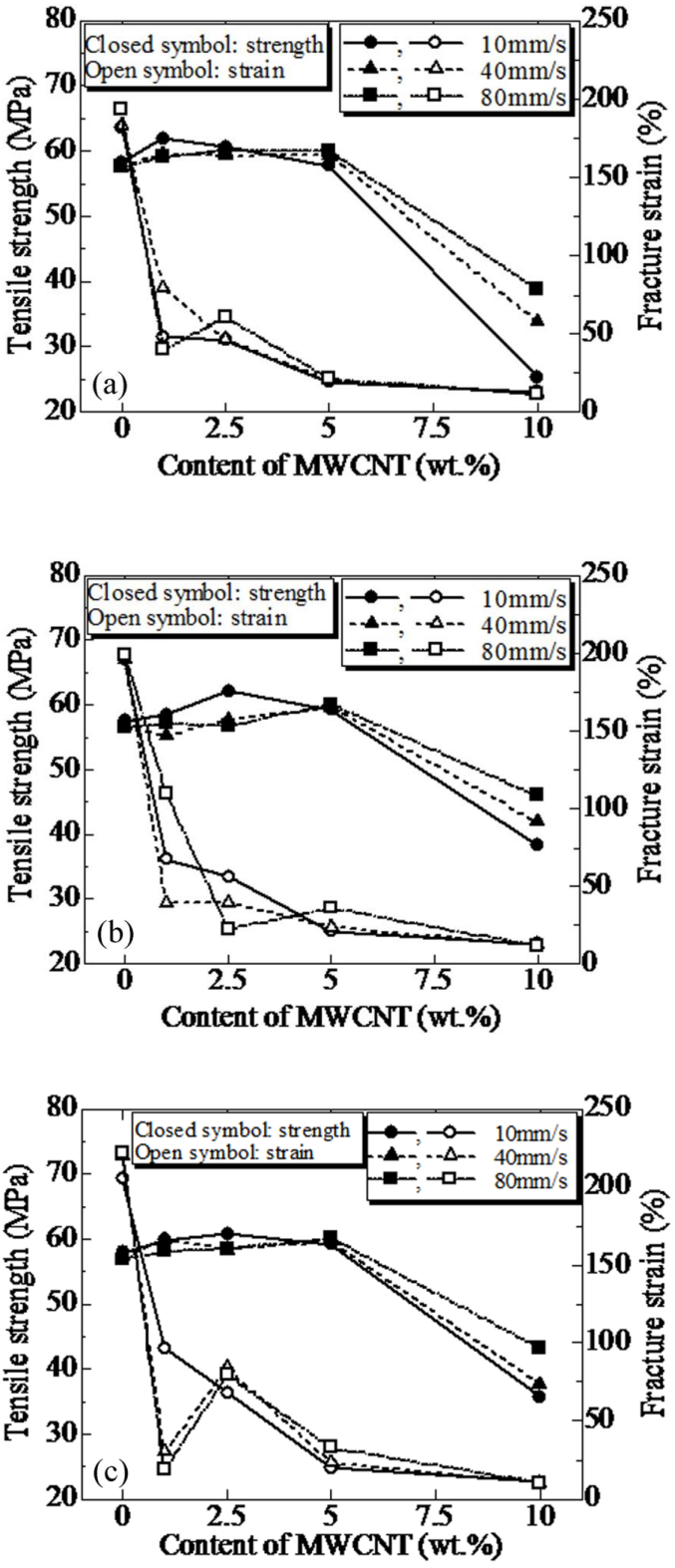

Fig. 3-5 Effect of MWCNT contents on tensile properties of pure PC and the MWCNT/PC composites prepared at injection temperatures of (a) 280 ℃, (b) 305 ℃, and (c) 330 ℃.

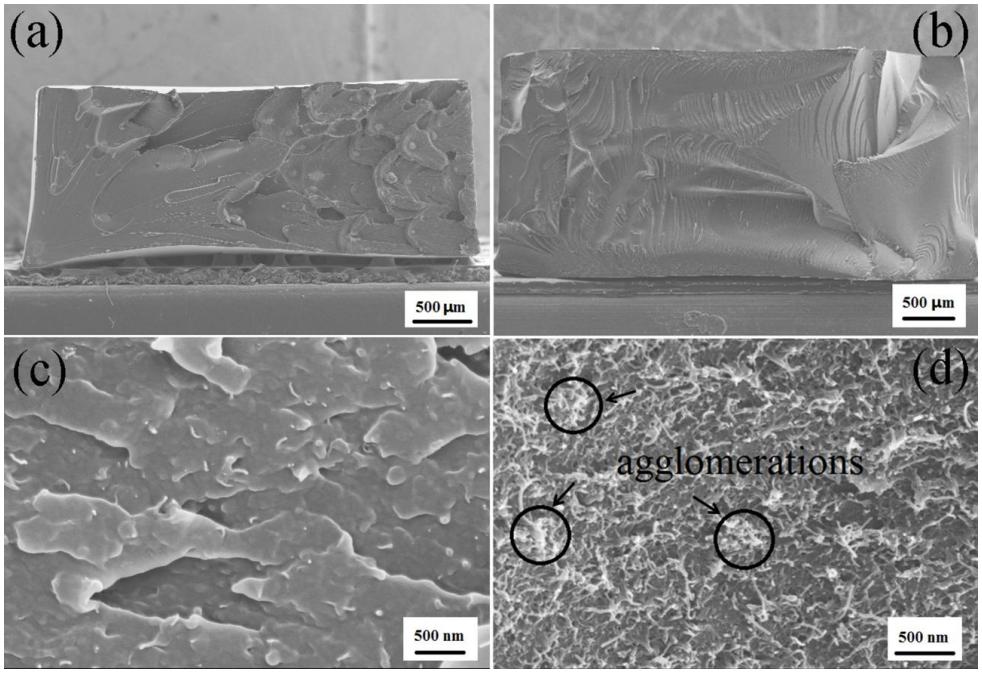

Fig. 3-6 SEM micrographs of tensile-fractured surfaces of MWCNT/PC composites with (a) 1 wt.% MWCNTs and (b) 10 wt.% MWCNTs; (c, d) high-magnification micrographs of (a) and (b), respectively. The composites were prepared at an injection temperature of 330 ℃ with an injection speed of 10 mm/s.

Generally, the tensile strain during the tensile test was partially transferred to MWCNTs embedded in the PC matrix under tensile stress, thus maintaining the tensile strength of PC. However, the incorporation of excessive MWCNTs would lead to MWCNT agglomeration, and the original excellent mechanical property of MWCNT could thus not be displayed. This might be the reason for the attenuation of tensile strength of the composite with 10 wt.% MWCNTs, and it was easy for the specimen to become brittle and fracture.

In view of the significant effect of the MWCNT content on their dispersion, which would affect the tensile properties, the distribution and dispersion of MWCNTs in the PC matrix were investigated by observing the tensile-fractured surfaces of the composites with different MWCNT contents via SEM. The typical SEM micrographs of composites with 1 wt.% and 10 wt.% MWCNTs are shown in Fig. 3-6.

Fig. 3-6 (a) shows that the entire fractured surface of the specimen with 1 wt.%

MWCNTs was uneven and its size became smaller than the original size (i.e., 5 mm × 2 mm), demonstrating that plastic deformation occurred during tensile testing. Moreover, Fig. 3-6 (c) shows that the MWCNTs were dispersed homogeneously without agglomeration, and the compatibility between MWCNTs and PC was reasonable without pulling out the MWCNTs, indicating that the tensile property of the composites with 1 wt.% MWCNTs was relatively strong. It was found from Fig. 3-6 (b) that the entire fractured surface of the composite with 10 wt.% MWCNTs was relatively smooth and its size was almost same as the original's, suggesting that brittle fracture occurred during tensile testing. The detailed microstructure of the fractured surface was further observed by an enlarging portion of the SEM image in Fig. 3-6 (b), shown as Fig. 3-6 (d). Obviously, a few minor agglomerations of MWCNTs (approximately 300–400 nm) formed in the preparation of the composite with 10 wt.% MWCNTs, implying that incorporation of excessive MWCNTs hindered the plastic deformation of PC, thereby attenuating the tensile properties.

Furthermore, it is from Fig. 3-5 known that when the MWCNT content was 1 wt.%, the effect of injection temperature on fracture strain was obvious; besides, as the MWCNT content increasing from 1 wt.% to 5 wt.%, the fracture strain greatly changed under the same injection condition. Therefore, the SEM micrographs of the tensile fractured surfaces of the 1 wt.% and 5 wt.% MWCNTs composites prepared at different injection conditions were contrasted again and are shown in Fig. 3-7. In Fig. 3-7 (b) and (d), MWCNTs were dispersed homogeneously and no agglomeration of MWCNTs was observed. The compatibility and interface interaction between MWCNTs and PC were reasonable since there was no MWCNT be pulled out. In addition, from observation of the whole cross section (Fig. 3-7 (a) and (c)), the specimen sizes were both smaller than the original size, it was considered that some plastic deformations occurred during tensile testing, indicating the tensile property of the 1 wt.% MWCNTs composites was relatively good. However, in Fig. 3-7 (e), there was a defect on the fractured surfaces. This defect was considered the cause of fracture during tensile testing, leading to a

distinct decrease of fracture strain. Moreover, even though the dispersibility of the MWCNTs in the PC matrix was sufficient, a few agglomerations of MWCNTs were still observed in Fig. 3-7 (f). Additionally, the specimen size did not change (Fig. 3-7 (e)), demonstrating the brittle fracture had occurred. It was inferred that the presence of more MWCNTs hindered plastic deformation of the PC, and the MWCNT agglomeration affected the interface interaction between MWCNT and PC, thereby attenuating the tensile property of the composites.

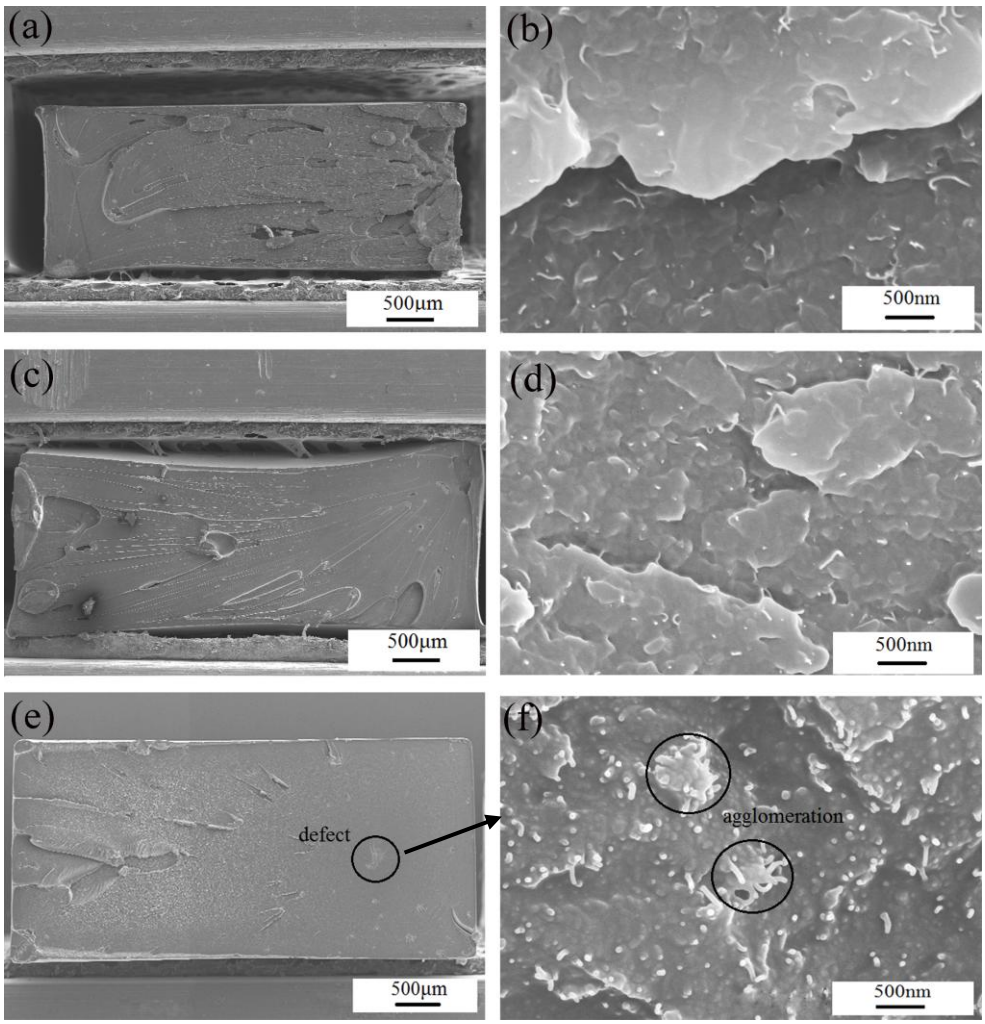

Fig. 3-7 SEM micrographs of the fractured surfaces of (a) 1 wt.% MWCNT/PC composites (330 ℃ and 10 mm/s), (c) 1 wt.% MWCNT/PC composites (280 ℃ and 10 mm/s), (e) 5 wt.% MWCNT/PC composites (280 ℃ and 10 mm/s). (b), (d) and (f) are large magnification micrographs of (a), (c) and (e), respectively.

Effects of injection speed and injection temperature

As discussed above, there was no noticeable effect of injection conditions on the tensile properties of all the composites, except the one with 10 wt.% MWCNTs. Therefore, the detailed investigation on the effect of injection conditions was performed only for the composite with 10 wt.% MWCNTs in this part. In Fig. 3-8 (a), regardless of the injection temperature, the tensile strength of this type of composite was enhanced by increasing the injection speed, whereas its fracture strain was affected very little by the injection speed. However, Fig. 3-8 (b) shows that both the tensile strength and the fracture strain reached their respective peaks at the same injection temperature of 305 ℃, although the effects on the fracture strain were very small compared with those on the tensile strength. It is, especially, worthy to note that as the injection speed was increased from 10 to 80 mm/s, the tensile strength was enhanced by 52.5% at an injection temperature of 280 ℃ (Fig. 3-8 (a)).

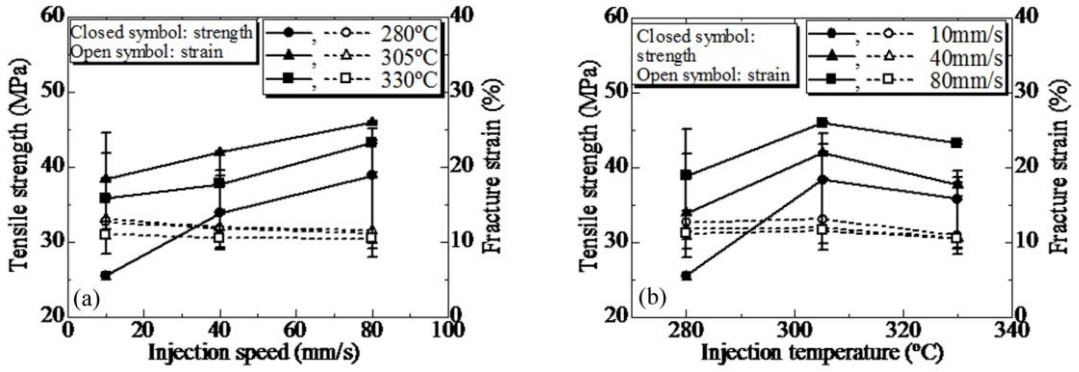

Fig. 3-8 Effects of injection conditions on tensile properties of MWCNT/PC composite with 10 wt.% MWCNTs.

A comparison of Fig. 3-8 (a) and (b) revealed that the tensile strength of the composite with 10 wt.% MWCNTs reached the maximum (approximately 45.9 MPa) at an injection temperature of 305 ℃ with an injection speed of 80 mm/s, and it was at the minimum at 280 ℃ with an injection speed of 10 mm/s. It was considered that the

injection temperature affected the viscosity and fluidity of the MWCNT/PC composite, and the higher injection speed made MWCNTs be subjected to a larger shear stress, resulting in the MWCNTs were more easily orientated in the flow direction of the polymer. Consequently, the different microstructures would lead to the variations of the mechanical properties through changing the injection conditions.

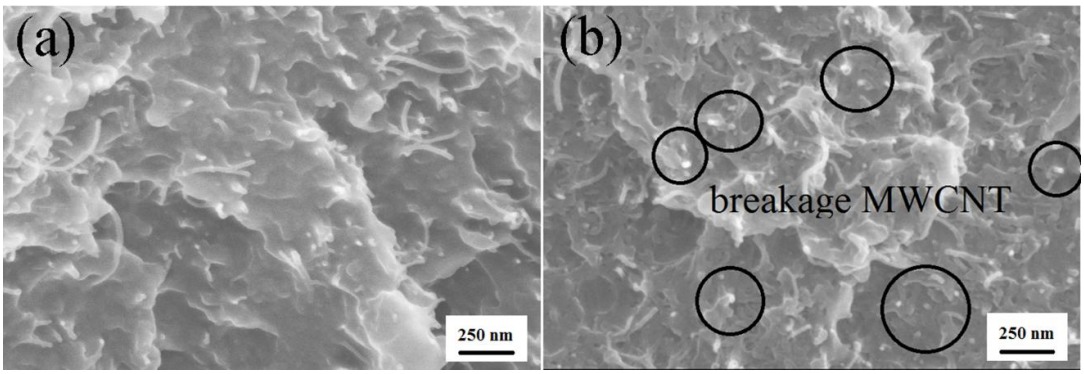

Fig. 3-9 SEM micrographs of tensile-fractured surfaces of MWCNT/PC composites with 10 wt.% MWCNTs prepared at (a) an injection temperature of 280 ℃ with an injection speed of 10 mm/s and (b) an injection temperature of 305 ℃ with an injection speed of 80 mm/s.

Moreover, to confirm the differences between the microstructures of the composites prepared under different injection conditions, SEM observations were carried out on the tensile-fractured surfaces of the composites with 10 wt.% MWCNTs prepared at different injection speeds and temperatures. Fig. 3-9 (a) and (b) show the SEM micrographs of the fractured surfaces of the specimen prepared at an injection temperature of 280 ℃ with an injection speed of 10 mm/s and the specimen prepared at an injection temperature of 305 ℃ with an injection speed of 80 mm/s, respectively. In Fig. 3-9 (a), some MWCNTs were pulled out, indicating that the MWCNTs could not strengthen the composite under these injection conditions. In contrast, a few minor white light dots are present in Fig. 3-9 (b), which represents the MWCNTs fractured during tensile testing. Therefore, it was confirmed that the injection conditions affected

the microstructures of the MWCNT/PC composites, resulting in the differences in tensile properties.

(b) Bending properties

It is well known that the bending property, as the same as tensile property, is the important parameters of the mechanical properties of a material, and the bending properties can reflect the interface strength of composites. Thus the bending properties of the composites at room temperature were investigated. Fig. 3-10 shows an example of the strain-stress curves of pure PC and the composites with different MWCNTs contents prepared at injection temperature of 330 ℃ with an injection speed of 10 mm/s. Paying the attention to the pure PC specimen shows that when its bending strength reached to approximately 90 MPa, the yield phenomenon happened, and the specimen was fractured at the strain of 26.7%. This was the typical characteristics of ductile materials. As a certain addition of MWCNTs (the MWCNT content ≤ 5 wt.%), although the bending strengths was increased, but the crack strains were decreased, and the composite samples were fractured before the occurrence of yielding phenomenon. However, when the content of MWCNTs was 10 wt.%, the bending strength and crack strain were evidently dropped.

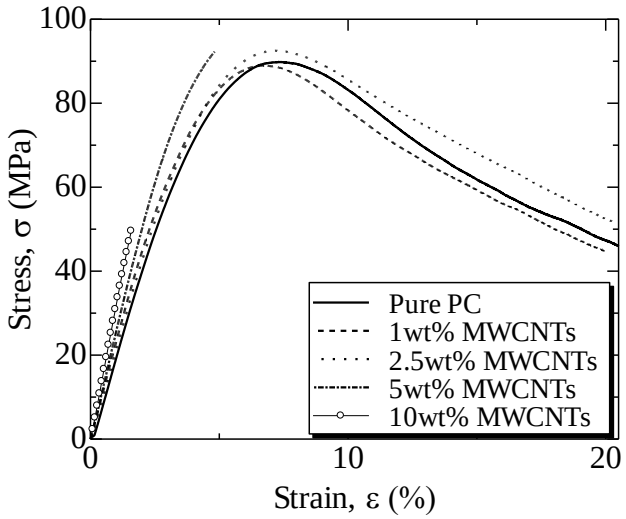

Fig. 3-10 Strain-stress curves of the composites prepared at an injection temperature of 330 ℃ with an injection speed of 10 mm/s.

Fig. 3-11 shows the effect of MWCNT content on bending strength and bending strain at different injection conditions. The bending strength of all composites specimens was increased with increasing the content of MWCNTs up to 5 wt.%; however, when the content of MWCNTs increased to 10 wt.%, the bending strength of the composites suddenly dropped, dropping above 50% than that of the composites with 5 wt.% MWCNTs. Moreover, the bending strain of the composites remained the same for the 1 wt.% and 2.5 wt.% MWCNTs content, and then decreased greatly. In general, the bending strength and bending strain of the composites had a minimum as the MWCNTs content was 10 wt.%, which was consistent with the changes of tensile properties. These phenomena were attributed to the reason that the interfacial defects in the composites were produced during injection molding process and the number of defects increased with the filler content [19]. As well, the three-point bending test was also sensitive to interfacial defects. On the other hand, the effect of injection conditions on the bending strength and bending strain was not obvious. Overall, the MWCNT content was a major factor to affect the bending properties of the prepared composites.

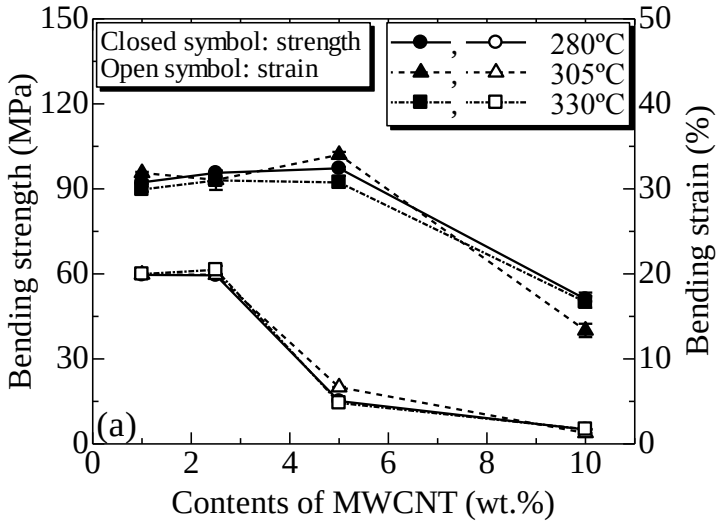

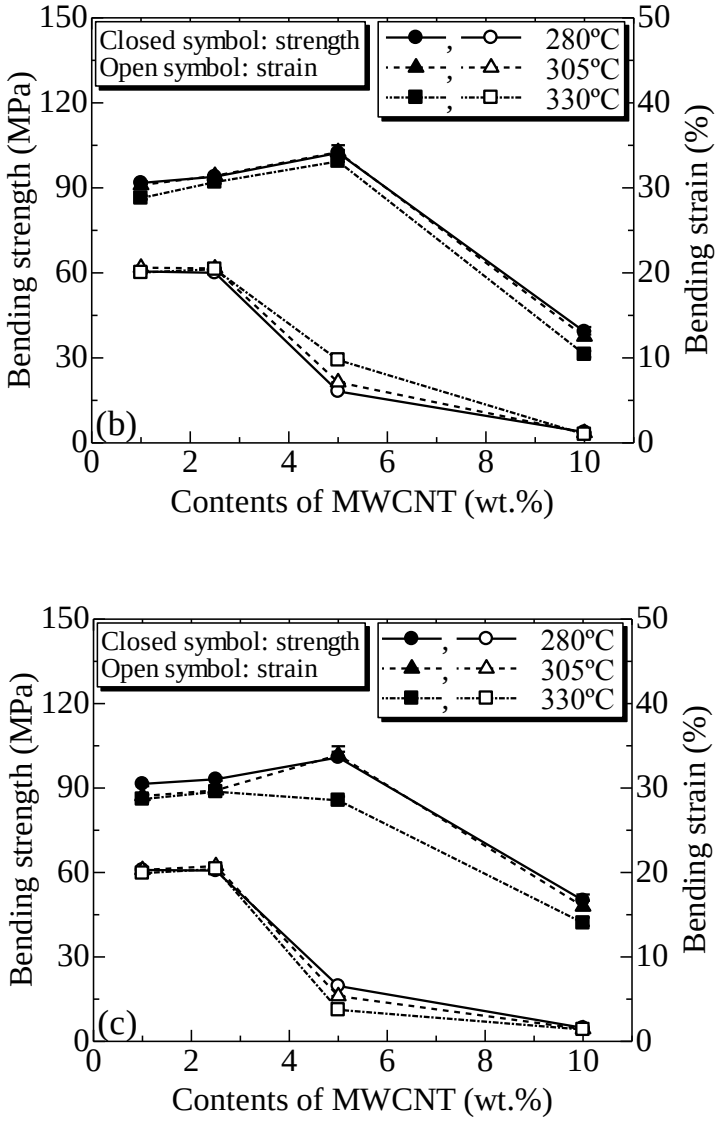

Fig. 3-11 Effect of the MWCNT contents on bending strength and bending strain: (a) Injection speed: 10 mm/s, (b) injection speed: 40 mm/s, (c) injection speed: 80 mm/s.

In general, during the injection molding, while a die is being filled with a high temperature molten state polymer, the three-layer structure of a skin layer, an intermediate layer and a core layer will be formed [20]. The skin layer is formed by the high temperature molten state polymer contacting with the cold die and then quickly cooling. Besides, the bending properties of composites were closely related to the skin layer of the composite specimens. Fig. 3-12 shows the SEM micrographs of the bending

fractured surfaces of the composites with 5 wt.% and 10 wt.% MWCNTs at the injection temperature of 330 ℃ and injection speed of 10 mm/s. Compared Fig. 3-12 (a) and (b) with each other, there were some differences between the two micrographs. In Fig. 3-12 (a), there was no defect on the surface of the composite specimen. However, from the Fig. 3-12 (b) to see, there were some defects on the fractured surface. It was considered that it was the primary reason which leaded the bending strength of the composites to weaken.

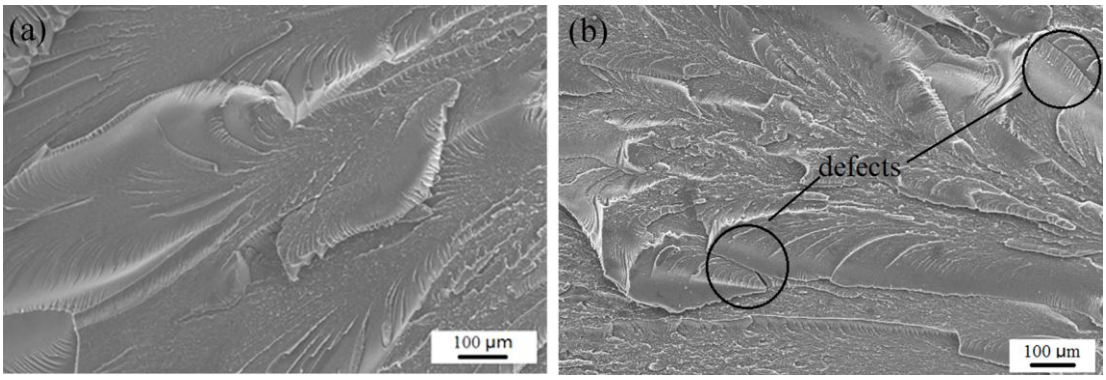

Fig. 3-12 SEM micrographs of bending fractured surfaces of the composites with (a) 5 wt.% MWCNTs and (b) 10 wt.% MWCNTs. The composites were prepared at an injection temperature of 330 ℃ with an injection speed of 10 mm/s.

The results showed that regardless of the injection temperature, the variation tendencies of the bending properties with the MWCNT content were almost the similar. Hereinafter, the discussions are therefore focused on the composites prepared at an injection temperature of 280 ℃ only. Fig. 3-13 shows that regardless of the injection speed, the bending strength did not show any obvious change when the MWCNT content was no more than 5 wt.%, a tendency similar to that shown for the tensile strength (Fig. 3-5); whereas once the MWCNT content was increased to 10 wt.%, the bending strength suddenly declined by 61.7% from 102.3 to 39.2 MPa. In addition, no matter what the injection speed was, the bending strain was in an overall downward trend. On the other hand, the effects of the injection speed were not distinct when the

MWCNT content was within 5 wt.%, but for the composites with10 wt.% MWCNTs, the bending strength at the injection speed of 40 mm/s was considerably smaller by 21.6% than those at two other injection speeds (i.e., 10 mm/s and 80 mm/s).

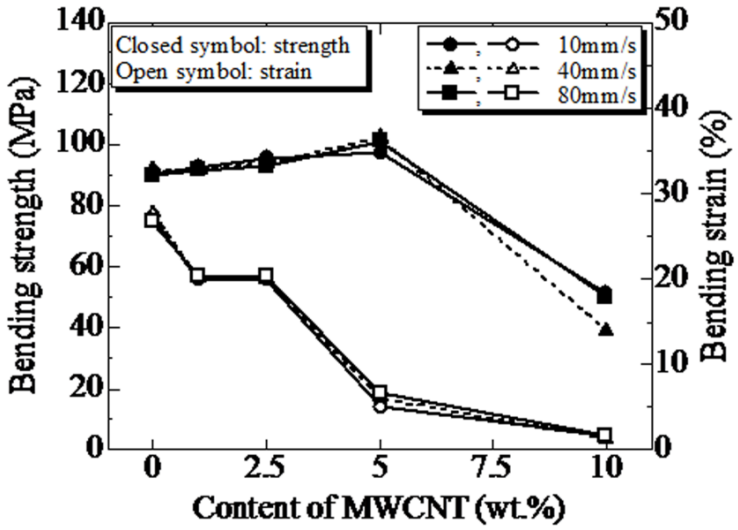

Fig. 3-13 Bending strength and bending strain of the composites prepared at injection temperature of 280 ℃.

As revealed above, the bending strength and bending strain reached their minima as the MWCNT content rose to 10 wt.%, the tendency was consistent with that of tensile properties. These phenomena could be attributed to the interfacial defects on the composite specimens during injection molding, and their number increased as the increase of filler content [19]. Moreover, the three-point bending test is also sensitive to interfacial defects. Therefore, the MWCNT content was the most important factor for forming different microstructures of the skin layer during injection molding, resulting in the composites having different bending properties.

Generally, during injection molding, while a die is being filled with a high-temperature molten-state polymer, a three-layered structure of a skin layer, an intermediate layer, and a core layer will be formed [20]. The bending properties are

closely related to the skin layer, which is formed by the high-temperature molten-state polymer coming into contact with the cold die and then quickly cooling.

Fig. 3-14 shows the SEM micrographs of the bending-fractured surfaces of the skin layer of the composites with 2.5 wt.% and 10 wt.% MWCNTs. A comparison of the two micrographs showed an obvious difference. In Fig. 3-14 (a), the dispersion of 2.5 wt.% MWCNTs was uniform and many fibrous MWCNTs were observed. However, in Fig. 3-14 (b), some minor agglomerations (solid circles) and a number of white bright spots (dashed circles) were observed in the specimen with 10 wt.% MWCNTs. It was considered that excessive MWCNTs led to the agglomerations in the hot polymer, and the high injection speed caused the orientation and breakage of MWCNTs [21], resulting in weakening of the bending strength.

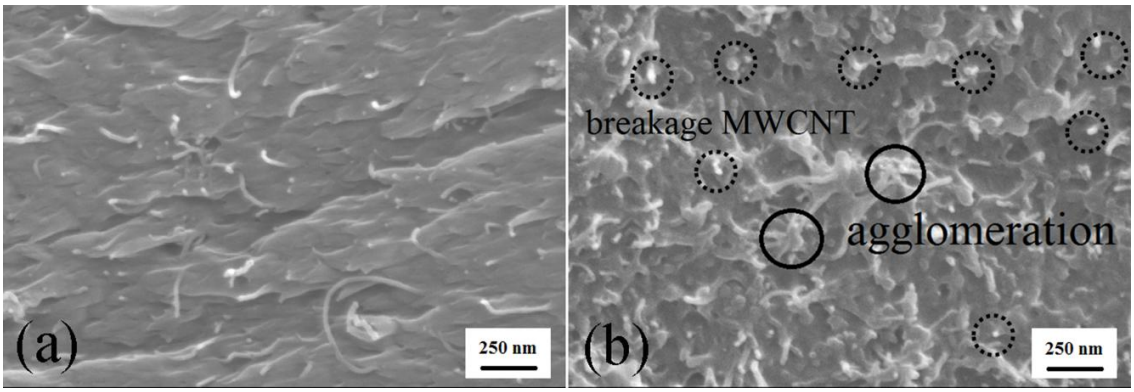

Fig. 3-14 SEM micrographs of bending-fractured surfaces of MWCNT/PC composites with (a) 2.5 wt.% MWCNTs and (b) 10 wt.% MWCNTs. The composites were prepared at an injection temperature of 280 ℃ with an injection speed of 80 mm/s.

(c) Impact strength

Impact strength is an indicator of material toughness [22]. The impact strength of pure PC and the MWCNT/PC composites at room temperature were measured and the impact strength is summarized in Table 3-2. The impact strength was obviously decreased as the increase of the MWCNT content up to 5 wt.%, then the impact strength was slightly increased as the MWCNT content of 10 wt.% . Besides, when the injection

temperature was 330 ℃, as the content of MWCNTs was increased, regardless of the injection speed (increased from 10 mm/s to 80 mm/s), the variation trend of impact strength was the same. Especially, the effect of injection speed on the impact strength was unconspicuous. It was found that the impact strength of the composites with 5 wt.% or 10 wt.% MWCNTs was the maximum under higher injection temperature and lower injection speed (e.g., injection temperature of 330 ℃ and injection speed of 10 mm/s).

Table 3-2 Impact strength of pure PC and the MWCNT/PC composites

No.	MWCNT content (wt.%)	Injection temperature (℃)	Injection speed (mm/s)	Impact strength (kJ/m^2)
1	0	330	10	13.345
2	5	330	10	1.473
3	10	330	10	1.686
4	0	330	40	12.994
5	5	330	40	1.313
6	10	330	40	1.576
7	0	330	80	13.923
8	5	330	80	1.299
9	10	330	80	1.532

(d) Microhardness and its distribution

Hardness is the ability to resist hard objects impressing into material surface. It is a comprehensive index of mechanical properties, such as elasticity, plasticity, strength and toughness of materials [23]. The effect of MWCNT content on the microhardness of the MWCNT/PC composites prepared under different injection conditions was thus examined, and the results are plotted in Fig. 3-15. Obviously, regardless of the injection temperature, with the increase of MWCNT content, the variation trend of microhardness is the same. Hereinafter, the discussions are therefore focused on the composites prepared at an injection temperature of 280 ℃ only (Fig. 3-15 (a)). When the injection temperature was 280 ℃, the variation trends of the microhardness were basically the same, regardless of the injection speed. Once the incorporation of MWCNT, overall, the

microhardness increased with increasing the MWCNT content, e.g., the microhardness of the composite with 10 wt.% MWCNTs had a maximum value of 17.3 kgf/mm^2. These phenomena might be attributed to the MWCNTs being incapable of serving the supporting role at low content (i.e., 1 wt.%), resulting in the microhardness of PC remaining at a low value; whereas the MWCNTs could play a supporting role when its content was 2.5–10 wt.%. Therefore, a proper incorporation of MWCNTs could distinctly improve the microhardness of the composites.

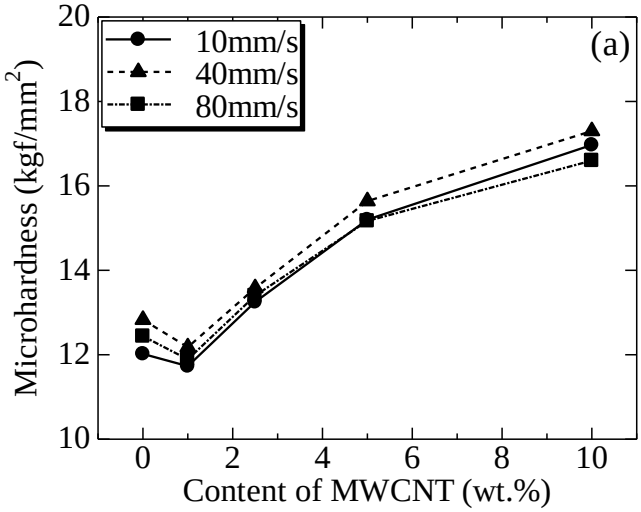

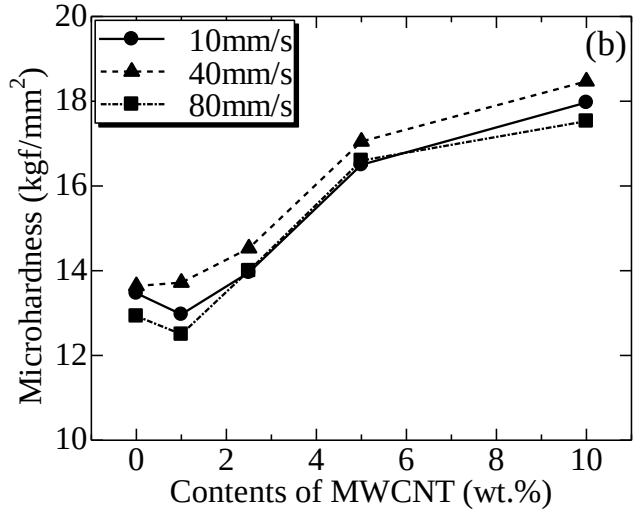

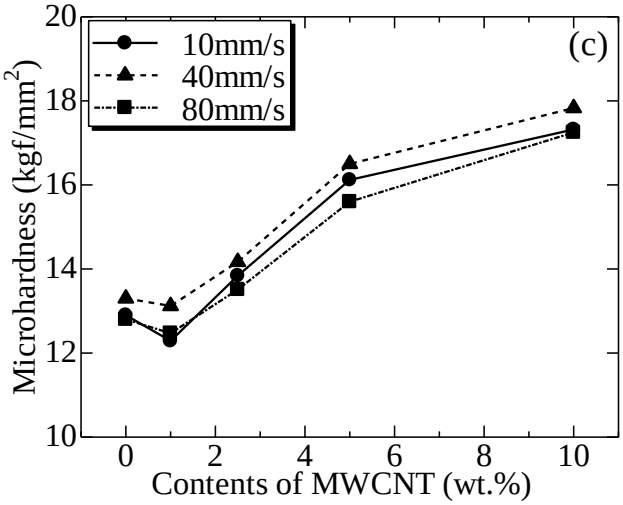

Fig. 3-15 Effect of MWCNT content on the microhardness of the composites prepared at injection temperature of (a) 280 ℃, (b) 305 ℃, (c) 330 ℃, respectively.

On the other hand, Fig. 3-16 (a) and (b) show the effects of the injection speed and injection temperature, respectively, on the microhardness of the composites with various MWCNT content. It can be seen that the variation tendencies of microhardness were the same, i.e., as the increase in injection speed or temperature, the microhardness first increased and then decreased. At an injection speed of 40 mm/s and an injection temperature of 305 ℃, the microhardness was the maximum. It was considered that the injection conditions would also change the microstructures of the composites specimen, leading to the difference in the microhardness of the MWCNT/PC composites. Similar observations were reported for other polymers prepared by the rolling process [24] or the injection molding process [25].

Based on the formation mechanism of the composite during injection molding, different MWCNT contents would result in obviously different internal microstructures, leading to different microhardness distributions. To confirm this hypothesis, the distributions of microhardness up to a depth of ~2000 μm from the surface were measured using a microscopic hardness meter. Moreover, to avoid the effect of surface roughness, all the test surfaces of specimen were ground using fine emery sandpaper

(#800) before the measurements. Fig. 3-17 shows the microhardness distributions of pure PC and the composites with various MWCNT contents prepared at an injection temperature of 330 ℃ with an injection speed of 10 mm/s. Overall, the microhardness at all distances from the surface rose as the MWCNT content was increased. For pure PC and the 1 wt.% MWCNTs composite, the microhardness basically remained unchanged at around 13 kgf/mm^2 from the surface to the interior. However, when the MWCNT content was 5 wt.%, the microhardness was increased by 24.03% at the core layer (at 2000 μm); when the MWCNT content reached 10 wt.%, the microhardness at the core layer was further increased by 35.94% compared with that of the composite with 5 wt.% MWCNTs.

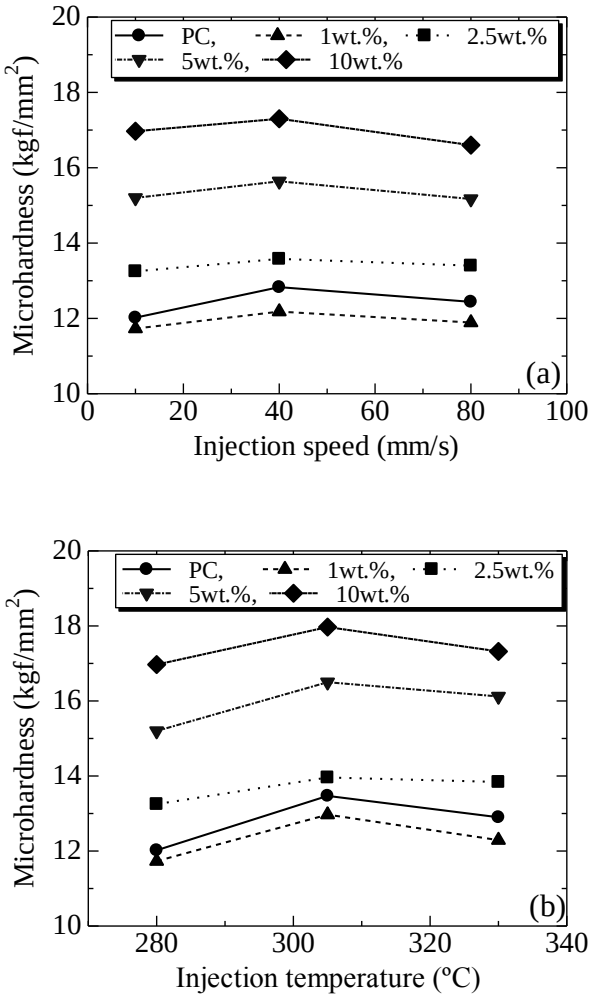

Fig. 3-16 Effect of injection conditions on the microhardness of composites prepared at (a) an injection temperature of 280 ℃ and (b) an injection speed of 10 mm/s.

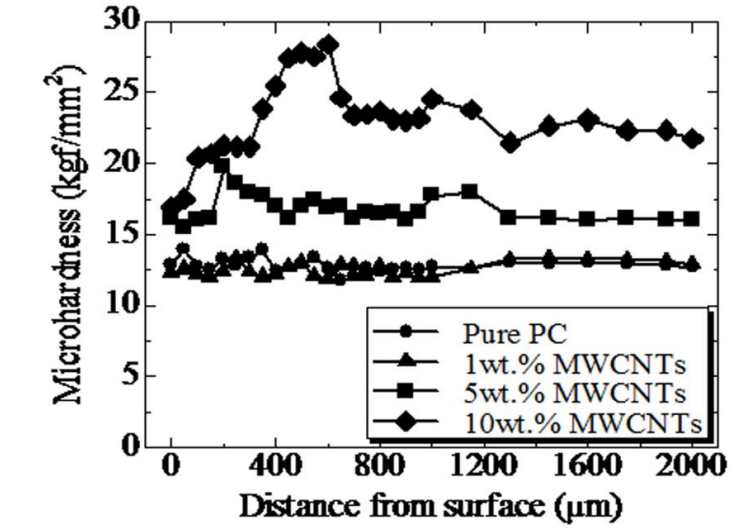

Fig. 3-17 Microhardness distributions of pure PC and the composites under various MWCNT contents. The PC and the composites were prepared at an injection temperature of 330 ℃ with an injection speed of 10 mm/s.

In particular, the values of microhardness of the composites with 5 wt.% and 10 wt.% MWCNTs reached their respective peaks at distances of 200 and 600 μm, respectively from the surface; the two peak values were 22.21 and 67.06% greater, respectively, than their corresponding values at the surface. When the MWCNT content was beyond a certain level, the microhardness was dramatically increased with the increase in distance from surface for a while, and after having reached the maximum value, the hardness gradually decreased, eventually reaching a stable value in the core layer. This indicates that the microhardness distribution from the surface to the interior could be divided into three regions, i.e., a rise, a decline, and a plateau. These phenomena might be: when the MWCNT content was beyond 5 wt.%, the MWCNTs in the core layer could more easily orient in a certain direction [26], and the thermal expansion coefficient of MWCNTs was lower than that of PC; thus a residual stress easily remained in the intermediate layer against with the pressure head of the meter, resulting in the enhancement of microhardness.

3.3.3 Dynamic mechanical behavior

The modulus will change with temperature because of the variations in molecular motions in a polymer [13]. DMA was performed to determine the storage modulus and tan δ of pure PC and the MWCNT/PC composites as functions of temperature, and the results are shown in Fig. 3-18. When the temperature was between 30 ℃ and 130 ℃, the composite could maintain its storage modulus at the same value irrespective of the MWCNT content. The storage modulus E' was increased by the stiffening owing to the MWCNTs, which was particularly outstanding at higher temperatures. The enhancement was significant below the glass translation temperature (T_g), at which the average reinforcement of 2.5 wt.% MWCNTs was achieved. As the temperature rose above T_g, the enhancement declined and E' of the composites with 10 wt.% MWCNTs was higher than that of other composites. For example, the storage modulus E' of the composite with 10 wt.% MWCNTs was 2.90×10^1 MPa at 170 ℃, which was a 3.8-fold increase than that of pure PC. In addition, the presence of MWCNTs also enabled the PC matrix to sustain a high modulus value. This suggested that PC was a typical amorphous polymer, and the crystallites in PC already imparted a high modulus; hence, the MWCNTs could not produce a dramatic increase in the stiffness of the PC matrix.

On the other hand, the tan δ was used to evaluate the energy loss of materials from segment rearrangements and internal friction during the measurement [27]. The position of the tan δ peak is commonly taken to indicate the value of T_g. The position of the peak shifted to a slightly lower temperature with the increase in MWCNT content. Moreover, the tan δ peak broadened slightly upon the incorporation of MWCNTs. However, the intensity of the tan δ peak decreased with increasing MWCNT content. It was considered that owing to the incorporation of MWCNTs, the original ductility of PC was reduced, whereas the brittleness was heightened, thus the intensity of the tan δ peak was decreased. In addition, when the temperature was above 160 ℃, there was a notable increase in tan δ of MWCNT/PC composites, which was due to the damping

effect of the MWCNTs as they restricted the molecular motion and increased the internal friction.

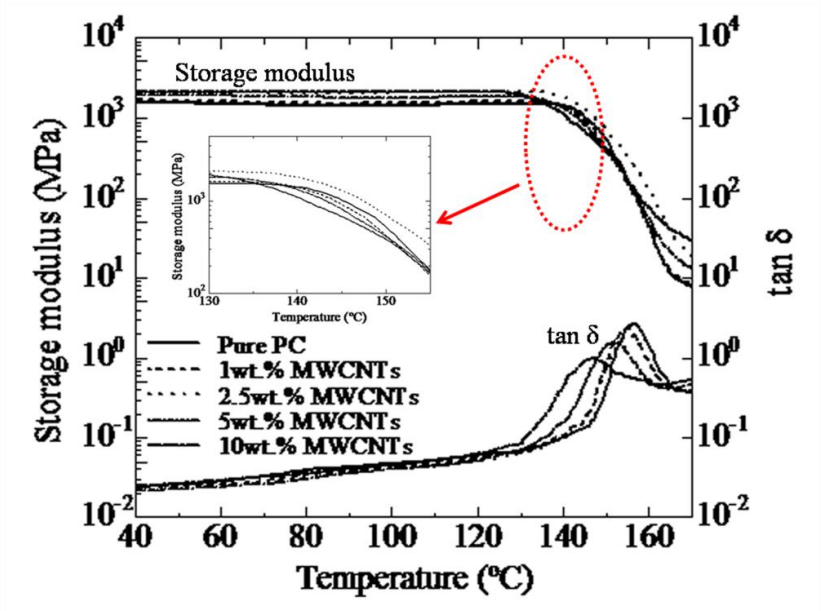

Fig. 3-18 Storage modulus and tan δ of pure PC and the MWCNT/PC composites prepared at an injection temperature of 280 ℃ with an injection speed of 10 mm/s.

Furthermore, Table 3-3 shows T_g and the maximum tan δ of the composites. Clearly, there was a slight overall decrease in T_g with the increase in MWCNT content; when the MWCNT content was increased from 0 wt.% to 10 wt.%, T_g was reduced by 6.21%. Meanwhile, $(\tan \delta)_{max}$ also decreased as the MWCNT content was increased. It was considered that MWCNTs hindered the deformation of PC and the incorporation of MWCNTs increased the internal friction between the molecules, resulting in the decrease in T_g.

Table 3-3 Glass translation temperature T_g and $(\tan\delta)_{max}$ of the MWCNT/PC composites

MWCNT content (wt.%)	0	1	2.5	5	10
T_g (℃)	156.41	154.65	155.34	151.77	146.70
$(\tan \delta)_{max}$	2.77	2.36	1.97	1.60	0.95

3.4 Conclusions

A two-step dispersion strategy, i.e., extrusion followed by injection molding, was employed for the preparation of MWCNT/PC composites. As a result, the MWCNT/PC composite specimens with well-dispersed MWCNTs were successfully obtained. The effects of MWCNT content and injection conditions on the thermal, mechanical, and dynamic mechanical properties of the prepared composites were investigated.

(1) Based on the above experimental results, the MWCNT content was the most dominant factor of the properties of the composites. As for thermal stability, the thermal-degradation temperature of the 1 wt.% MWCNT/PC composite was enhanced by 100 ℃ compared to that of PC.

(2) When the MWCNT content was within 5 wt.%, the tensile strength and bending strength of the composite could basically be maintained at values of those of pure PC, even with some increases. However, when the MWCNT content increased to 10 wt.%, the tensile and bending strengths were obviously reduced by approximately 35% and 47%, respectively. In contrast, the impact strength and microhardness of the composites were reinforced by increasing the MWCNT content. Furthermore, dynamic mechanical analysis of the composites proved that the storage modulus of the composite with 10 wt.% MWCNTs was increased by 3.8-fold of that of pure PC at 170 ℃, but the glass translation temperature T_g was slightly decreased with the increase in MWCNT content.

(3) The injection temperature and injection speed were also major factors of the properties of MWCNT/PC composites. When the MWCNT content was within 5 wt.%, the effects of injection temperature and speed on the tensile strength and bending strength were not obvious; when the content increased to10 wt.%, the effects were obvious. In particular, when the injection temperature was 305 ℃ and the injection speed was 80 mm/s, the tensile strength had a maximum value of 45.9 MPa, basically meeting the strength of engineering plastic.

(4) For different practical applications, MWCNT/PC composites with different properties can be prepared by changing MWCNT content and injection conditions. For a composite with low conductive properties, the addition of a small amount of MWCNTs (e.g., 5 wt.%) could achieve not only the conductivity but also higher mechanical properties. For a composite with high conductivity, the excessive addition of MWCNTs may result in the decrease in mechanical properties. In other words, enhanced mechanical properties can be achieved by changing the injection conditions. Therefore, the injection molding method offers a convenient way to prepare the MWCNT/PC composites in practical applications.

References

[1] J.C. Kearns and R. L. Shambaugh. Polypropylene Fibers Reinforced with Carbon Nanotubes. J. Appl. Polym. Sci. 86 (2002) 2079-2084.

[2] T. Filleter, R. Bernal, S. Li and H.D. Espinosa. Ultrahigh Strength and Stiffness in Cross-Linked Hierarchical Carbon Nanotube Bundles. Adv. Mater. 23 (2011) 2855-2860.

[3] M.F. Yu, O. Lourie, M.J. Dyer, K. Moloni, T.F. Kelly and R.S. Ruoff. Strength and Breaking Mechanism of Multiwalled Carbon Nanotubes under Tensile Load. Science 287 (2000) 637-640.

[4] J. Gao, D. Yan, B. Yuan, H. Huang and Z. Li. Large-Scale Fabrication and Electrical Properties of an Anisotropic Conductive Polymer Composite Utilizing Preferable Location of Carbon Nanotubes in a Polymer Blend. Composites Science and Technology 70 (2010) 1973-1979.

[5] P. Potschke, A. R. Bhattacharyya and A. Janke. Melt Mixing of Polycarbonate with Multiwalled Carbon Nanotubes: Microscopic Studies on the State of Dispersion. Eur. Polym. J. 40 (2004) 137-148.

[6] M. T. Muller, B. Krause, B. Kretzschmar and P. Potschke. Influence of Feeding Conditions in Twin-Screw Extrusion of PP/MWCNT Composites on Electrical and Mechanical Properties. Compos. Sci. Technol. 71 (2011) 1535-1542.

[7] T. Villmow, P. Pötschke, S. Pegel, L. Häussler and B. Kretzschmar. Influence of Twin-Screw Extrusion Conditions on the Dispersion of Multi-walled Carbon Nanotubes in a Poly(lactic acid) Matrix. Polymer 49 (2008) 3500-3509.

[8] T. Villmow, B. Kretzschmar and P. Pötschke. Influence of Screw Configuration, Residence Time, and Specific Mechanical Energy in Twin-screw Extrusion of Polycaprolactone/Multi-walled Carbon Nanotube Composites. Compos. Sci. Technol. 70 (2010) 2045-2055.

[9] T. Villmow, S. Pegel, P. Potschke and U. Wagenknecht. Influence of Injection Molding Parameters on the Electrical Resistivity of Polycarbonate Filled with Multi-walled Carbon Nanotubes. Compos. Sci. Technol. 68 (2008) 777-789.

[10] D. Lellinger, D. Xu, A. Ohneiser, T. Skipa and I. Alig. Influence of the Injection Molding Conditions on the In-line Measured Electrical Conductivity of Polymer–Carbon Nanotube Composites. Phys. Status Solidi B. 245 (2008) 2268-2271.

[11] A. Chandra, A.J. Kramschuster, X. Hu and L.S. Turng. Effect of Injection Molding Parameters on the Electrical Conductivity of Polycarbonate/Carbon Nanotube Nanocomposites. Mech. Eng. 4 (2007) 2184-2188.

[12] A. Ameli, P.U. Jung and C.B. Park. Through-plane Electrical Conductivity of Injection-molded Polypropylene/Carbon-fiber Composite Foams. Compos. Sci. Technol. 76 (2013) 37-44.

[13] Z. Jin, K.P. Pramoda, G. Xu and S.H. Goh. Dynamic Mechanical Behavior of Melt-processed Multi-walled Carbon Nanotube/Poly(methyl methacrylate) Composites. Chemical Physics Letters 337 (2001) 43-47.

[14] Q. Jiang, X. Wang, Y. Zhu, D. Hui and Y. Qiu. Mechanical, Electrical and Thermal Properties of Aligned Carbon Nanotube/Polyimide Composites. Composites Part B: Engineering 56 (2014) 408-412.

[15] J. Guo, Y. Liu, R. Prada-Silvy, Y. Tan, S. Azad, B. Krause, P. Pötschke and B.P. Grady. Aspect Ratio Effects of Multi-walled Carbon Nanotubes on Electrical, Mechanical, and Thermal Properties of Polycarbonate/MWCNT Composites. Journal of Polymer Science: Part B: Polymer Physics 52 (2014) 73-83.

[16] S.M. Yuen, C.C. M. Ma; H.H. Wu, H.C. Kuan, W.J. Chen, S.H. Liao, C.W Hsu and H.L. Wu. Preparation and Thermal, Electrical, and Morphological Properties of Multiwalled Carbon Nanotubeand Epoxy Composites. J.Appl. Polym. Sci. 103 (2007) 1272-1278.

[17] V.J. Mkhabela, A.K. Mishra and X.Y. Mbianda. Thermal and Mechanical

Properties of Phosphorylated Multiwalled Carbon Nanotube/Polyvinyl Chloride Composites. Carbon 49 (2011) 610-617.

[18] L. Lei, J. Qiu and E. Sakai. Preparing Conductive Poly(lactic acid) (PLA) with Poly(methyl methacrylate) (PMMA) Functionalized Graphene (PFG) by Admicellar Polymerization. Chem. Eng. J. 209 (2012) 20-27.

[19] T. Takeda, Y. Shindo, F. Narita and Y. Mico. Tensile Characterization of Carbon Nanotube-reinforced Polymer Composites at Cryogenic Temperatures: Experiments and Multiscale Simulations. Mater. Trans. 50 (2009) 436-445.

[20] J. Qiu. Effect of Hot Roll Process on the Morphology and Tensile Properties of Injection Molded Polypropylene (in Japanese). Kobunshi Ronbunshu 63 (2006) 397-403.

[21] A. Ameli, M. Nofar, S. Wang and C.B. Park. Lightweight Polypropylene/ Stainless-steel Fiber Composite Foams with Low Percolation for Efficient Electromagnetic Interference Shielding. ACS Appl. Mater. Interfaces 6 (2014) 11091-11100.

[22] http://baike.haosou.com/doc/6963845-7186500.html. Retrieved in October 1st, 2015.

[23] http://baike.haosou.com/doc/3596256-3781286.html. Retrieved in October 1st, 2015.

[24] J. Qiu, M. Kawagoe, W. Mizuno, M. Morita and T. Miyati. Changes of Microstructure and Mechanical Properties of Injection-molded Polypropylene Sheets by Rolling Process (in Japanese). Kobunshi Ronbunshu 54 (1997) 778-784.

[25] J. Qiu, M. Kawagoe, W. Mizuno and M. Morita. Change of Morphology and Mechanical Properties of PP by Injection-molded Speed (in Japanese). Trans.Jpn. Soc. Mech. Eng. A. 67 (2001) 1017-1023.

[26] J. Qiu, L. Wang, K. Uchiya and E. Sakai. Effects of Injection Molding Conditions on the Electrical Properties of Polycarbonate/Carbon Nanotube Nanocomposites. Polym. Compos. (2015) DOI: 10.1002/ pc.23523.

[27] J. Bai, R. D. Goodridge, Richard J.M. Hague, M. Song and M. Okamoto. Influence of Carbon Nanotubes on the Rheology and Dynamic Mechanical Properties of Polyamide-12 for Laser Sintering. Polym. Test. 36 (2014) 95-100.

Chapter 4 Effects of Molding Conditions on Microstructures and Electrical Properties of Carbon Nanotube-Reinforced Polycarbonate Conductive Composites

4.1 Introduction

For conductive polymer composites (CPCs), the most prominent is electrostatic phenomenon which will lead to performance degradation of photographic films; and polymer products will cause catastrophic accidents in flammable and explosive occasions. To resist electromagnetic interference (EMI) and radio frequency interference (RFI), the shielding performance of the polymers also urgently needs to be solved. All these require the polymers with new conductive properties and lower surface resistivity, so as to promote the rapid development of CPCs.

For actual applications, it is particularly necessary to control the electrical resistivity within a certain range [1, 2]. In recent years, the EMI shielding capabilities of CPCs with CNTs have been studied [3-5]. Compared to the conventional CPCs, composites with carbon nano-fillers present lower percolation threshold and superior electrical properties. Accordingly, a uniform dispersion of CNTs in a polymer matrix and a strong interfacial interaction [6, 7] between CNTs and polymers are necessary conditions to maximize the advantages of CNTs as effective reinforcing filler in polymer composites. Generally, there are two major approaches to improve the electrical properties of a polymer at a given content of conductive fillers [8], while obtaining excellent mechanical and electrical properties. One approach is to rely on surface treatment to modify and functionalize CNTs [9-11]. This method has been confirmed to not only improve the solubility and dispersibility of CNTs, but also enhance the electrical properties and the interfacial interaction between CNTs and

polymers [12, 13]. However, the main drawbacks of this method are time consuming and environmentally unfriendly. Another approach is to prepare CPCs by different molding processes, such as melt mixing, extrusion molding and injection molding. Many studies have reported that the melt processing conditions must be optimized to achieve homogeneous MWCNT dispersion in the composites [14-17]. Villmow et al. [16] indicated that the extrusion conditions influenced the dispersion of MWCNTs in polylactide (PLA) matrix while using twin-screw extrusion whereas MWCNTs were added together with the polymer when using an extruder. Besides, Lee′s group [17] found that the electrical percolation threshold of PMMA/SAN/MWCNTs remained around 1.5 wt.%. Although MWCNT/polymer composites have been widely studied using different molding methods, there are few published reports on the effects of MWCNT content on microstructures and electrical resistivity of the composites prepared by injection molding. Especially, during the injection molding process, while the high temperature polymer contacts with the low temperature die, a three-layer structure of skin layer, intermediate layer and core layer of the nanocomposites are formed from the surface to the inside [18-20].

Considering the formation mechanism of the internal microstructures of the nanocomposites specimens in injection molding, the molten polymer will be constrained by the die wall, thus forming the three-layer structure with different orientations or dispersions [21-26]. In addition, the different injection conditions will affect the filler state in the polymer matrix, so the control of electrical resistivity becomes difficult. In this study, the MWCNT/PC composites prepared by injection molding were used, and the effects of injection temperature, injection speed and MWCNT contents on electrical resistivity of the composites were researched. Furthermore, the effects of injection molding conditions on the distribution of electrical resistivity in the cross section (i.e., from skin layer to interior) of the specimens were investigated. Accordingly, the relationship between the internal microstructures and the electrical resistivity, and the formation mechanism of the internal microstructure were both elucidated.

4.2 Experimental

4.2.1. Preparation composites specimens

The MWCNT/PC composites with 0–10 wt.% MWCNTs were prepared at various injection conditions by a two-step dispersion method (mentioned as chapter 3). The dimension of the standard rectangle shaped specimens was 80 mm × 10 mm × 4 mm (JIS K 7171 1(1/2), Fig. 2-7), which was prepared by using the injection molding machine (shown in Fig. 2-5).

Also, the flat shaped specimens with a size of 60 mm × 60 mm × 3 mm (Fig. 4-1) were also prepared by the injection molding machine (ROBOSHTO-100C, FANUC Co., Ltd., Japan). And, the MWCNT contents were 0–5 wt.%. This purpose of production of different shapes specimens is to compare the differences in the electrical resistivity of different shapes. Besides, Table 4-1 summarizes the ability to measure electrical resistivity and to mold the flat shaped specimens at different injection conditions.

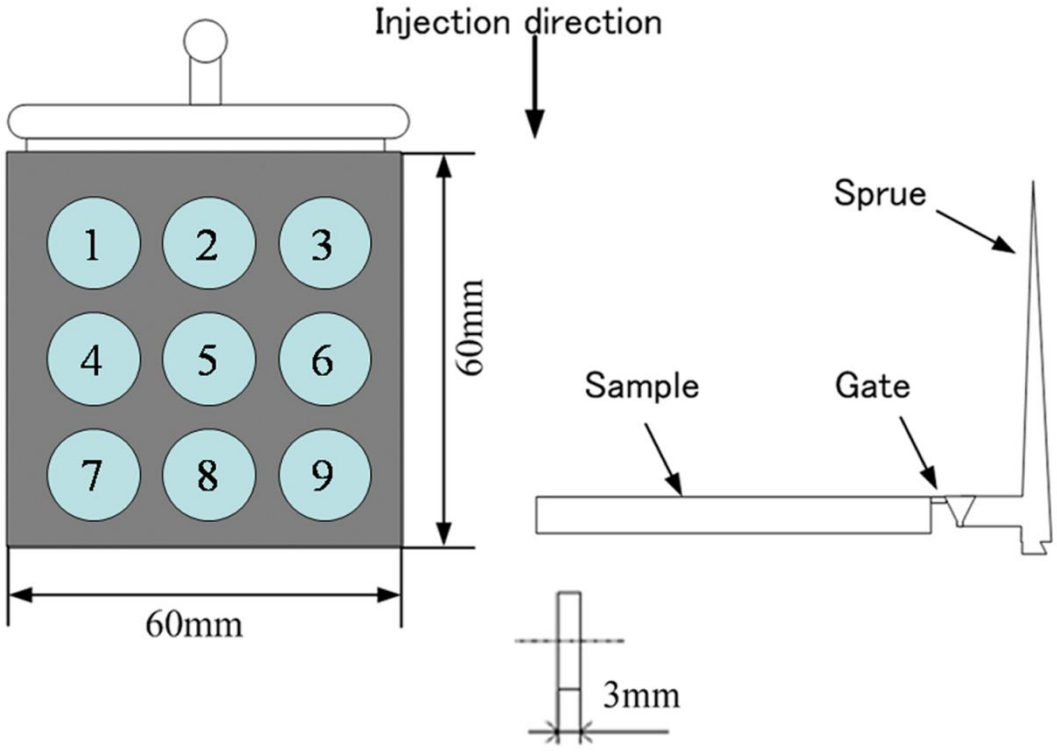

Fig. 4-1 The flat shaped specimen for electrical resistivity test.

Table 4-1 Abilities to injection mold the MWCNT/PC composite specimens at different injection conditions and to measure surface resistivity

	Temperature (℃)	280			295			310			340		
	Speed(mm/s)	10	40	80	10	40	80	10	40	80	10	40	80
MWCNT content (wt.%)	1	○	×	×	○	×	×	○	×	×	○	○	×
	3	○	○	○	○	○	○	○	○	○			
	5	○	○	○	○	○	○	○	○	○			

○: measurable; ×: cannot be measured; slash: cannot be molded

4.2.2. Measurement of electrical resistivity

For the rectangle shaped specimens, the middle of the specimen was measured to ensure the measurement accurately. While for the flat shaped specimens, the measurement of electrical resistivity was performed from $1^{\#}$ point to $9^{\#}$ point, and the results are shown in Fig. 4-1. The electrical resistivity of each type specimen was tested repeatedly at least five times. And the electrical resistivity of the composites was determined by the means of the average value.

4.3 Results and discussions

4.3.1 Dispersion of MWCNTs

The excellent properties of MWCNT are attributed to their large surface area and high aspect ratios. However, these properties easily lead to significant agglomeration because of Van der Waals attraction among tubes, thus preventing an efficient transfer of their superior properties to the polymer matrix. To create a composite with higher electrical conductivity, more MWCNTs should be added; however, this would lead to additional agglomerations and reduction of the attractive electrical properties of the MWCNTs. In general, for MWCNT/polymer composites, since the lack of interfacial interactions among MWCNTs, they are agglomerated in the host polymer. In the present work, homogeneously dispersed MWCNT/PC composites were prepared by a

two-step dispersion method. In the first step, MWCNTs were dispersed in a twin-screw extruder machine by mechanical force. In the second step, MWCNTs were dispersed again through injection molding by mechanical force. Namely, MWCNTs were dispersed twice during the preparation process. Fig. 4-2 shows an optical micrograph of a 2.5 wt.% MWCNTs composite (prepared at injection temperature of 280 ℃ and injection speed of 10 mm/s). It is evident that the MWCNTs were homogeneously dispersed in the PC matrix with minor agglomeration, confirming that the two-step dispersion method was effective at improving the dispersibility of the MWCNTs in the host polymer.

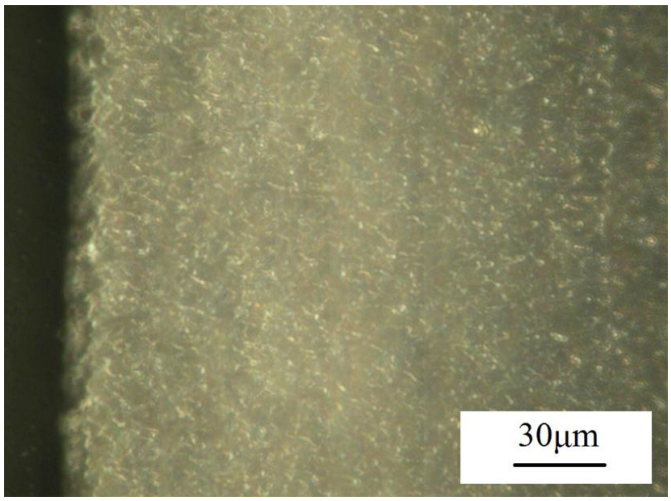

Fig. 4-2 Optical micrograph of 2.5 wt.% MWCNT/PC composite prepared at the injection temperature of 280 ℃ and injection speed of 10 mm/s.

4.3.2 Electrical properties

Injection molding conditions generally include, mold temperature, injection speed, and injection temperature. These conditions would be potential factors which affect the electrical resistivity of the composites. Therefore, in this part, the effect of the mold temperature, the MWCNT content, the injection speed and the injection temperature on the electrical resistivity of the composites was mainly discussed.

(a) Effect of measurement position on the electrical resistivity

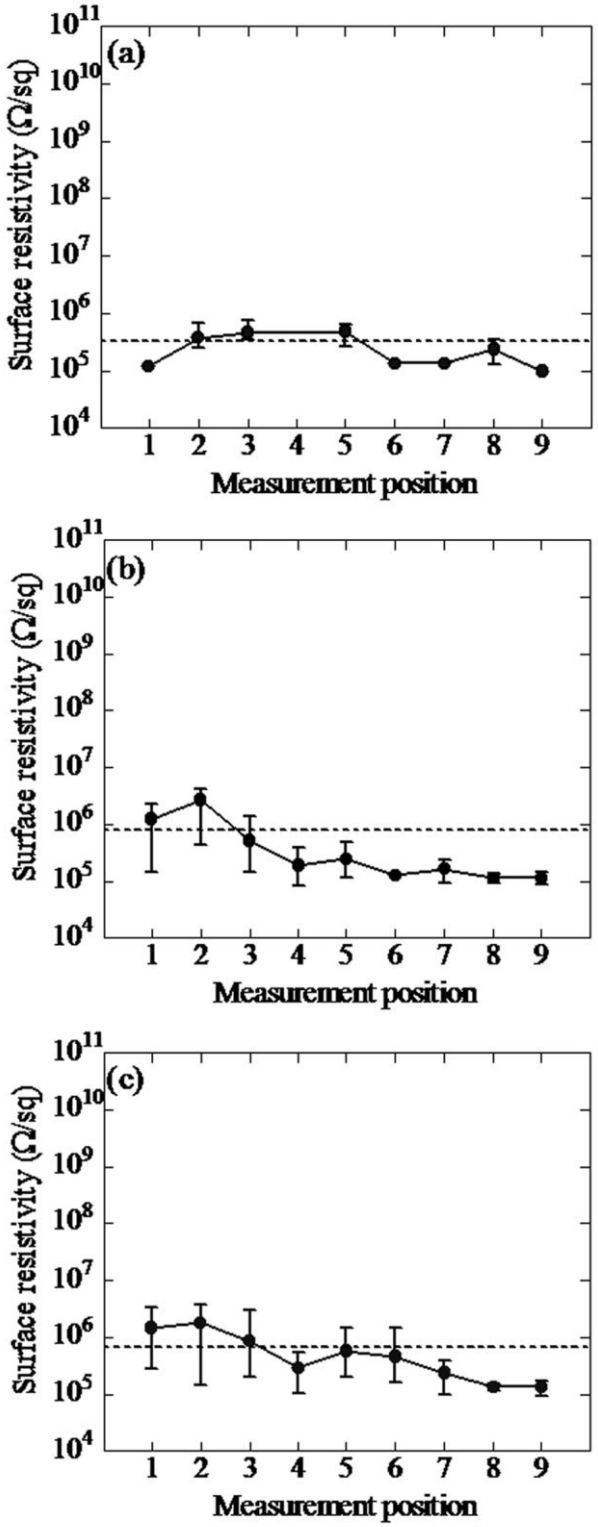

Fig. 4-3 Effect of measurement position on surface resistivity of the 3 wt.% MWCNT composites prepared at injection temperature of 310 ℃ and injection speed of (a) 10 mm/s; (b) 40 mm/s; (c) 80 mm/s.

To investigate the effect of measurement position, the electrical resistivity of each position ($1^{\#}$–$9^{\#}$) was tested. And the specimens were the flat shaped specimens (shown as Fig. 4-1). Fig. 4-3 shows an example of the surface resistivity of the 3 wt.% MWCNT composites prepared at injection temperature of 310 ℃. From the experimental results, the difference of the electrical resistivity was not obvious, when the injection temperature was 310 ℃. In fact, the specimens of other injection temperatures were also measured, and the results were as similar as that. Thus the effect of measurement position on the electrical resistivity was very small. Therefore, to obtain the stable results, only $4^{\#}$, $5^{\#}$, $6^{\#}$ three points of the flat shaped specimen were tested in latter part. And then the average value was used as the electrical resistivity of the specimen.

(b) Effect of mold temperature on the electrical resistivity

Generally, during the injection molding of polymers, the effect of the mold temperature on the electrical resistivity was similar to that of the injection temperature. Thus the composite specimens of 3 wt.% MWCNTs prepared at the injection speed of 10 mm/s and injection temperature of 310 ℃ were examined in terms of the effect of mold temperature on the electrical resistivity. The flat shaped specimens were measured and the results are shown in Fig. 4-4. It is evident that as the mold temperature was dropped from 80 ℃ to 40 ℃, the electrical resistivity rose from $4\times10^{5}\,\Omega$/sq to $10^{7}\,\Omega$/sq, an increase of 25 times. In other words, the changes of mold temperature had a considerable effect on the electrical resistivity. It had the advantage of improving the electrical conductivity of the composites. This might be because while the mold temperature was low, the solidification rate of the molten polymer would become quick, so the thickness of the MWCNT orientation layer in the surface vicinity was increased. Therefore the electric resistivity would be considerable increased.

Accordingly, the experimental results showed that the mold temperature would affect the electrical resistivity; in particular the results pointed out the fact that the higher mold temperature had the advantage of improving the electrical conductivity of the composites [27]. In the following sections, the used specimens were all prepared at

the mold temperature of 80 ℃.

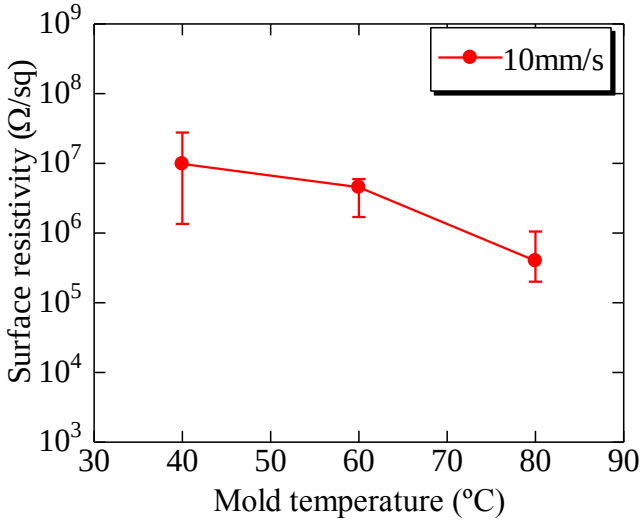

Fig. 4-4 Effect of mold temperature on surface resistivity of the 3 wt.% MWCNT composites prepared at injection temperature of 310 ℃.

(c) Effect of MWCNT content on the electrical resistivity

To avoid non-uniformity or occasionality of electrical resistivity of the composites, the electrical resistivity was measured on the middle of the rectangle shaped specimens at different locations and was determined by the average values. The relationship between MWCNT contents and electrical resistivity under different injection temperatures is shown in Fig. 4-5. These results showed that the electrical conductivity exponentially increased with the MWCNT content, regardless of the injection temperature. According to the large number of experimental data showed that all volume resistivity values were lower than the surface resistivity values by approximately 1 order of magnitude, although the change trends were basically the same. Subsequently, in this work only the surface resistivity of the composites is discussed. More importantly, with the increase of MWCNT content from 1 wt.% to 5 wt.%, the surface resistivity of the composites was decreased several orders of magnitude, especially in the case of lower injection speed (i.e., Fig. 4-5 (a)). Regarding

this behavior, previous research studies have described the percolation threshold as being within 5 wt.% MWCNT [3, 28].

In addition, Fig. 4-5 shows that as the MWCNT content was increased from 1 wt.% to 10 wt.%, the surface resistivity decreased by 9 orders of magnitude (from 10^{11} Ω/sq to 10^{2} Ω/sq), regardless of the injection speed and injection temperature. However, the trend of surface resistivity was not the same. When the injection speed was low (i.e., injection speed of 10 mm/s, Fig. 4-5 (a)) and the MWCNT content was from 1 wt.% increased to 5 wt.%, the surface resistivity dropped linearly by 6–9 orders of magnitude. However, when the MWCNT content exceeded 5 wt.% (MWCNT content > 5 wt.%) and the injection temperature was higher (e.g., injection temperature of 330 ℃), the effect of the MWCNT content on the surface resistivity was not noticeable and the surface resistivity decreased by only 1 order of magnitude. It was hypothesized that more MWCNTs agglomerated in the PC matrix, leading to the conductivity of MWCNT not being transferred to the PC. Moreover, when the injection speed was high (injection speed of 40 mm/s or 80 mm/s, fig. 4-5 (b) and (c)), the effect of MWCNT content on the surface resistivity was also great. As the MWCNT content was increased from 1 wt.% to 10 wt.%, the surface resistivity uniformly decreased. This was ascribed to the melt viscosity and different alignment of the MWCNTs which would affect MWCNT network formation under various injection temperatures [3].

Overall, it was significant that the percolation threshold of the MWCNT/PC composites remained the same (within 5 wt.% MWCNT), irrespective of injection temperature. Moreover, even when the MWCNT contents were in the small range of 1 wt.% to 10 wt.%, the electrical conductivity of the composites was drastically increased. This implied that the composites specimens with various electrical resistivities and a wide range of conductivities could be produced by changing the MWCNT content. In general, the effect on the conductivity was a larger MWCNT content, the conductive network formed more easily. It was confirmed that the MWCNT content was an important factor affecting the electrical resistivity of the MWCNT/PC composites.

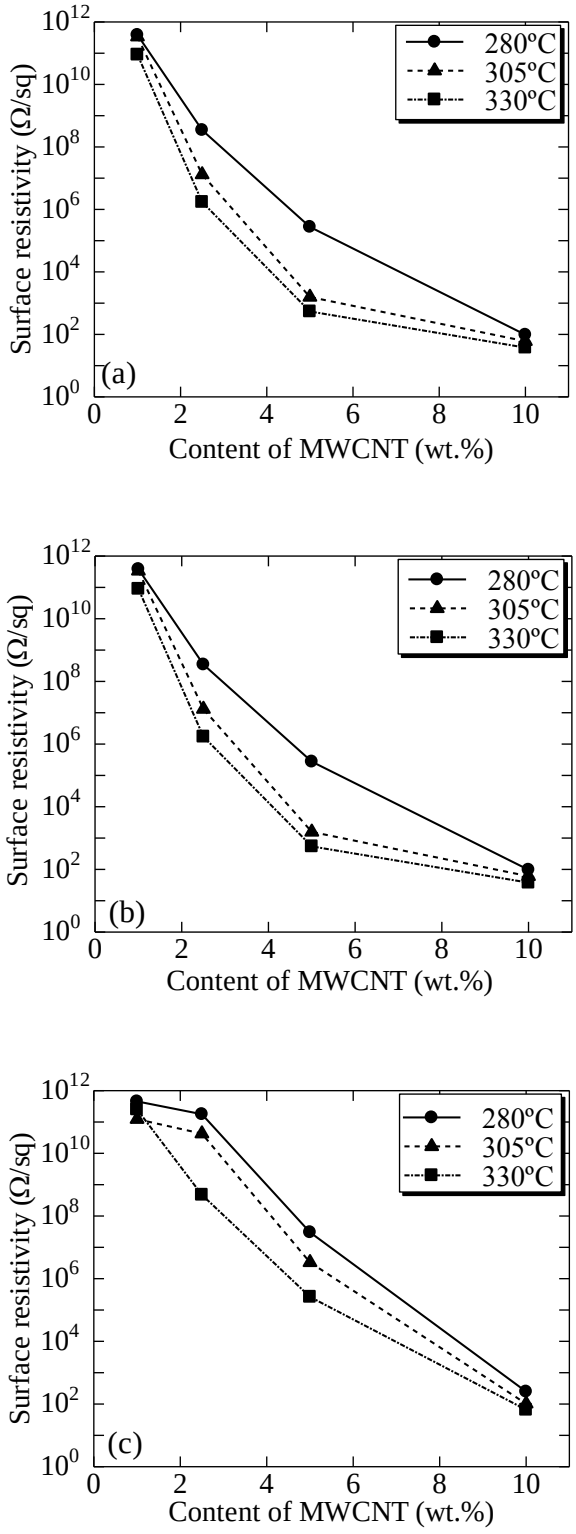

Fig. 4-5 Effect of MWCNT content on the surface resistivity of the composites obtained at injection speeds of (a) 10 mm/s, (b) 40 mm/s and (c) 80 mm/s, respectively.

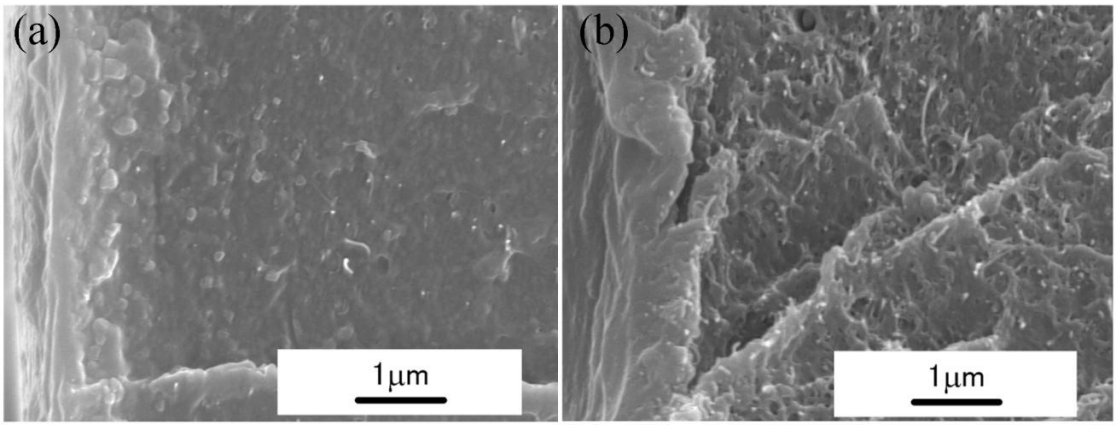

Fig. 4-6 SEM micrographs of the surface layer of the MWCNT/PC composites with (a) 1 wt.% MWCNTs and (b) 5 wt.% MWCNTs. The left side of each micrograph shows the specimen surface. The MWCNT/PC composites were prepared at an injection temperature of 280 ℃ with an injection speed of 10 mm/s.

Fig. 4-6 shows SEM micrographs of the fractured surfaces of the 1 wt.% and 5 wt.% MWCNTs composites prepared at an injection temperature of 280 ℃ and injection speed of 10 mm/s (perpendicular to the injection direction, and similarly hereinafter). The left side of the micrographs shows the specimen surface (similarly in all micrographs hereinafter). No matter what the types of fracture surfaces were, within the depth of approximately 1 μm from the surface, the plastic deformation of PC occurred; even the MWCNT content increased to 5 wt.%, distinct carbon nanotubes could not be observed. This meant that during the injection molding process, while the high temperature molten polymers flowed into the die, they immediately contacted with the cold die and were quickly cooled, thus the distribution of MWCNTs in the surface layer was less. Moreover, the MWCNT agglomeration was not observed on the two fractured surfaces of the specimens in Fig. 4-6, indicating the good dispersion of MWCNTs. It was considered that the electrical properties of MWCNTs were the best displayed yet, and the electrical conductivity of the composites was almost linearly enhanced with the increase of the MWCNT contents.

Additionally, Fig. 4-7 (a) and (b) show SEM micrographs of the fractured surfaces

of the composites with 5 wt.% and 10 wt.% MWCNTs, respectively. Comparing Fig. 4-7 (a) with Fig. 3-7 (b), no matter the types of fractured surfaces were, even if the MWCNT content increased to 5 wt.%, MWCNT agglomeration was not observed while the electrical networks were distinctly observed. These results showed that the dispersion of MWCNTs was very good. Therefore, during the injection molding, as the high temperature molten polymers flowed into the cold die and were cooled slowly, and even with a slow injection speed, MWCNTs were not oriented along the injection direction, which contributed to the formation of conductive networks. The conductive properties of the MWCNTs played the best effect at this time, and the electrical resistivity of the composites was significantly improved with the increase of the MWCNT contents. However, from Fig. 4-7 (b), it was found that, although the dispersion of MWCNTs was not bad, some MWCNTs agglomerated with a combined size of 150–250 nm, hampering the formation of conductive networks.

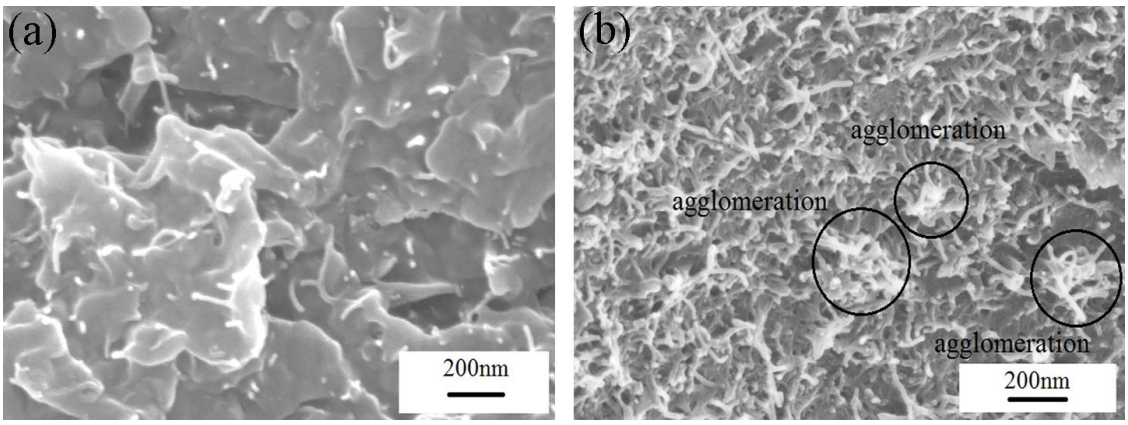

Fig. 4-7 SEM micrographs of the interior of (a) 5 wt.% MWCNT/PC composites and (b) 10 wt.% MWCNT/PC composites, which are prepared at the injection temperature of 330 ℃ and injection speed of 10 mm/s.

(d) Effect of injection speed on the electrical resistivity

The effect of the injection speed on the electrical resistivity of the composites with different MWCNT contents formed at different injection temperatures was investigated

and the obtained results are shown in Fig. 4-8. From the four plots of electrical resistivity versus injection speed, for the 1 wt.% or 10 wt.% MWCNT composites, no matter what the injection temperatures were, even though the injection speed was increased from 10 mm/s to 80 mm/s (an 8-fold increase), the variation of electrical resistivity was slight, within 1 order of magnitude. For the resistivity variation tendency of the composites with 1 wt.% MWCNTs (Fig. 4-8 (a)), the changes of electrical resistivity were unobvious. This might be because when the MWCNT content was small (i.e., 1 wt.%) the percolation threshold had not been reached [29], the contact probability of MWCNT was low and conductive networks were not formed, thus the effect of the injection speed on the electrical resistivity was not noticeable. In addition, in the case of 10 wt.% MWCNT, the resistivity variation tendency of the composites with 10 wt.% MWCNTs (Fig. 4-8 (d)) was the same as that with 1 wt.%, and the variation was narrower. It was considered that even though the MWCNTs had reached the percolation threshold, the MWCNTs agglomerated and the inherent conductivity of MWCNT was hindered, thus the effect of the injection speed on the electrical resistivity was unobvious. Furthermore, when the MWCNT content was 2.5 wt.% or 5 wt.% (Fig. 4-8 (b) or (c)), the variation of surface resistivity with injection speed was strong. At the same injection temperature, the surface resistivity increased by 3 orders of magnitude as the 8-fold increase of injection speed. From the overall results, the electrical conductivity of the composites was improved under a lower injection speed and higher injection temperature, particularly in the case of 2.5 wt.% and 5 wt.% MWCNTs composites.

In general, according to the formation mechanism of the internal microstructure, in the case of the same injection temperature, the formation of the composite specimen was affected by higher sheer stress under a higher injection speed, and the MWCNTs were easily oriented along the polymer flow direction, resulting in a decrease in the contact probability of the MWCNTs. Similarly, when the polymer filled into the die cavity, the chance of CNT breakage was increased at high injection speed, which would

lead to attenuating the probability of the formation of the conductive network [30]. Consequently, the electrical conductivity of the composites was decreased. However, regarding the percolation phenomenon, when the MWCNT content was below 5 wt.%, the effect of the internal microstructure on the electrical resistivity was noticeable.

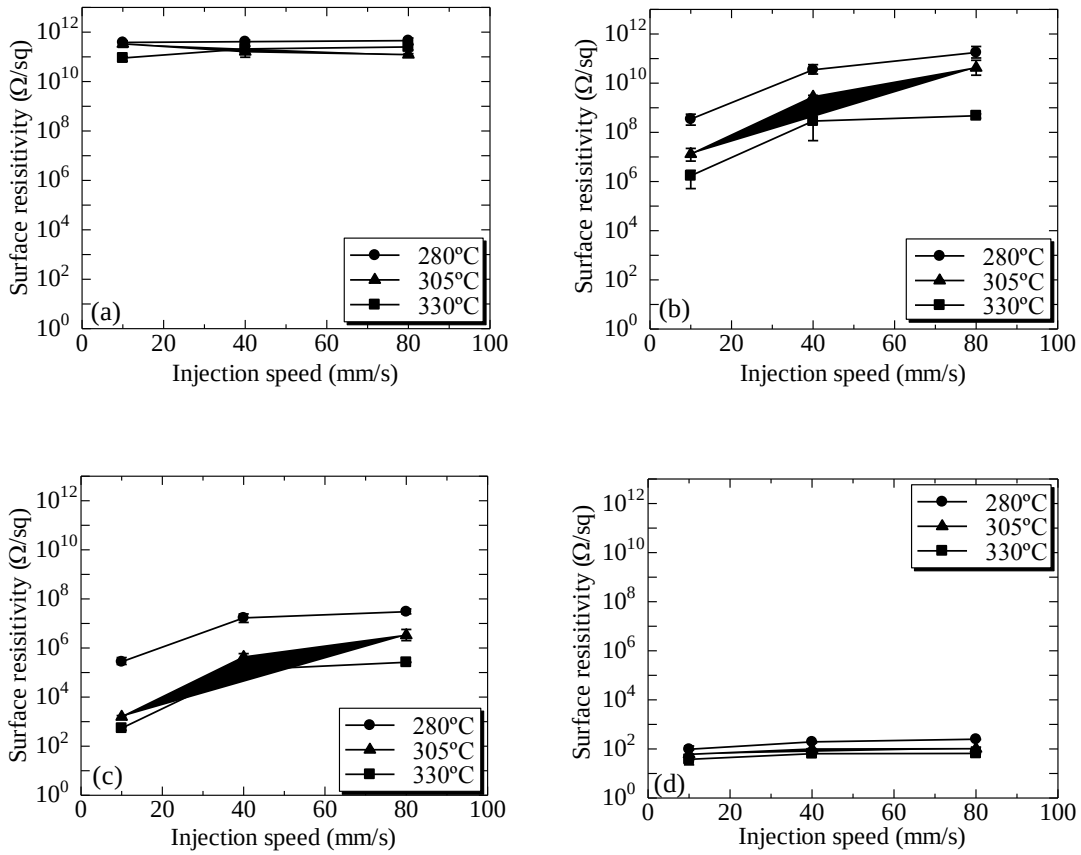

Fig. 4-8 Effect of injection speed on surface resistivity of the MWCNT/PC composites with (a) 1 wt.% MWCNT, (b) 2.5 wt.% MWCNT, (c) 5 wt.% MWCNT, (d) 10 wt.% MWCNT.

Fig. 4-9 (a) and (b) show SEM micrographs of fractured surfaces of the 2.5 wt.% MWCNTs composites prepared at injection speed of 10 mm/s and 80 mm/s, respectively. Comparing the two micrographs showed that when the injection speed was increased from 10 mm/s to 80 mm/s, the changes of the MWCNT dispersion were observed, and

the microstructures were markedly different. When the injection speed was low (i.e., 10 mm/s, Fig. 4-9 (a)), conductive networks formed. While the injection speed was high (i.e., 80 mm/s, Fig. 4-9 (b)), many small white dots (i.e., MWCNTs) were observed. It was considered that the MWCNTs were oriented in the injection direction. Therefore, injection speed could easily affect the internal microstructure of the composite specimens, resulting in a large variation in electrical resistivity between the two composite specimens.

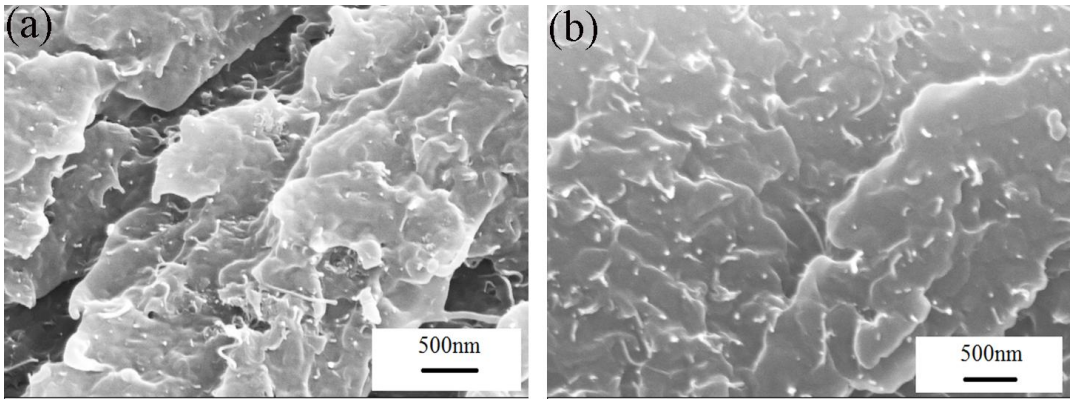

Fig. 4-9 SEM micrographs of the fractured surfaces of the 2.5 wt.% MWCNT/PC composites obtained at the injection temperature of 280 ℃ with (a) the injection speed of 10 mm/s and (b) the injection speed of 80 mm/s.

(e) Effect of injection temperature on the electrical resistivity

The effects of the injection temperature on the surface resistivity of the composites with various MWCNT contents prepared at different injection speeds are shown in Fig. 4-10. In Fig. 4-10 (a), when the MWCNT content was small (i.e., 1 wt.%), no matter the injection speed was, even if the injection temperature was increased by 50 ℃ (in the range from 280 ℃ to 330 ℃), the variation of surface resistivity was small, in the range of 10^{10}–10^{11} Ω/sq. Besides, Fig. 4-10 (d) shows the similar case as the previously mentioned, the variation of surface resistivity for the 10 wt.% MWCNTs composite was slight, the surface resistivity was decreased by only 1 order of magnitude (the same as previously mentioned for the influence of injection speed). This demonstrated that

regardless of the injection temperature and injection speed, the variation of surface resistivity of the 1 wt.% or 10 wt.% MWCNTs composites was within 2 orders of magnitude. Namely, when the MWCNT content was too small or too large, the effect of the injection temperature on the electrical resistivity was not noticeable. In contrast, when the MWCNT content was 2.5 wt.% or 5 wt.% (Fig. 4-10 (b) or (c)), the electrical resistivity was easily affected by the injection temperature. For example, the surface resistivity of the 2.5 wt.% MWCNTs composites was in the range of 10^6–10^{11} Ω/sq, and the surface resistivity of the 5 wt.% MWCNTs composites was in the range of 10^2–10^7 Ω/sq, both varying by 5 orders of magnitude. This meant no matter what the injection temperatures and injection speeds were, compared with that of the composites with 1 wt.% MWCNTs, the variation of electrical resistivity of the composites with 2.5 wt.% or 5 wt.% MWCNTs was obvious. It was considered that the injection temperature would change the internal microstructure of the composites and this greatly affected the electrical resistivity of the composites, and the higher injection temperature was favorable for obtaining lower resistivity.

Moreover, comparing the electrical resistivity plots showed that at a high injection temperature and low injection speed (i.e., 330 ℃ and 10 mm/s), the composites were superior to those prepared by other injection conditions, especially a low injection temperature and high injection speed (i.e., 280 ℃ and 80 mm/s). This improvement was attributed to the distinctive microstructure of the composites at high injection temperature and low injection speed, which contributed to the favorable dispersion of MWCNTs for improving the electrical conductivity of PC. Therefore, composites with various electrical resistivities could be prepared through changing the injection temperature and injection speed.

In general, during injection molding, while a die is being filled with a high temperature molten state polymer, a three-layer structure of a skin layer, an intermediate layer and a core layer will be formed from the surface to the inside with different orientations or dispersions [31]. The skin layer is formed by the high temperature

molten state polymer contacting with the cold die and then quickly cooling. The intermediate layer is formed by the molten polymer flowing into the die and at the same time experiencing a high shear stress, so that the molecular chains and microscopic structures are more easily orientated. The core layer is formed by the polymer slowly cooling at the end of the filling, so the anisotropy of the core layer microstructures is low [32].

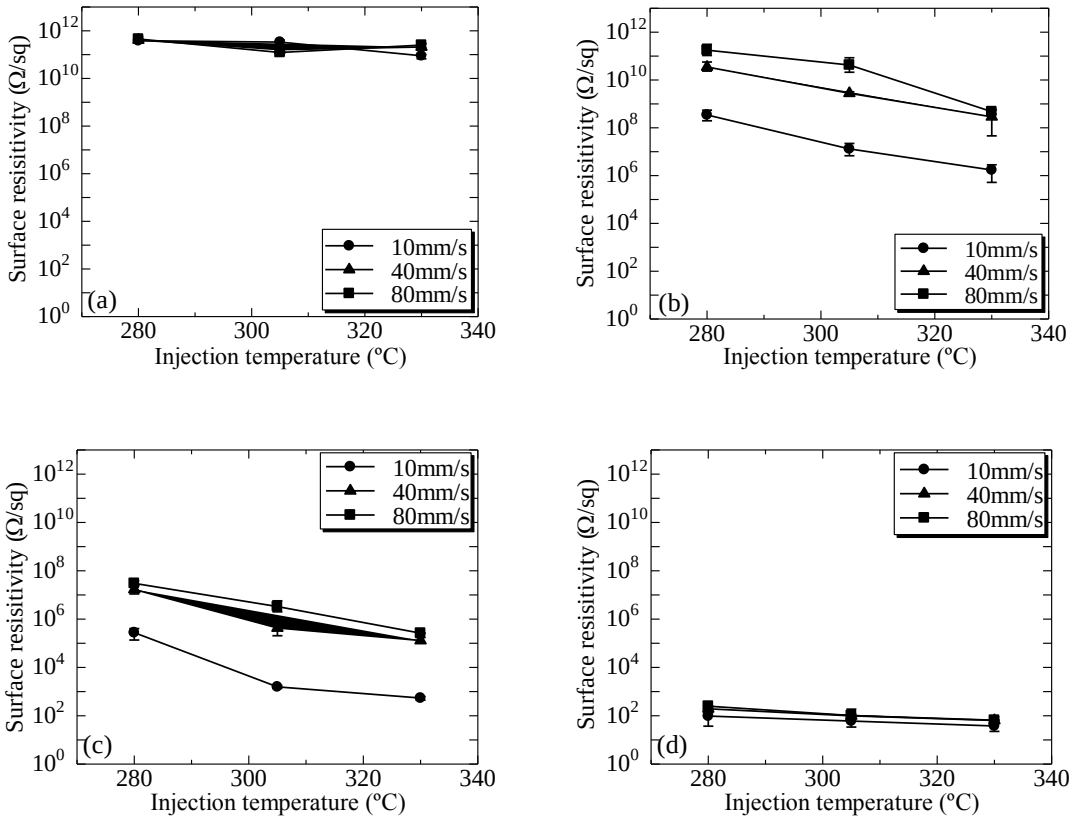

Fig. 4-10 Effect of injection temperature on surface resistivity of the MWCNT/PC composites with (a) 1 wt.% MWCNT, (b) 2.5 wt.% MWCNT, (c) 5 wt.% MWCNT, (d) 10 wt.% MWCNT.

Fig. 4-11 shows an SEM image of the fractured surface of the 2.5 wt.% MWCNTs composite prepared at an injection temperature of 330 ℃ and injection speed of 10 mm/s. Comparison of Fig. 4-11 with Fig. 4-9 (a), which is a specimen with 2.5 wt.%

MWCNTs prepared at the same injection speed, but using a different injection temperature (i.e., 280 ℃), showed that although the MWCNT contents of the two specimens were both small, and MWCNTs were distributed on the fractured surfaces, no obvious difference was observed between the two micrographs. In addition, according to the formation mechanism of the internal microstructure during injection molding, when the injection temperature was lower, the viscosity of the molten polymer was higher. At the same injection speed, if the injection temperature was low (e.g., 280 ℃), when the polymer filled into the die, the solid fibrous MWCNTs were affected by high sheer stress, thus MWCNTs were easily orientated along the flow direction of polymer and the contact probability between MWCNTs was lower. Consequently, during the injection molding process, it was considered that the change of injection temperature would cause a difference in the internal microstructure, resulting in a variation of electrical conductivity of the composite.

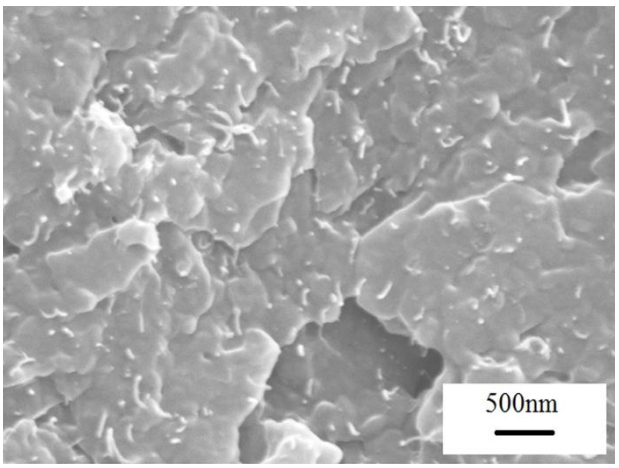

Fig. 4-11 SEM image of the fractured surface of the 2.5 wt.% MWCNT/PC composite obtained at the injection temperature of 330 ℃ and injection speed of 10 mm/s.

In addition, Fig. 4-12 shows the SEM micrographs of 5 wt.% MWCNT composites obtained at different injection conditions. It is obviously seen that when the injection temperature was 280 ^{o}C and injection speed was 80 mm/s, MWCNTs were pulled out to

be visible distinctly and dispersed unevenly in the matrix and thus the conductive paths weren't formed, resulting in the higher electrical resistivity of MWCNT/PC composites. However, when the injection temperature was 330 ^{o}C and injection speed was 10 mm/s, MWCNTs weren't pulled out and dispersed evenly, playing a key role to form the conductive paths in the matrix, and hence the electrical resistivity of MWCNT/PC composites was lower, below 10^3 Ω/sq. Overall, the higher injection temperature and lower injection speed was favorable for obtaining lower electrical resistivity.

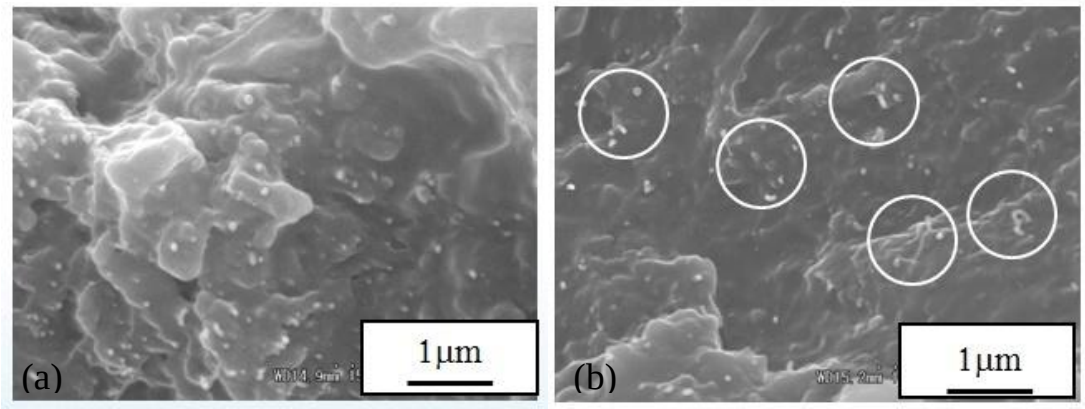

Fig. 4-12 SEM micrographs of MWCNT/PC composites with 5 wt.% MWCNTs: (a) injection temperature: 280 ^{o}C, injection speed: 80 mm/s, (b) injection temperature: 330 ^{o}C, injection speed: 10 mm/s.

Overall, in the same change range of the injection temperature, the effect of injection temperature on the electrical resistivity of 2.5 wt.% and 5 wt.% MWCNTs composites differed more greatly from that of 1 wt.% and 10 wt.% MWCNTs composites. This was considered to be the effect of the percolation phenomenon. In the percolation phenomenon, when the content of conductive filler reaches the percolation thresholds, the filler species are in close contact with each other and they form a conductive network in the system to enhance the electrical conductivity [33]. Therefore, under the current experimental conditions in this work, the MWCNT content over 5 wt.% might be achieved or exceeded the percolation thresholds, and thus even if the

MWCNT contents had some changes, there was not a huge impact on the formation of the conductive network. In other words, when the MWCNT content was beyond a certain value (e.g., 10 wt.%), even though the injection conditions were changed, the variation of the electrical resistivity was not obvious. Therefore, the electrical resistivity had a very strong dependence on the orientation and alignment of CNTs in the PC [34], and there was a great impact on the electrical resistivity from the difference of injection molding conditions.

(f) Effect of surface roughness on the electrical resistivity

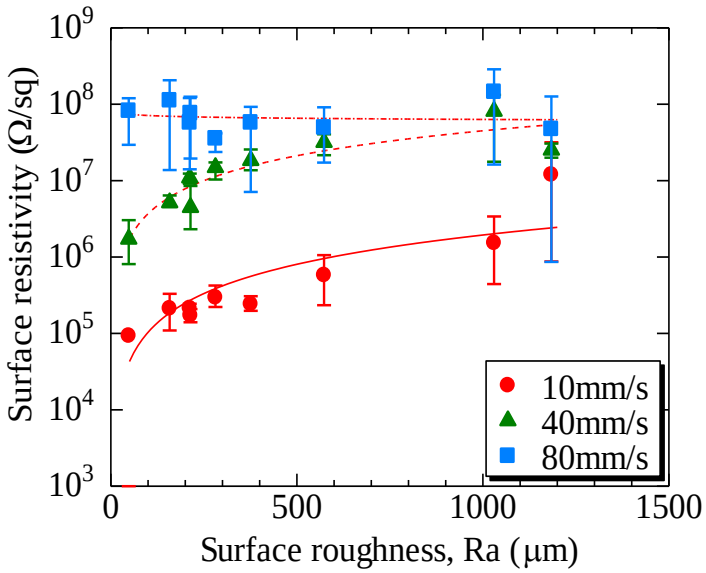

Fig. 4-13 Effect of the surface roughness on surface resistivity of the 3 wt.% MWCNT composites prepared at an injection temperature of 280 ℃.

The relationship between the surface roughness and the surface resistivity was examined and the results are shown in Fig. 4-13 (i.e., 280 ℃). From the overall results, when the surface roughness was Ra≤500 μm, the electrical resistivity changed considerably with the variation of surface roughness in the parallel direction; but once the surface roughness exceeded 500 μm (i.e., Ra＞500 μm), the variation of electrical resistivity was small. These phenomena implied that it was necessary to pay particular attention to the effect of surface roughness on the resistivity electrical measurement.

Therefore, all the specimen surfaces were ground using fine emery paper (#1000) firstly and then polishing with abrasive agent to avoid the effect of the surface roughness. The electrical resistivity was measured whenever the specimen was ground to a certain thickness and polished.

(g) Distribution of electrical resistivity from surface to core

Different electrical resistivities of the composites are likely related to the difference in dispersibility of the MWCNTs [35]. The formation mechanism of the composites specimens during the injection molding indicates that the microstructures of the specimen are most easily affected by the injection conditions. In this part of the work, the distributions of the surface resistivity along a distance from the composite surface to core were measured to examine the effect of the injection conditions on the distribution of the electrical resistivity. Prior to the measurement of electrical resistivity, all specimen surfaces were ground using fine sandpaper and polished with an abrasive agent to avoid the surface roughness effects. The electrical resistivity of the composite was measured each time a certain thickness (i.e., 50 μm) was ground off the specimen and polished.

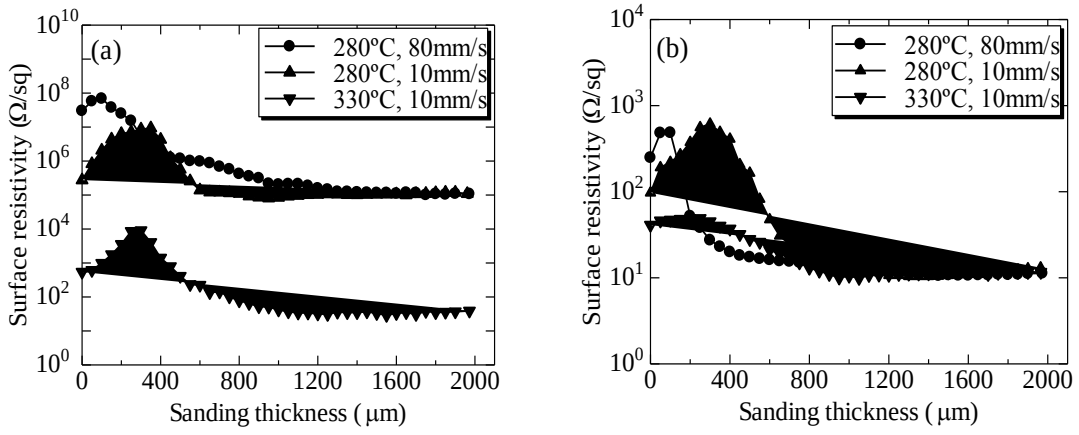

Fig. 4-14 Distributions of surface resistivity of the MWCNT/PC composites with (a) 5 wt.% MWCNT and (b) 10 wt.% MWCNT.

Fig. 4-14 shows the electrical resistivity distributions of the 5 wt.% and 10 wt.% MWCNTs composites prepared at different injection conditions. Overall, regardless of the injection conditions and the MWCNT content, the electrical resistivity of the composites dramatically increased with the increase in distance from the surface to a maximum value. After having reached this maximum value, the electrical resistivity gradually decreased and at an interior distance of 1000 μm retained a constant value.

For the composite with 5 wt.% MWCNTs (Fig. 4-14 (a), injection temperature of 280 ℃), as the injection speed was increased (from 10 increased to 80 mm/s), the surface resistivity increased by 2 orders of magnitude. The position of the maximum resistivity value varied, and it was observed that with a lower injection speed, the maximum resistivity value was closer to the specimen surface. At a distance of ~1000–2000 μm from the composite surface, the order of magnitude of the electrical resistivity was the same, approximately 10^5 Ω/sq. As for the effect of the injection temperature, at an injection speed of 10 mm/s, when the injection temperature was increased by 50 ℃ (from 280 ℃ to 330 ℃), the surface resistivity integrally dropped by approximately three orders of magnitude and the internal electrical resistivity also differed by 3 orders of magnitude. It was hypothesized that when the MWCNT content was 5 wt.%, which might reach the percolation threshold, the electrical resistivity of the core layer was easily affected by the injection temperature, and the MWCNTs were oriented easily in the PC matrix under low injection temperatures.

However, for the 10 wt.% MWCNTs composite (Fig. 4-14 (b)), at the same injection temperature, as the injection speed was increased 8-fold, the variation of the electrical resistivity was small, even though the position of the maximum resistivity value was different, the order of magnitude of the electrical resistivity was in the same range. In addition, the distribution of electrical resistivity was within 1 order of magnitude in the case of injection temperature of 330 ℃ and injection speed of 10 mm/s. Moreover, even though the injection temperature was increased from 280 ℃ to 330 ℃, the maximum values of electrical resistivity were only differed by 1 order of

magnitude. Comparing Fig. 4-14 (a) and (b) with each other, the electrical resistivity of the 5 wt.% MWCNTs composite (i.e., 330 ℃ and 10 mm/s) and that of the 10 wt.% MWCNTs composite (i.e., 280 ℃ and 80 mm/s) had no significant difference in the order of magnitude. This also indicated that a lower injection speed and a higher injection temperature were very effective in the improvement of the electrical conductivity.

For all composites specimens, the distribution of electrical resistivity from the specimen surface to the core consisted of three regions of increasing, decreasing, and constant resistivity. It was hypothesized that this trend was attributed to the formation mechanism of the internal microstructure during injection molding. For the region of the sharp increase in the electrical resistivity, the composites were solidified quickly and the MWCNTs were affected by sheer stress to orient along the flow direction of the polymer. For the regions where the electrical resistivity decreased or remained constant, the polymer stopped flowing and MWCNTs were randomly dispersed, finally the hot polymer solidified and then the core layer was formed. It was considered that the formation of electrical networks was associated with the injection conditions, which subsequently affected the electrical resistivity.

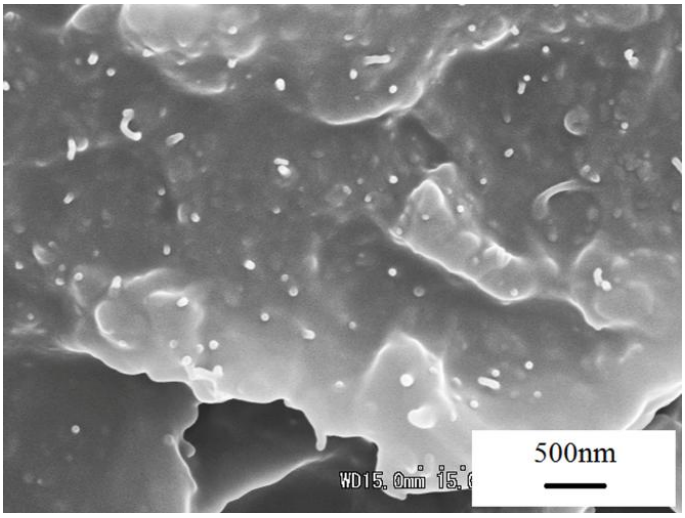

Fig. 4-15 SEM image of the core layer of the 5 wt.% MWCNT/PC composite prepared at the injection temperature of 280 ℃ and injection speed of 10 mm/s.

Fig. 4-15 shows an SEM image of the core layer of a MWCNT/PC composite with 5 wt.% MWCNTs (i.e., 280 ℃ and 10 mm/s). Comparing Fig. 4-15 with Fig. 4-7 (a), the MWCNTs were both dispersed well, but many small white dots and few networks could be observed in Fig. 4-15. It was realized that when the injection temperature was low, the composite specimens were solidified quickly and the MWCNTs were affected by high sheer stress to orient along the flow direction of the PC. In Fig. 4-7 (a), more MWCNTs were observed, there was no obvious orientation of the MWCNTs, and electrical networks had formed. Therefore, when the MWCNT content reached the percolation threshold, the internal microstructure was easily affected by the injection conditions, and the orientation of the MWCNTs under a low injection temperature was higher than that of the MWCNTs under a high injection temperature.

4.4 Conclusions

In this study, the effects of the MWCNT content and injection conditions on the electrical resistivity of the MWCNT/PC composites were investigated. The obtained results can be summarized as follows:

(1) The electrical resistivity of the MWCNT/PC composites with 5 wt.% MWCNTs considerably decreased down to 10^2 Ω/sq in the case of an injection temperature of 330 ℃ and injection speed of 10 mm/s, and the electrical resistivity was ~15 orders of magnitude lower than that of PC.

(2) The electrical properties of the MWCNT/PC composites with 2.5 wt.% or 5 wt.% MWCNTs were more easily affected by the injection conditions. In addition, a lower injection speed and a higher injection temperature (i.e., 330 ℃ and 10 mm/s) were conducive to obtaining the MWCNT/PC composite with lower electrical resistivity.

(3) The distribution of the electrical resistivity from the surface to the core had three regions exhibiting increasing, decreasing, and constant behaviors. It was known that not only the injection conditions but also the heat dissipation rate would

affect the value of the maximum electrical resistivity and the position where the maximum electrical resistivity occurred. Basically, the observed phenomena were due to the formation mechanism of the internal microstructures of the MWCNT/PC composites during injection molding.

References

[1] The Institute of Electrostatics Japan, Seidenki handbook, Ohmsha. Ltd., Japan, (1998) 365-383.

[2] M. Futazawa. Seidenki Kannrigijuku no Kiso, Plastics Age Co., Ltd., Japan, (2009) 25-65.

[3] M. Arjmand, T. Apperley, M. Okoniewski and U. Sundararaj. Comparative Study of Electromagnetic Interference Shielding Properties of Injection Molded Versus Compression Molded Multi-walled Carbon Nanotube/Polystyrene Composites. Carbon 50 (2012) 5126-5134.

[4] M. Arjmand, M. Mahmoodi, G.A. Gelves, S. Park and U. Sundararaj. Electrical and Electromagnetic Interference Shielding Properties of Flow-induced Oriented Carbon Nanotubes in Polycarbonate. Carbon 49 (2011) 3430-3440.

[5] S.M. Yuen, C.C.M. Ma, C.Y. Chuang, K.C. Yu, S.Y. Wu, C.C. Yang and M.H. Wei. Effect of Processing Method on the Shielding Effectiveness of Electromagnetic Interference of MWCNT/PMMA Composites. Comp Sci Technol. 68 (2008) 963-968.

[6] A. Thionnet, H.Y. Chou and A. Bunsell. Fibre Break Failure Processes in Unidirectional Composites. Part 1: Failure and Critical Damage State Induced by Increasing Tensile Loading. Appl. Compos. Mater. 22 (2015) 119-140.

[7] M.A. Bily, Y.W. Kwon and R.D. Pollak. Study of Composite Interface Fracture and Crack Growth Monitoring Using Carbon Nanotubes. Appl. Compos. Mater. 17 (2010) 347-362.

[8] M. Naebe, C. Hurren, A. Maazouz, K. Lamnawar and X. Wang. Improvement in Mechanical Properties of Aluminum Polypropylene Composite Fiber. Fibers and Polymers 10 (2009) 662-666.

[9] D. Tasis, N. Tagmatarchis, A. Bianco and M. Prato. Chemistry of Carbon Nanotubes. Chem. Rev. 106 (2006) 1105-1136.

[10] S. Wang, R. Liang, B. Wang and C. Zhang. Covalent Addition of Diethyltoluenediamines onto Carbon Nanotubes for Composite Application. Polym. Compos. 30 (2009) 1050-1057.

[11] L. Meng, C. Fu and Q. Lu. Advanced Technology for Functionalization of Carbon Nanotubes. Progress in Natural Science 19 (2009) 801-810.

[12] N. Tekin, S.K. Beyaz, A. Kara, E. Simsek, F.D. Lamari, G. Cakmak and H.Y. Guney. The Synthesis of Covalent Bonded Single-walled Carbon Nanotube/Polyvinylimidazole Composites by in Situ Polymerization and Their Physical Characterization. Polymer Composites 33 (2012) 1255-1262.

[13] S. Xu, A. Akchurin, T. Liu, W. Wood, X.W. Tangpong, I.S. Akhatov and W.H. Zhong. Mechanical Properties, Tribological Behavior, and Biocompatibility of High-density Polyethylene/Carbon Nanofibers Nanocomposites. Journal of Composite Materials 49 (2015) 1503-1512.

[14] Y.Y. Leu, Z.A. Mohd Ishak and W.S. Chow. Mechanical, Thermal, and Morphological Properties of Injection Molded Poly(lactic acid)/SEBS-g-MAH/ Organo-Montmorillonite Nanocomposites. J Appl Polym Sci. 124 (2012) 1200-1207.

[15] G.R. Kasaliwal, S. Pegel, A. Goldel, P. Potschke and G. Heinrich. Analysis of Agglomerate Dispersion Mechanisms of Multiwalled Carbon Nanotubes during Melt Mixing in Polycarbonate. Polymer 51 (2010) 2708-2720.

[16] T. Villmow, P. Potschke, S. Pegel, L. Haussler and B. Kretzschmar. Influence of Twin-screw Extrusion Conditions on the Dispersion of Multi-walled Carbon Nanotubes in a Poly (lactic acid) Matrix. Polymer 49 (2008) 3500-3509.

[17] M. Lee, H. Jeon, B.H. Min and J.H. Kim. Morphology and Electrical Properties of Polymethylmethacrylate/Poly(styrene-co-acrylonitrile)/Multi-walled Carbon Nanotube Nanocomposites. Journal of Applied Polymer Science 121 (2011) 743-749.

[18] J. Qiu, M. Kawagoe, W. Mizuno, M. Morita, T. Kumazawa and Y. Takahashi.

Combined Effects of Rolling and Blending with Liquid Crystalline Polyester on the Fatigue Properties of Polypropylene under High Rolling Ratio (in Japanese). Kobunshi Ronbunshu 58 (2001) 427-434.

[19] J. Qiu. Microstructure and Tensile Property of Cold Rolled PP/LCP Blends (in Japanese). Transactions of the Japan Society of Mechanical Engineers (A) 67 (2001) 1458-1463.

[20] J. Qiu. Effect of the Stress Amplitude on the Inner Structure and Fatigue Fracture Property of PP/LCP Polymer Blends (in Japanese). Transactions of the Japan Society of Mechanical Engineers (A) 68 (2002) 266-272.

[21] P. Liu. Modifications of Carbon Nanotubes with Polymers. European Polymer Journal 41 (2005) 2693-2703.

[22] H. Ikeda and Y. Seinoh. Flow Induced Fiber Orientation in the Moldings of Potassium Titanate Fiber/Polystyrene Composites (in Japanese). Seikei-Kakou (The Journal of JSPP) 1 (1989) 197-204.

[23] K. Kato, Y. Zhang and N. Otake. Numerical Analysis of Fiber Orientation and Velocity Distribution in Slit Channel Flow of Concentrated Short Fiber Composites (in Japanese). Seikei-Kakou (The Journal of JSPP) 11 (1999) 847-855.

[24] J. Qiu, M. Kawagoe, W. Mizuno and M. Morita. Enhancement of Resistance to Fatigue in Polypropylene/Liquid Crystalline Polyester Blends by Rolling Process (in Japanese). Kobunshi Ronbunshu (The Journal of JSPP) 56 (1999) 151-158.

[25] J. Qiu. Changes of the Microstructure and Mechanical Properties in the Flow Direction of Injection-molded Polypropylene Sheet (in Japanese). Kobunshi Ronbunshu (The Journal of JSPP) 62 (2005) 50-54.

[26] J. Qiu, M. Kawagoe, W. Mizuno and M. Morita. Microstructure and Fatigue of Injection-molded PP Sheets (in Japanese). Transactions of the Japan Society of Mechanical Engineers (A) 63 (1997) 2105-2113.

[27] J. Qiu, L. Wang, K. Uchiya and E. Sakai. Effects of Injection Molding Conditions on the Electrical Properties of Polycarbonate/Carbon Nanotube Nanocomposites.

Polymer Composites (2015), DOI: 10.1002/ pc.23523.

[28] A. Ameli, P.U. Jung and C.B. Park. Electrical Properties and EMI Shielding Effectiveness of Polypropylene/Carbon Fiber Composite Foams. Carbon 60 (2013) 379-391.

[29] P. Potschke, A. R. Bhattacharyya and A. Janke. Melt Mixing of Polycarbonate with Multiwalled Carbon Nanotubes: Microscopic Studies on the State of Dispersion. Eur. Polym. J. 40 (2004) 137-148.

[30] A. Ameli, P.U. Jung and C.B. Park. Through-Plane Electrical Conductivity of Injection-Molded Polypropylene/Carbon Fiber Composite Foams. Composites Science and Technology 76 (2013) 37-44.

[31] J. Qiu. Effects of Flow Distance and Injection-modeled Speed on the Fatigue Property of Injection-Molded Polypropylene Sheet (in Japanese). Kobunshi Ronbunshu (The Journal of JSPP) 62 (2005) 425-431.

[32] J. Qiu, M. Kawagoe, W. Mizuno, M. Morita and T. Miyati. Changes of Microstructure and Mechanical Properties of Injection-Molded Polypropylene Sheets by Rolling Process (in Japanese). Kobunshi Ronbunshu (The Journal of JSPP) 54 (1997) 778-784.

[33] T. Odagaki. The Science of Percolation. Shokabo Publishing Co., Ltd., Japan, (1993) 1-5.

[34] J. Guo, Y. Liu, R. Prada-Silvy, Y. Tan, S. Azad, B. Krause, P. Pötschke and B. P. Grady. Aspect Ratio Effects of Multi-walled Carbon Nanotubes on Electrical, Mechanical, and Thermal Properties of Polycarbonates/MWCNT Composites. Journal of Polymer Science: Part B: Polymer Physics 52 (2014) 73-83.

[35] B. Krause, M. Mende, P. Potschke and G. Petzold. Dispersability and Particle Size Distribution of CNTs in an Aqueous Surfactant Dispersion as a Function of Ultrasonic Treatment Time. Carbon 48 (2010) 2746-2754.

Chapter 5 Polylactic acid-based conductive composites by a cold rolling process

5.1 Introduction

According to our previous studies, the MWCNT/PC composites are not suitable for rolling processing, due to the strong hygroscopicity of the PC. To improve the possibility of second stage processing method and expand the composite applications, we use a new polymer which is easy to process instead of the original matrix material (i.e., PC), and expect to prepare a new-style composite with better mechanical properties (especially the ductility).

In recent years, recycling is one of the most important technologies to conserve resources and to reduce waste. For this purpose, the biodegradable polymer has attracted more and more interests as an alternative matrix material. Out of these polymers, Polylactic acid (PLA) is considered as one of the most promising biodegradable compostable, thermoplastic, and crystalline polymer. Additionally, PLA can be derived from renewable resources such as starch and is a sustainable alternative to petrochemical-derived products [1]. PLA is a well-studied environmental friendly polymer because of its good strength and stiffness [2-4] and is being used in several applications [5-7]. Therefore, it is considered that PLA as an environmentally friendly polymer could replace traditional polymers in potential industrial applications. However, because PLA belongs to the group of brittle material, to improve its ductility and extend its industrial applications, many researchers have proposed various methods to increase its ductility while maintaining or reinforcing its original strength. Unfortunately, the effect was not as good as expected [8].

Additionally, as the conductive filler—CNT, literature reviews indicated that the matching between the solubility parameter (SP) of CNT and the polymer matrix is propitious to achieve higher electrical conductivity in CNT/polymer composites [9].

According to some literatures, the SP of CNT is approximately 17.8 $MPa^{1/2}$ [9-11], while the SP of PLA is approximately 18.5 $MPa^{1/2}$ [12, 13]; their SP values are similar, which will result in continuous conductive pathways and good compatibility, leading to the achievement of a high electrical conductivity and good mechanical properties.

Commonly, injection molding, extrusion molding, blow molding and rolling molding are available for composite preparation. Moreover, it is well known that microstructures, including the crystalline structure, molecular orientation, and crystallinity, can affect the mechanical properties of crystalline polymers. Some researchers have attempted to take advantage of the molecular chain orientation of polymer during extending to improve the mechanical properties of degradable polymer through various molding processes [14-19]. Many researchers have reported that plastic processing, such as die-drawing [20], roller drawing [21], tensile drawing [22], equal channel angular extrusion [23], hydrostatic extrusion [24], and the rolling process [25], can achieve good mechanical properties. In particular, the rolling process can achieve high molecular orientation for polymers, while preventing the generation of voids during processing, which has been reported by Nakayama et al. [26]. Therefore, the rolling process has been extensively employed for producing polymers with good properties, such as polyethylene (PE) [27], polyoxymethylene (POM) [28], polypropylene (PP), [29] and others. Both Qiu et al. [30] and Murata et al. [19] investigated the changes of morphology and mechanical property in molded polymers. During plastic processing, a multilayer structure will form because of the different cooling processes on the surface as well as in the inner part [31]. Moreover, the crystallinity is decreased and the molecular orientation is increased by the rolling process, as observed with micro Fourier transform infrared (FT-IR) spectroscopy [32]. These researchers obtained the internal structure information in the whole cross section of the polymer and accurately assessed the change of the PP microstructure via the rolling process. To the best of our knowledge, there has been no research conducted on the effect of crystallinity and orientation on microstructures (i.e., crystal morphology, crystallinity, and molecular orientation) and mechanical properties of PLA produced by a

cold rolling process. Therefore, it is essential to know whether the rolling process changes the microstructure of PLA, which is key for improving the mechanical properties of PLA, especially its ductility.

In this study, the MWCNT/PLA conductive composites with various MWCNT contents (1–10 wt.%) were prepared by extrusion process followed by a cold rolling process. The effects of the rolling conditions on the mechanical and electrical properties of the prepared composites were investigated. Furthermore, like most other aliphatic polyesters, PLA presents a slower crystallization rate and variations in crystal structure and crystallinity after different molding processes [33, 34], as well as its orientation which strongly affects mechanical properties [35, 36]. Therefore, the variations of crystallization and orientation of the PLA composites prepared at different rolling ratios were also investigated by DSC, the density method and XRD, respectively. It offers an alternative green and easy solution to produce conductive MWCNT/PLA composites as an environmentally friendly CPC.

5.2 Experimental

5.2.1 Preparation of MWCNT/PLA composites

The compounding processes of MWCNT/PLA mater batches were manufactured using a twin screw extruder (KZX25TW-60MG-NH (-1200)-AKT, Technovel Co., Ltd, Japan), with a screw speed of 100 rpm, and the temperature profile was varied from 150 ℃ at the feeding zone to 190 ℃ (TP1) or 210 ℃ (TP2) at the die. The mixtures were vacuum-dried at 50 ℃ for 8 h prior to the process whereby the PLA and its composites were compounded with 0, 1, 3, 5 and 10 wt.% MWCNT contents, followed by the pelletizing step. All master batches were cooled down in a water bath and pelletized after the first extrusion process. The mechanical blending process conditions of prepared mater batches are presented in Table 5-1.

Then the prepared mater batches were dried at 50 ℃ for 8 h again prior to extrusion

process and the composite plates were produced by the same extruder. Temperature profile 3 (TP3) was designed with a low temperature level to prepare the MWCNT/PLA mater batches with 0, 1, 3 and 5 wt.% MWCNTs, whereas temperature profile 4 (TP4) was conceived to promote the fluidity of composite mater batches with high MWCNT content (i.e., 10 wt.%). The extrusion conditions refer to Table 5-2. Five different plates were produced under different processing conditions. A variation of MWCNT content, temperature profile, rotation speed and extrusion speed was executed (Table 5-3).

Table 5-1 Mechanical blending process conditions

	Heating zone (℃)						Rotation speed (rpm)
	C1	C2	C3	C4	H	SD/AD	
Temperature profiles 1 (TP1)	150	160	170	180	180	190	100
Temperature profiles 2 (TP2)	150	160	180	190	190	210	

Table 5-2 Temperature profiles TP3 and TP4 designed to perform different extrusion tasks

	Heating zone (℃)							
	C1	C2	C3	C4	H	SD/AD	SD1	SD2
Temperature profiles 3 (TP3)	150	160	170	180	180	190	180	180
Temperature profiles 4 (TP4)	150	160	180	190	190	210	180	180

Table 5-3 Extrusion molding conditions for preparing composite plates

No.	MWCNT content (wt.%)	Temperature profile	Rotation speed (rpm)	Extrusion speed (mm/s)
1	0	TP1, TP3	144	1.54
2	1	TP1,TP3	144	1.54
3	3	TP1,TP3	144	1.54
4	5	TP1,TP3	144	1.37
5	10	TP2,TP4	144	1.33

5.2.2 Rolling process and specimen preparation

The extruded plates were used for the rolling process under different rolling conditions. The rolling process was performed according to Table 5-4 with different rolling ratios to evaluate the effect of the rolling ratio on the properties and morphology of PLA and MWCNT/PLA composites. Because the ductility of the composites with different MWCNT contents had a certain difference, the maximum rolling ratio of the composites was different. 2000 mm (length) × 100 mm (width) × 1.2 mm (thickness; the maximum thickness was 1.6 mm) extruded plates were machined into specimens with dimensions of 100 mm (length) × 80 mm (width) × 1.2 mm (thickness; the maximum thickness was 1.6 mm) (shown in Fig. 5-1). The rolling process was carried out by a rolling machine (TKE-0; Imoto Machinery Co., Ltd., Tokyo, Japan) at room temperature (23±2 ℃) with a rotation speed of 3 m/min (shown as Fig. 2-10). The rolling direction was matched to the extrusion direction, and the effective width and diameter of each roller were 150 mm and 100 mm, respectively. The rolling ratio ξ was calculated using the following equations:

$$\xi = [(H_0 - H_1) / H_0] \times 100\% \quad (5\text{-}1)$$

where, H_0 – the initial thickness of the specimen (cm);

H_1 – the thickness of the rolled specimen, which was measured by a micrometer after the rolling process (cm).

Table 5-4 The rolling molding conditions for prepared composite plates

No.	MWCNT content (wt.%)	Rolling temperature (℃)	Rolling speed (m/min)	Rolling ratio (%)	Ambient humidity (%)
1	0	23 ±2	3	0, 20, 40, 60, 75	30 ±2
2	1	23 ±2	3	0, 20, 40, 60, 75	30 ±2
3	3	23 ±2	3	0, 20, 40, 60, 80	30 ±2
4	5	23 ±2	3	0, 20, 40, 60, 77	30 ±2
5	10	23 ±2	3	0, 20, 40, 60, 80	30 ±2

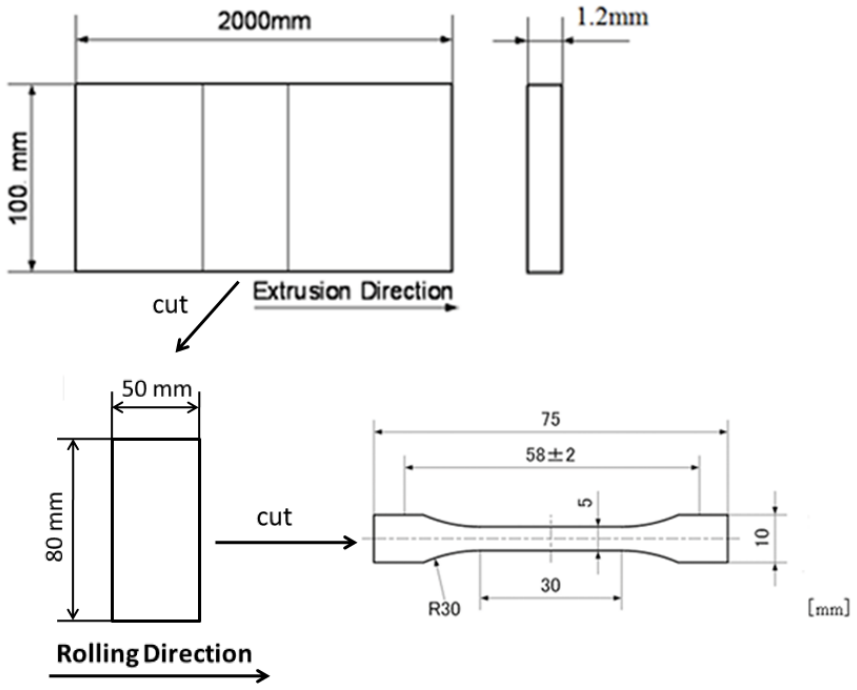

Fig. 5-1 The preparation of specimens.

Finally, the rolled plates were cut using a dumbbell-shaped mold to obtain specimens with dimensions of 75 mm (length) × 10 mm (width), but with different thicknesses based on the different rolling ratios, both in parallel to the rolling direction (i.e., 0 °) and vertical to the rolling direction (i.e., 90 °) (shown as Fig. 5-2). The different thicknesses of the rolled plates were achieved by adjusting the distance between the two

rollers (Fig. 2-9). The specimens were used for evaluation of the mechanical and electrical properties, and other characterizations.

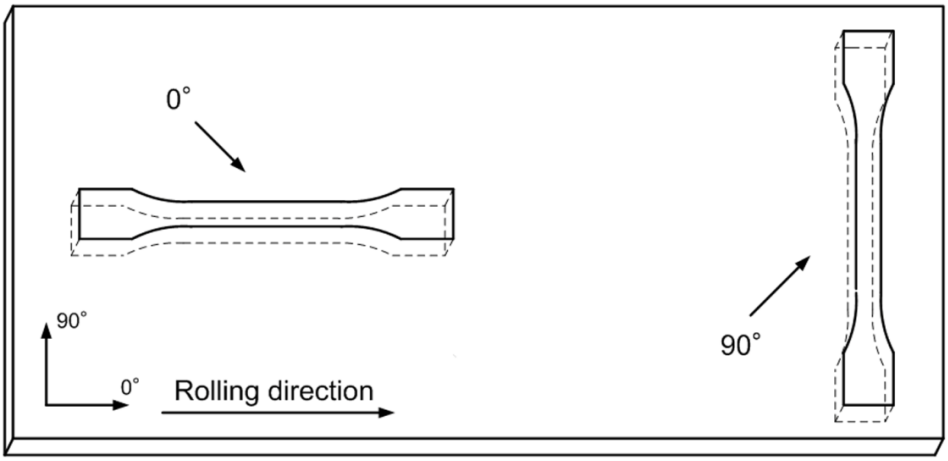

Fig. 5-2 The angle between the specimens and the rolling direction.

5.3 Results and discussions

5.3.1 Microstructures

(a) Variation of the internal structure of PLA

It is well known that different plastic processes will lead to the formation of a multilayer and different microstructures between the surface and the interior of the obtained polymer products [31]. Based on this view, the internal microstructures of unrolled and rolled PLA were investigated, and the morphologies are shown in Fig. 5-3.

Fig. 5-3 (a) shows a micrograph near the surface of unrolled PLA, and it is obvious that the structure, as well as the structure of Fig. 5-3 (b), showed a columnar microstructure. The size of the columnar microstructure was approximately 3–10 μm, while in the core layer, the size was approximately 5–12 μm, which was slightly larger than that of the surface. This may be because the surface layer was rapidly cooled, and only small size microstructures were formed during the extrusion process. And in the core layer (Fig. 5-3 (b)), columnar crystals with sizes of 5 μm could be clearly observed.

These phenomena might have resulted because the surface of the specimen was subjected to forces from the extruder during the extrusion process and was cooled rapidly in the air; thus the crystals were small. The impact on the interior was very small, leading to the differences between the surface and the interior of the specimen. Moreover, for the PLA with a low rolling ratio (i.e., ξ = 20%, Fig. 5-3 (c)), distinct changes in the microstructures of the interior were not observed compared to that of the unrolled PLA (Fig. 5-3 (b)), but the microstructures were destroyed slightly and became smaller than before. Unexpectedly, for the specimens with high rolling ratios (i.e., ξ = 40%, 60%, and 75%), the microstructures exhibited dramatic changes in the core layer. Most of the crystals were refined, but there were still unrefined parts, as shown in Fig. 5-3 (g). In Fig. 5-3 (d), columnar microstructures were mostly not observed, and the microstructures became very orderly. Furthermore, the size of these microstructures was smaller. This was because the surface of the specimen was subjected to a strong shear stress from the two rollers during the rolling process, resulting in the destruction of the original microstructures and crystal refinement; thus, the shape of the microstructures changed. A similar case can be observed in Fig. 5-3 (e) and (f), which shows the microstructure near the surface and the microstructure of the core layer of 60% rolled PLA. Regardless of the surface vicinity and core layer, the size of the microstructures was smaller than that of the unrolled PLA. It was considered that the microstructures from the surface to the core layer were completely refined under the high rolling ratio. Fig. 5-3 (g) shows the heart part of the 60% rolled PLA, and it was found that there were still some large microstructures in the heart part (this case was similar to the 40% rolled PLA, which was omitted in this paper). However, the range of the large microstructures was small (approximately 60 μm). It was considered that the rolling ratio was not too high to be refined completely. Moreover, these microstructures of the core layer were regularly arranged and orientated along the rolling direction. As the rolling ratio increased (Fig. 5-3 (h)), the microstructures were further refined in the core layer. This phenomenon might due to that PLA was a brittle polymer, and the original

columnar microstructures were completely destroyed by a strong shear stress and were further refined under a high rolling ratio (i.e., ξ = 75%).

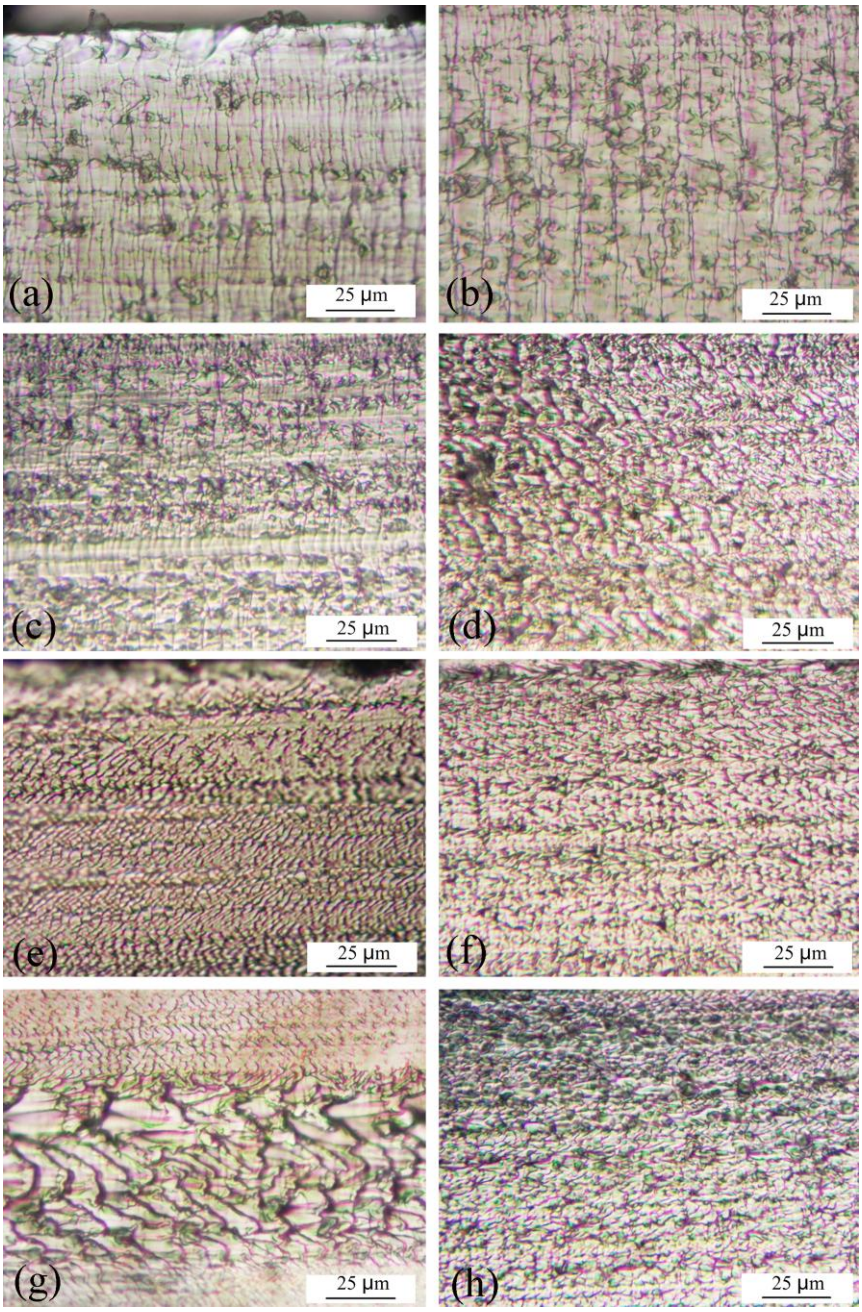

Fig. 5-3 Micrographs of PLA with different rolling ratios: (a) ξ: 0%, near the surface; (b) ξ: 0%, core layer; (c) ξ: 20%, core layer; (d) ξ: 40%, core layer; (e) ξ: 60%, near the surface; (f) ξ: 60%, core layer; (g) ξ: 60%, heart part and (h) ξ: 75%, core layer.

In general, plastic deformation occurred more easily on the specimen surface which

was in contact with the two rollers than in the core layer. The deformed layer was expanded as the rolling ratio increased. Furthermore, crystalline destruction and high molecular orientation occurred more easily in the case of high rolling ratios.

(b) Distribution and dispersion of the MWCNTs in PLA

As MWCNT contents in the PLA 1 wt.%, 3 wt.%, 5 wt.% and 10 wt.% were selected to investigate the distribution and dispersion of MWCNTs in the PLA matrix. Comparison with the four composite specimens, the investigation of MWCNT distribution and dispersion via optical microscopy revealed great differences in the remaining agglomerate size and number, as shown in Fig. 5-4.

The three composites containing 1 wt.%, 3 wt.% and 5 wt.% MWCNT processed with the same screw profile, temperature profile, and rotation speed (TP1, TP3 and 1.54 mm/s) indicated significantly a better distribution and a higher dispersion as compared to that of 10 wt.% MWCNT (TP2, TP4 and 1.33 mm/s). These differences are clearly reflected in the number of visible MWCNT agglomerates and their distribution in the PLA. In Fig. 5-4 (a), (b) and (c), it was clear that the number of MWCNT agglomerates in Fig. 5-4 (a) (1 wt.% MWCNT composite) was less than that of Fig. 5-4 (b) (3 wt.% MWCNT composite) and (c) (5 wt.% MWCNT composite), and the size of the agglomerates was approximately 5–10 μm, which was 2-fold smaller than that of the 3 wt.% and 5 wt.% MWCNT composites. Moreover, the difference in the remaining agglomerate size and number for 3 wt.% and 5 wt.% MWCNT composites was not obvious. Overall, for the composites with a low MWCNT content, the distribution and dispersion of MWCNT were both good. However, for the composite with higher MWCNT content, the size of MWCNT agglomerates was greater than others (approximately 30–50 μm), due to the excessive incorporation of MWCNT.

As aforementioned as the MWCNT/PC composites [14], Van der Waals attraction among tubes plays an important role in dispersing agglomerated nanofillers, as well as the effect of shear stress during extrusion process [37]. Therefore, excessive MWCNTs (i.e., 10 wt.%) would prevent an efficient transfer of their superior properties to the

polymer matrix. Besides, the observed differences in the distribution and dispersion were ascribed to differences in the flow properties of the melts. As the MWCNT content increased, the viscosity of the composites was increased, resulting in that the dispersed MWCNT in the PLA matrix was much greater in case of the higher MWCNT content which leaded to bigger MWCNT agglomerations.

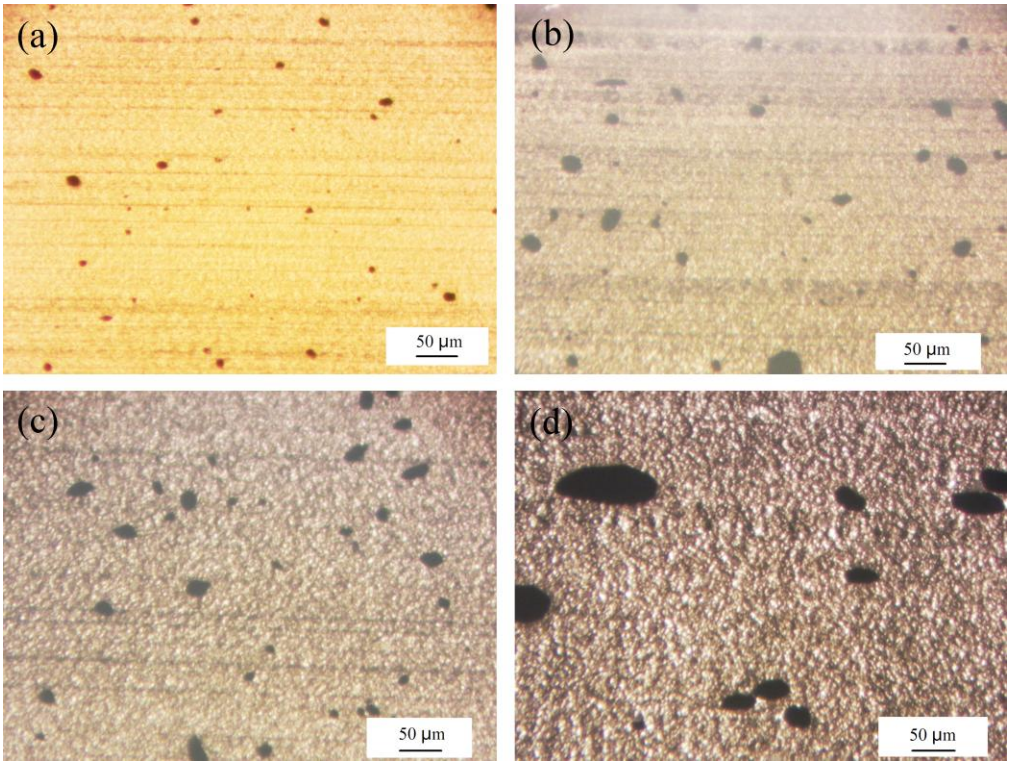

Fig. 5-4 Optical micrograph of the unrolled composites illustrating the effect of the MWCNT content on the macro dispersion of MWCNT in PLA: (a) 1 wt.% MWCNT; (b) 3 wt.% MWCNT; (c) 5 wt.% MWCNT and (d) 10 wt.% MWCNT.

5.3.2 Thermal behaviors

As a reinforced filler, CNT has been reported to enhance the thermal stability of the host polymer matrices [38, 39]. TGA and DTA curves of pure PLA and the MWCNT/PLA composites with 1 wt.% and 10 wt.% MWCNTs are illustrated in Fig. 5-5. In Fig. 5-5 (a), both pure PLA and the composites possessed single-stage

decomposition. For PLA, the thermal degradation of pure PLA started at around 302 ℃, and closured at approximately 380 ℃. The incorporation of 1 wt.% MWCNT exhibited no obvious changes in thermal stability compared with pure PLA; the thermal degradation temperature was around 300–385 ℃. However, when the MWCNT content increased to 10 wt.%, the degradation temperature had some decline (approximately 265–370 ℃). This behavior was attributed to the minor agglomerations and the breakage of MWCNTs [40], resulting in the excellent properties of MWCNT not being displayed. Moreover, it can be found that the residue weight fractions at 800 ℃ were all consistent with the additive amount of MWCNT (i.e., MWCNT content). As well, the DTA curves (Fig. 5-5 (b)) clearly showed thermal degradation temperatures of the PLA and its composites. Evidently, as the MWCNT content increased to 10 wt.%, the thermal degradation temperature was decreased by approximately 30 ℃.

Overall, the results confirmed that the compatibility between MWCNTs and PLA was good, and a proper incorporation of MWCNTs was a favorable method for maintaining good thermal properties of the PLA; however, excessive MWCNT would lead to the reduction on the original thermal properties of PLA, which was attributed to some MWCNT agglomerations in the PLA matrix.

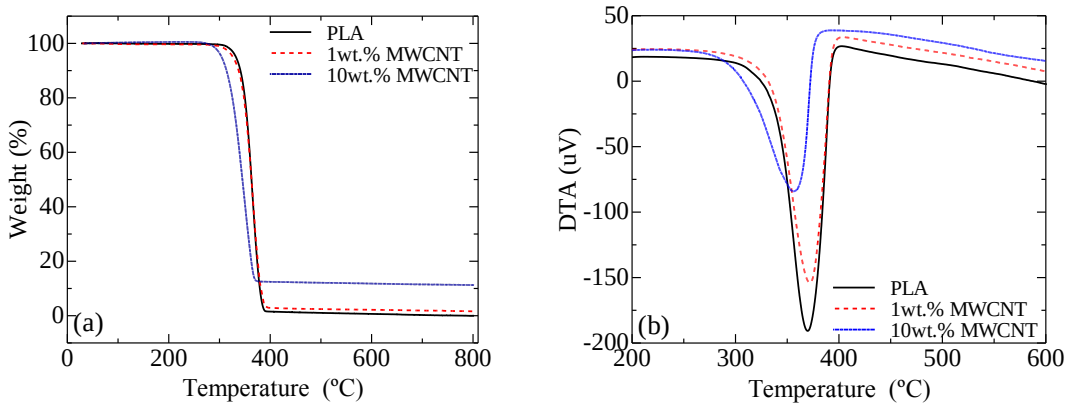

Fig. 5-5 TG and DTA curves of the unrolled composites.

5.3.3 Effect of the rolling ratio on the crystallization behaviors

(a) Variation of PLA

DSC measurements were carried out to investigate the effect of the rolling ratio on the crystallization behaviors of PLA and MWCNT/PLA composites, which was expected to affect their mechanical and electrical properties.

First, the variation of crystallization behavior for pure PLA was investigated. Fig. 5-6 shows the DSC curves of pure PLA for various rolling ratios. All specimens exhibited three distinct peaks, corresponding to the glass transition at approximately 60 ℃, cold crystallization at approximately 107–110 ℃, and melting at approximately 171–173 ℃. In other words, the thermal properties of the PLA were not distinctly changed during the rolling process. Moreover, it was interesting to note that there were double-melting peaks for the semi-crystalline PLA specimens after rolling at higher rolling ratios (e.g., ξ = 40%, 60% and 75%). Double-melting peaks, which were related mainly to the cooling rate, have been reported previously [41].

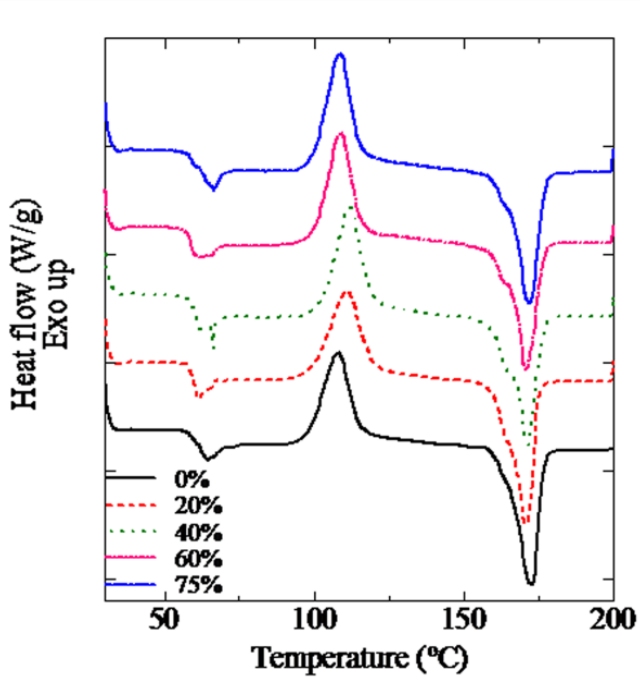

Fig. 5-6 DSC curves of unrolled and rolled PLA.

The crystallization and melting behaviors of the PLA were examined, and the glass-transition temperature (T_g), cold crystallization temperatures (T_c), melting temperature (T_m), melting enthalpy (ΔH_m), crystallization enthalpy (ΔH_c), and the degree of crystallization (χ_c) were obtained, as tabulated in Table 5-5. Obviously, the T_g was basically maintained at approximately 59 ℃, and the T_m was slightly decreased with the increase of the rolling ratio. However, the T_c first increased and then decreased as the rolling ratio increased, which demonstrated that the rolling process was beneficial for the recrystallization of PLA up to a rolling ratio of 40%. Additionally, χ_c of PLA decreased with the increase of the rolling ratio (as shown in Fig. 5-7, and the maximum deviation of the crystallinity was approximately 3%). When the rolling ratio increased from 0% to 40%, χ_c decreased by 34.0%. Furthermore, as the rolling ratio was raised to 75%,χ_c dropped by approximately 61.7% to 1.8%. It can be inferred that the decrease of the crystallinity was due to crystalline deformation and crystals destruction, which led to the increase of plastic deformation during the rolling process. Similar results were reported by Qiu and Jia for polypropylene (PP) using other evaluation methods (i.e., Fourier transform infrared spectroscopy (FT-IR) [18] and X-ray diffraction (XRD) [42]. In addition, during the rolling process, the molecular chains may orientate highly in the amorphous phase, and the quasi-crystals were destroyed, which resulted in the decrease of χ_c.

Table 5-5 DSC data measured on unrolled and rolled PLA specimens

Rolling ratio (%)	T_g (℃)	T_c (℃)	T_m (℃)	$\triangle H_m$ (mJ/mg)	$\triangle H_c$ (mJ/mg)	χ_c (%)
0	59.7	107.8	173.2	34.0	29.6	4.7
20	59.1	110.4	172.5	33.7	29.9	4.0
40	59.4	110.9	172.2	32.7	29.8	3.1
60	58.7	108.5	171.6	30.6	28.6	2.1
75	59.0	107.4	171.5	32.6	30.9	1.8

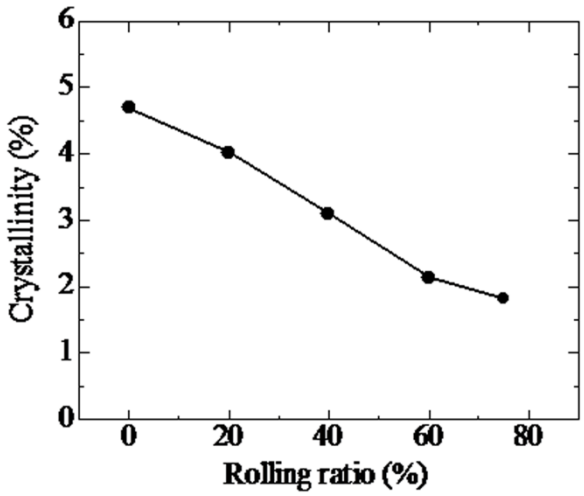

Fig. 5-7 Variation of the crystallinity of PLA as a function of rolling ratio.

(b) Variation of MWCNT/PLA composites

In general, nanofillers, particularly carbon nanotubes have been reported to act as nucleating agent in composites [43] and crystalline layers may cover nanotubes [44] reducing or hindering contact probability between carbon nanotubes. The DSC measurements of the rolled plates reflected indirectly the results concerning the state of MWCNT dispersion within PLA that were obtained by light microscopy. Therefore, the crystallization and melting behavior of the unrolled and 75% rolled MWCNT/PLA composites were also examined (Fig. 5-8), from which the melting temperature (T_m), the melting enthalpy (ΔH_m), the crystallization enthalpy (ΔH_c) and the degree of crystallization (χ_c) could be obtained, as listed in Table 5-6.

All specimens exhibited three distinct peaks corresponding to glass transition at around 60 ℃, cold crystallization peaks at approximately 80–110 ℃ and melting peaks at around 170 ℃, respectively. It was observed that the incorporation of MWCNTs led to an enhanced ability of PLA crystallization due to the nucleating effect of the filler. Especially, the composite with higher MWCNT content (e.g., 10 wt.%) was improved highly as compared to the composite with lower MWCNT content (e.g., 1 wt.%). Because of the large aspect ratio, high specific surface area and strong interfacial interaction of –OH and –COOH on MWCNTs with PLA matrix [45], the PLA

molecules can be easily bounded on the surface of MWCNTs, which can form a sufficient number of nucleation centers and play the role of crystal nucleus [46, 47].

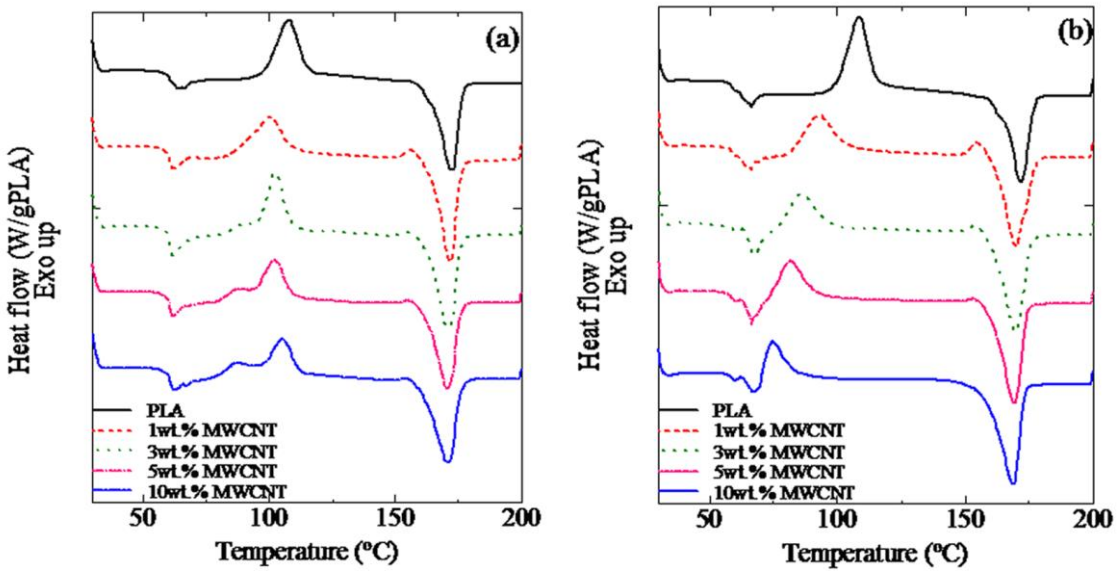

Fig. 5-8 DSC curves of different MWCNT/PLA composites (a) ξ: 0% and (b) ξ: 75%.

A comparison of Fig. 5-8 (a) and (b) shows a conclusion that a correlation between rolling ratio and crystallization behavior exists. Although the composite specimens exhibiting the MWCNT nucleating effect, the crystal nucleus were destroyed during rolling processing, leading to a decrease in crystallinity (the same results showed in Table 5-6). More interestingly, the exothermic peak of PLA was obviously close to the lower temperature with the increase of MWCNT content after rolling process (Fig. 5-8 (b)). This might be because that during rolling processing, the original crystallization of PLA was destroyed, and the nucleating effect of MWCNT attenuated, leading to the crystallization temperatures and crystallization of PLA composites decreased.

In Table 5-6, obviously, whether unrolled PLA or 75% rolled PLA, the T_g and T_m were almost not changed as the increase of MWCNT content. But the T_c was changed greatly. Regardless of the MWCNT content, the T_c of the unrolled composite was greater than that of rolled composite, particularly in the case of 10 wt.% MWCNT composite. When the MWCNT content was 10 wt.%, the T_c was decreased by 30 ℃

after rolling process. Besides, for the unrolled composites, the T_c basically maintained at 100 ℃ or more; however, for the rolled composites, the T_c was from 93.0 ℃ dropped to 75.7 ℃, dropped by 18.6%. Moreover, the χ_c of the unrolled composites were increased with the MWCNT content increasing. When the MWCNT content was increased from 1 wt.% to 10 wt.%, the χ_c was increased by 53.8%. The case of the rolled composites was the similar as the unrolled composites. It was inferred that the CNT played a role as a nucleating agent in the PLA, and prompted the increase of PLA crystallization. The similar results have been reported by Barrau [48].

Table 5-6 DSC data measured on unrolled and 75% rolled MWCNT/PLA composite specimens

MWCNT content (wt.%)	Rolling ratio (%)	T_g (℃)	C_p (mJ/deg.mg)	T_c (℃)	T_m (℃)	$\triangle H_m$ (mJ/mg)	$\triangle H_c$ (mJ/mg)	χ_c (%)
1	0	59.3	0.18	100.8	172.0	35.2	27.7	8.1
1	75	59.5	0.38	93.0	169.9	33.4	29.1	4.6
3	0	59.1	0.33	102.7	171.4	34.9	27.0	8.7
3	80	60.2	0.40	85.8	169.8	33.7	27.0	7.4
5	0	59.1	0.24	102.3	170.9	33.0	23.1	11.1
5	77	59.4	0.46	81.6	169.3	35.7	27.5	9.2
10	0	58.8	0.25	105.6	170.8	32.3	21.8	12.5
10	80	60.2	0.50	75.7	168.6	37.1	27.9	10.9

5.3.4 Relationship between density and crystallinity

To further confirm the aforementioned experimental results, the density method was utilized to measure the density of PLA, and then the variation of the PLA crystallinity was obtained. The density and crystallinity of pure PLA as a function of the rolling ratio are shown in Fig. 5-9. The density of PLA decreased linearly with the increase of the rolling ratio from 1.2499 g/cm^3 to 1.2487 g/cm^3 at the rolling ratio of 75%, indicating a decrease of approximately 0.1%. Likewise, the degree of crystallinity decreased as the rolling ratio increased, which was in accord with the DSC results. According to

calculation by the equation 2-11, the crystallization of unrolled PLA was 4.72%, but after being rolled by a 75% rolling ratio, the crystallinity suddenly dropped by approximately 62.3% to 1.78% (this results were as similar as Table 5-5). This suggested that the crystallinity of PLA was relatively low, and the original crystals were destroyed during the rolling process; thus, the crystallinity decreased greatly. Similar results on other crystalline polymers (POM and PP) have been reported by Pielichowski et al. [49] and Qiu et al. [32], respectively.

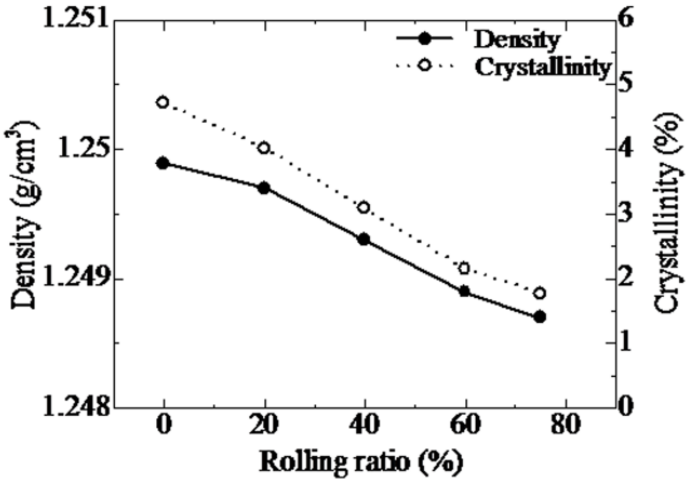

Fig. 5-9 Density and crystallinity of pure PLA as a function of rolling ratio.

In addition, the obtained density and crystallinity of the unrolled MWCNT/PLA composites were plotted in Fig. 5-10. The density of the PLA was linearly raised with the increasing MWCNT content, from 1.2499 g/cm^3 raised to 1.2534 g/cm^3. Also, the crystallinity ratio was monotonically increased as the MWCNT content increased, which was in accord with the results of the DSC. When the MWCNT content increased to 10 wt.%, the crystallization of the composites was 2.8 times compared with that of pure PLA.

Overall, MWCNT played a role as a nucleating agent in PLA matrix, and it was advantageous to enhance the crystallization of PLA, leading to reinforce the mechanical properties of the composites, even the electrical properties.

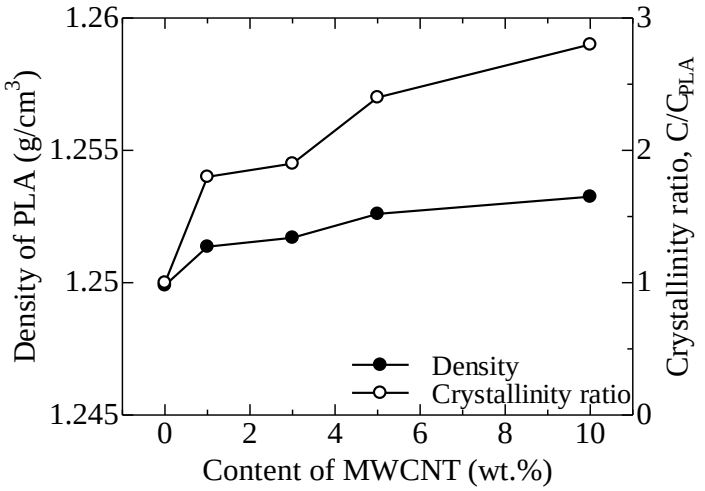

Fig. 5-10 Effect of MWCNT content on the density and crystallinity of unrolled MWCNT/PLA composites.

As the above mentioned, the rolling process would make the original crystals of PLA destroy; however, the MWCNT played a role as a nucleating agent which would enhance the crystallization of PLA. Therefore, how the rolling process affect the crystallization of the MWCNT/PLA composites was investigated also by the density method.

Fig. 5-11 shows the variations of the density and the crystallization of the composites with different MWCNT contents. It is obviously that the density and the crystallization are both decreased as the increase of rolling ratio. The tendency of the 1 wt.% MWCNT composite is the most obvious. Comparing the four figures with each other, it is found that the density of the composite was raised as the increase of the MWCNT content. Besides, the crystallization of the composites was also enhanced by the MWCNT content increasing. These results are associated with the DSC results.

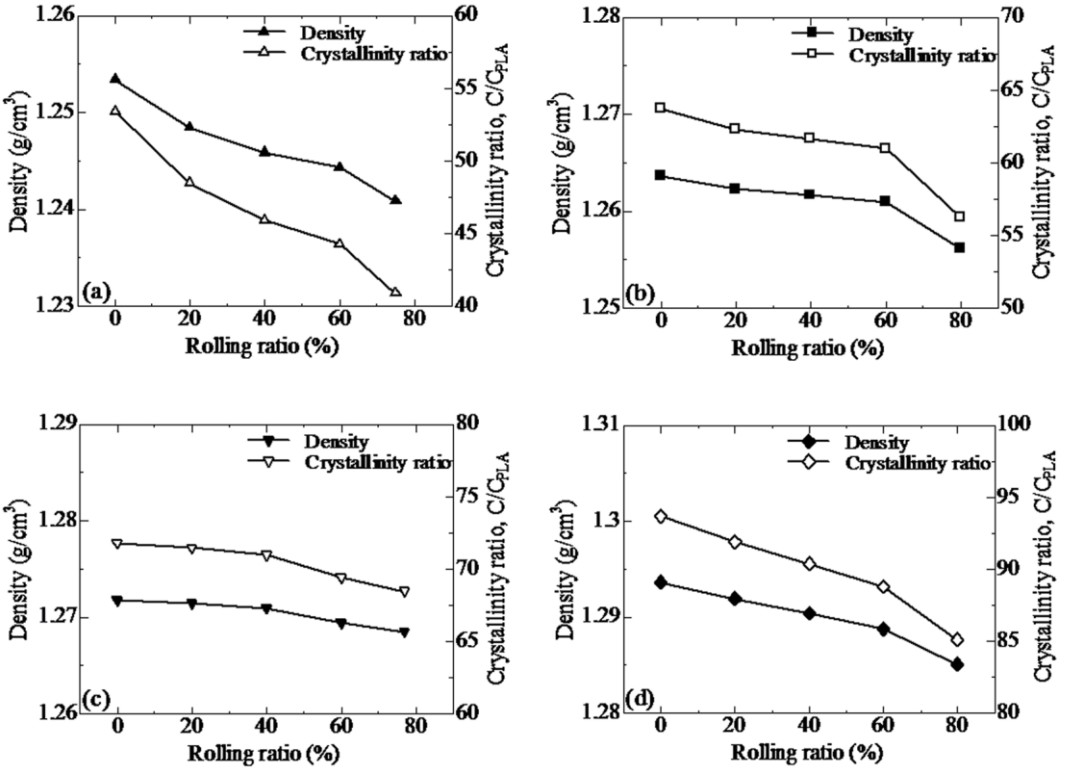

Fig. 5-11 Effect of rolling ratio on the density and crystallinity of (a) 1 wt.% MWCNT/PLA, (b) 3 wt.% MWCNT/PLA, (c) 5 wt.% MWCNT/PLA and (d) 10 wt.% MWCNT/PLA.

5.3.5 Effect of rolling ratio on the molecular orientation

XRD measurements were performed to evaluate the variation of the molecular orientation of pure PLA and the composites during the rolling process. Fig. 5-12 displays the XRD patterns in the range of 2θ=5 °–50 ° for the pure PLA and the MWCNT/PLA composites. The specimens before rolling process exhibit the most intense diffraction peak at 2θ=16.7 °, corresponding to reflections from (110) and (200) planes [48], which belonged to the α-crystal form of PLA as reported previously [50]. Moreover, it shows that the diffraction peak position of oriented PLA and MWCNT/PLA composites with different rolling ratios had no obvious variation; however, there were significant differences in the intensity; namely, the intensity of the diffraction peak at 2θ=16.7 °, as the rolling ratios increased. The intensity of the

diffraction peak represented the degree of order in the composite, including the orientation and crystallization. Therefore, these results indicated that rolling process did not change the crystal type, but it significantly affect the orientation and crystallization of PLA.

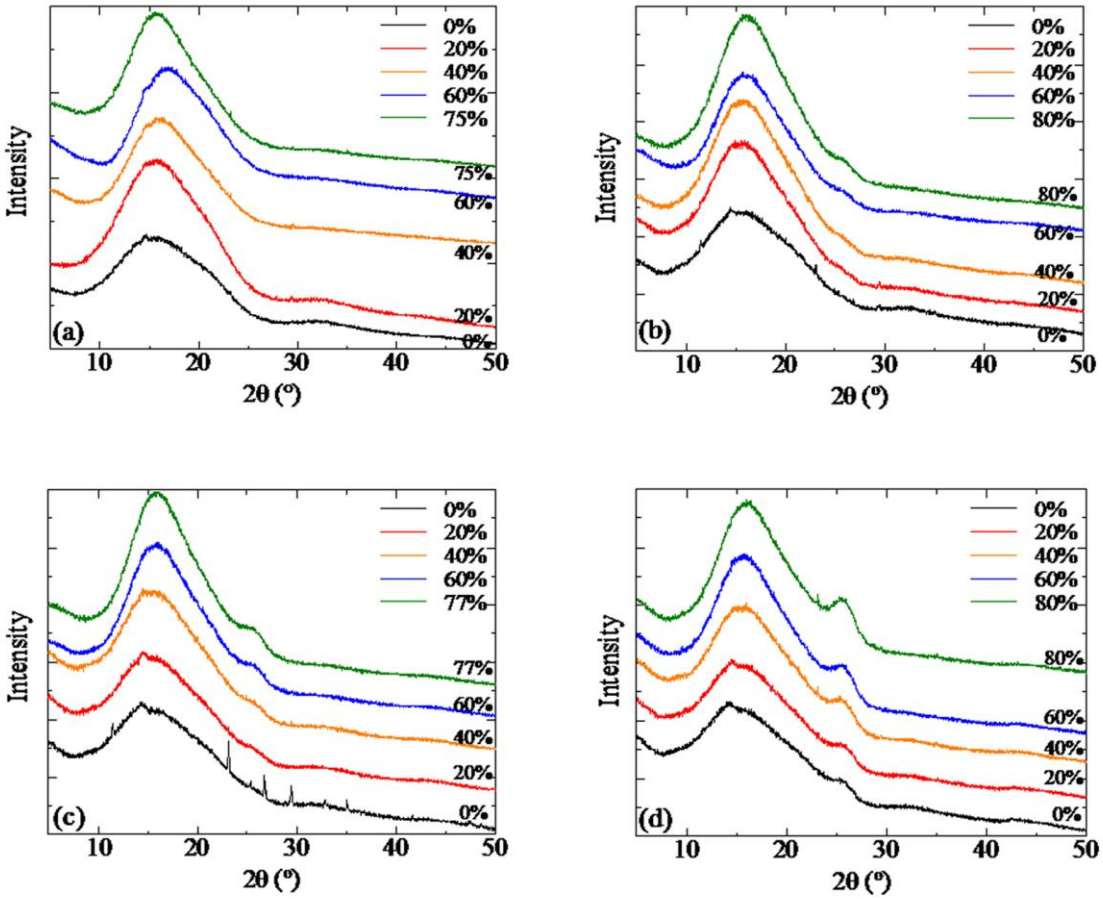

Fig. 5-12 XRD curves of (a) pure PLA, (b) 3 wt.% MWCNT/PLA composites, (c) 5 wt.% MWCNT/PLA composites and (d) 10 wt.% MWCNT/PLA composites.

Compared to pure PLA, in addition to the diffraction peak attributed to PLA, the patterns of the MWCNT/PLA composites presented a new less intense diffraction peak around 2θ=26.1°, corresponding to a d-spacing of 3.4Å, which was the inter-shell spacing within the nanotubes [47]. Before rolling process, the MWCNTs were randomly dispersed in the polymer matrix, which was expected a relative low intensity distribution. As the increasing of rolling ratio, the diffraction intensity of the MWCNTs

increased, suggesting that the MWCNTs were preferentially oriented along the rolling direction. The trend of orientation obtained from XRD was close to that of oriented PLA reported in the literature [47].

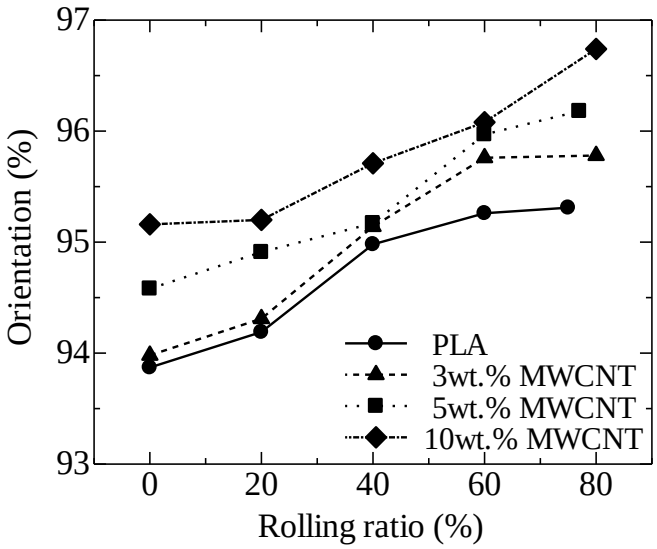

Fig. 5-13 Variation of the orientation of PLA and MWCNT/PLA composites as a function of the rolling ratio.

According to the data of the Fig. 5-12, the molecular orientation of the composites was calculated by equation 2-8 and is shown in Fig. 5-13. It is obvious that the degree of molecular orientation increased as the rolling ratio increased, no matter what the specimen type. In particular, when the rolling ratio was less than 60%, the degree of molecular orientation increased linearly, but once the rolling ratio was beyond 60% (e.g., ξ = 75%), the increased degree became smaller. During the rolling process, the molecular chains were highly orientated in the amorphous phase, resulting in the increase of orientation. In other words, the rolling process contributed to the orientation of PLA in the amorphous phase.

Besides, the data of the orientation degree of the composites with different MWCNT contents were summarized in Table 5-7. Obviously, irrespective of the MWCNT content,

the orientation was raised by the increase of rolling ratio, raised by approximately 1.5%–1.9%. Moreover, under the same rolling ratio, the orientation was slightly increased with the MWCNT content increasing.

Table 5-7 The orientation degree of the MWCNT/PLA composites

MWCNT content (wt.%)	Rolling ratio （%）	Half-width （°）	Orientation （%）
0	0	11.04	93.87
0	20	10.45	94.19
0	40	9.04	94.98
0	60	8.54	95.26
0	75	8.44	95.31
3	0	10.84	93.98
3	20	10.24	94.31
3	40	8.74	95.14
3	60	7.64	95.76
3	80	7.59	95.78
5	0	9.75	94.58
5	20	9.17	94.91
5	40	8.70	95.17
5	60	7.26	95.97
5	77	6.88	96.18
10	0	8.72	95.16
10	20	8.64	95.20
10	40	7.72	95.71
10	60	7.05	96.08
10	80	5.86	96.74

5.3.6 Microhardness and its distribution for PLA

Microhardness is related to the microstructures of crystal polymers in cross and longitudinal sections, such as the degree of molecular orientation, crystallinity, crystal size and crystal structure, as reported by Qiu [51]. In this part, we only discuss the variation of microhardness of pure PLA during the rolling process. The microhardness

of the specimen surface and the microhardness distribution in the longitudinal sections were measured, and the results are shown in Fig. 5-14. Fig. 5-14 (a) shows that the surface microhardness of unrolled PLA was approximately 18.5 kgf/mm^2, whereas as the rolling ratio increased, the microhardness decreased up to a rolling ratio of 60%, and then a slight increase occurred. The results showed that the specimen was significantly softened after the rolling process, but when the rolling ratio reached 75%, the orientation was at the maximum (from the result of Fig. 5-13), and stress concentration was generated during the rolling process, leading to a slight increase in the microhardness of PLA.

Fig. 5-14 (b) shows the microhardness distributions of the specimens with different rolling ratios in the longitudinal sections. The left side of the horizontal axis represented the specimen surface, and the right side represents the core. To make the relative position of the specimens of each layer (surface layer, intermediate layer, and core layer) consistent, the horizontal axis is the ratio of the distance from the surface and the half thickness. Overall, for the specimens with lower rolling ratios (i.e., ξ = 0% and 20%), the microhardness distributions could be divided into three regions from the surface to the core, i.e., a rise, a decline, and a plateau. In particular, for the unrolled PLA specimen, the microhardness of the intermediate layer was the largest, which was probably due to the extrusion process. It is well known that the intermediate layer was formed by rapid cooling and the impact of shear stress during the extrusion process. Therefore, the crystallinity and molecular orientation of the intermediate layer were higher, and the residual stress was greater, leading to a higher microhardness. However, in the case of the higher rolling ratios (i.e., ξ = 40%, 60%, and 75%), the microhardness distribution integrally dropped, and the difference of the microhardness between each layer became more and more indistinct. This might because the specimens were softened and became homogenized during the rolling process. Even for the 40% and 60% rolled specimens, although the heart part contained large microstructures, the microhardness of the specimens was not affected. In other words, an appropriate rolling

ratio was necessary to produce a homogenized polymer, which perhaps improved the original mechanical properties of the polymer. Qiu [52] also reported similar results on PP.

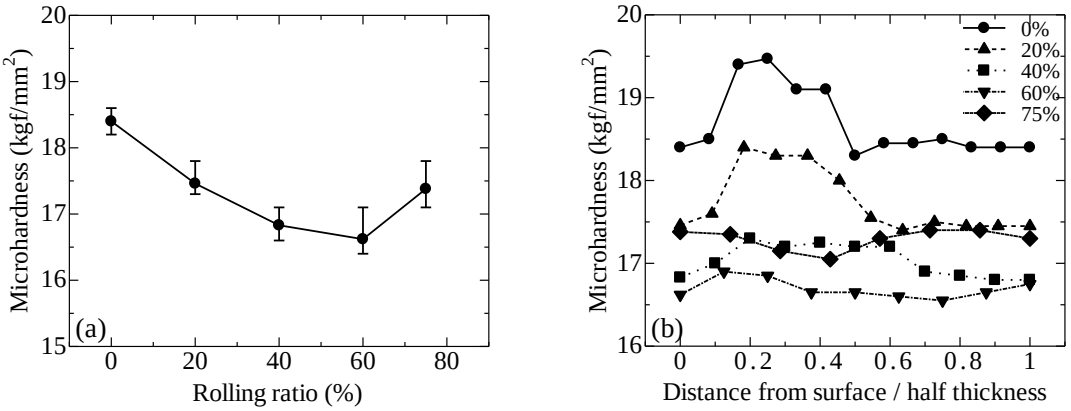

Fig. 5-14 Microhardness of PLA with different rolling ratios: (a) Surface microhardness and (b) microhardness distributions.

5.3.7 Dynamic mechanical behaviors

First, the dynamic mechanical properties of rolled PLA were tested, and the curves are shown in Fig. 5-15. The storage modulus E' and tan δ under different rolling ratios were clearly shown as a function of temperature. From Fig. 5-15, it can be found that at temperatures over 55 ℃, E' sharply declined; the onset temperature was the glass transition temperature (T_g) of PLA. Overall, regardless of the rolling direction, E' decreased with the increase of temperature, but tan δ showed an increasing trend. In Fig. 5-15 (a), in the region below the glass transition temperature, as the rolling ratio increased (i.e., ξ = 20%, 40, 60%, and 75%), E' increased. In the high temperature region (e.g., 90 ℃), E' was the same. For tan δ， in the region below the glass transition temperature, the values of rolled PLA were all higher than that of unrolled PLA, but in the high temperature region（e.g., 90 ℃），the change of tan δ was not significant. In Fig. 5-15 (b), when the temperature was below the glass transition temperature, the variation

trend of tan δ was similar as that in Fig. 5-15 (a). However, in the high temperature region (e.g., 90 ℃), the E' trend was somewhat different, i.e., little difference was observed in the E' of the specimens with different rolling ratios. This proved that the microstructures of PLA were changed by the rolling process, including the crystallinity, molecular orientation and so on; thus, PLA produced anisotropy during the rolling process. Moreover, as shown in both Fig. 5-15 (a) and (b), E' exhibited a slight increase at 90 ℃; this effect was due to cold crystallization at high temperatures (i.e., above 90 ℃).

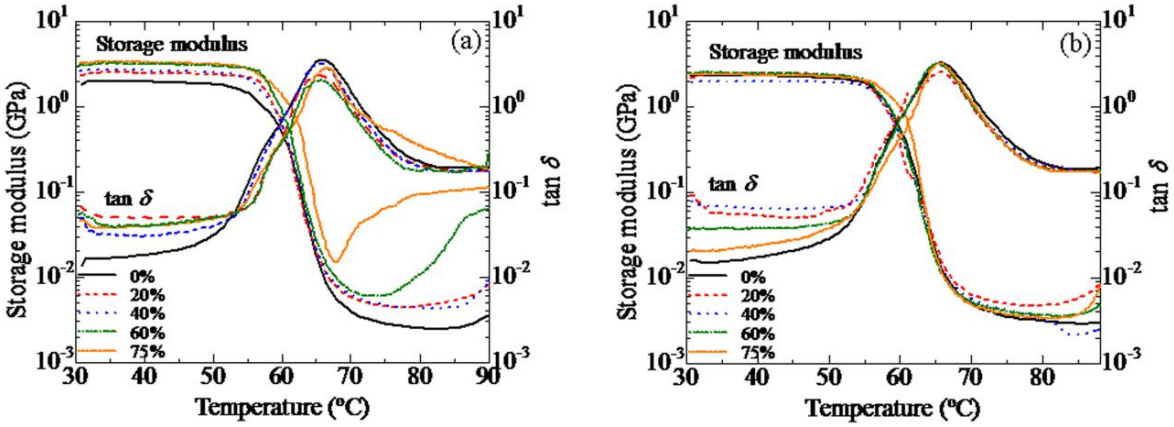

Fig. 5-15 Storage modulus and tan δ of unrolled and rolled PLA: (a) Parallel to the rolling direction and (b) vertical to the rolling direction.

In addition, to discuss the effects of the rolling ratio on E' and tan δ in detail, the data of Fig. 5-15 (E' and tan δ at 30 ℃) were plotted in Fig. 5-16. Comparing Fig. 5-16 (a) and (b), it can be found that due to the different directions (parallel and vertical to the rolling direction), the trends of E' and tan δ were different with each other. For the parallel direction (Fig. 5-16 (a)), E' dramatically increased with the increase of the rolling ratio, and eventually reached a maximum value at a rolling ratio of 75%. E' was increased from 1.8 GPa to 3.3 GPa, i.e., an increase of 83%, compared to the unrolled PLA. However, the tan δ of the 20% rolled PLA suddenly increased, and then the change of tan δ was not obvious. In contrast, in the vertical direction (Fig. 5-16 (b)), the

change of E' was not obvious with an increase of the rolling ratio. Nevertheless, the effect of the rolling ratio on tan δ was significant, especially in the case of the 20% rolling ratio. Tan δ increased by 3.1-fold from 2.0×10^{-2} to 8.1×10^{-2}, and subsequently decreased linearly with the increase of the rolling ratio. Overall, regardless of the direction, i.e., parallel vs. vertical, when the rolling ratio was 20%, tan δ was at a maximum. It was considered that PLA was softened during the rolling process, and the mobility of the molecules was enhanced, leading to the increase of tan δ.

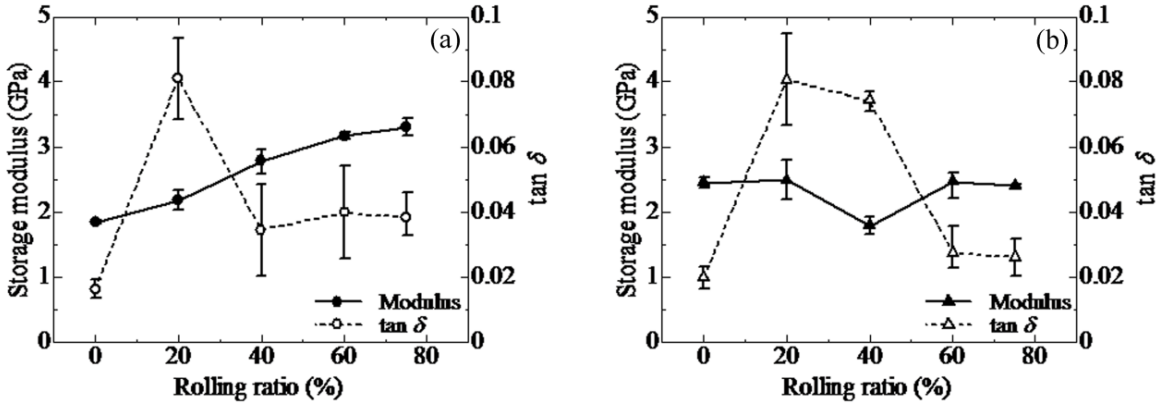

Fig. 5-16 Dynamic mechanical properties of the PLA at 30 ℃: (a) Parallel to the rolling direction and (b) vertical to the rolling direction.

Furthermore, the curves of the dynamic mechanical properties of unrolled MWCNT/PLA composites are shown as a function of temperature in Fig. 5-17. Regardless of the MWCNT content and the direction, E' were decreased with the increase of temperature but the tan δ showed an increasing trend. In Fig. 5-17 (a), when the temperature was over 55 ℃, E' sharply declined; the onset temperature was the glass transition temperature (T_g) of PLA. Besides, as the increase of the MWCNT content, E' was slightly increased, but tan δ did not changed obviously. Also, the similar case was found in Fig. 5-17 (b); however, the tan δ had a difference at 30 ℃. Moreover, comparing the two figures, it was found that the tan δ began to drop at the temperature of 65 ℃, and the E' was also increased at the high temperature (i.e., 90 ℃). It was

considered that the reason was the effect of cold crystallization, which was associated with the DSC results.

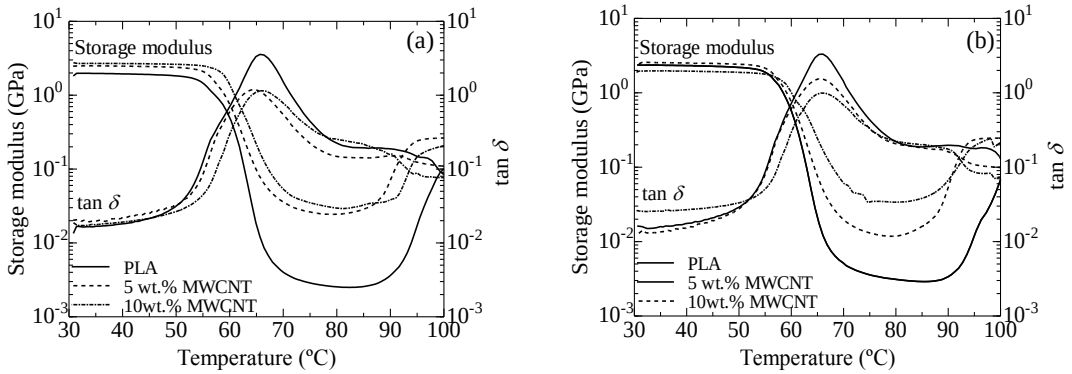

Fig. 5-17 Storage modulus and tan δ of unrolled MWCNT/PLA composites: (a) Parallel to the rolling direction and (b) vertical to the rolling direction.

5.3.8 Effect of rolling ratios on the tensile properties

To investigate the effect of MWCNT content on the tensile properties, the composite tensile properties in the parallel and vertical to the extrusion direction (i.e., 0 ° and 90 °) were measured, and are displayed in Fig. 5-18. It can be seen from Fig. 5-18 (a) that the tensile strength of the composites was increased with the increase of MWCNT content up to 3 wt.%, then the tensile strength was linearly decreased. At the incorporation of 3 wt.% MWCNT, the tensile strength was from 51.1 MPa increased to 68.0 MPa, an increase by 33.12%. Also, the variation trend of elongation at break was the similar as that of the tensile strength. The elongation at break of the 3 wt.% MWCNT composite was increased by 37.83% compared with that of pure PLA. In Fig. 5-18 (b), the maximum values of the tensile strength appeared at the 3 wt.% MWCNT content. Nevertheless, the elongation at break of the composites with different MWCNT content basically unchanged, maintaining at approximately 5%.

Comparing with Fig. 5-18 (a) and (b) indicates that when the MWCNT content was

3 wt.%, the tensile strength was the greatest, regardless of the parallel and vertical direction. It was considered that the MWCNT/PLA composites showed an anisotropy during extrusion process, which resulting the obvious difference in the mechanical properties.

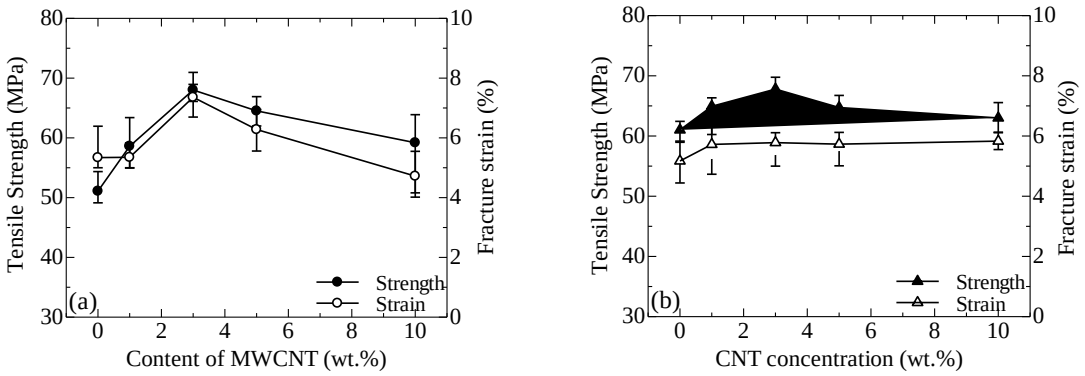

Fig. 5-18 Tensile properties of unrolled MWCNT/PLA composites: (a) Parallel to the extrusion direction and (b) vertical to the extrusion direction.

The internal microstructures of pure PLA and the MWCNT/PLA composites was examined by SEM. Fig. 5-19 displays the representative SEM micrographs of the tensile-fractured surfaces of the PLA and the composites with 3 wt.% and 10 wt.% MWCNTs. In Fig. 5-19 (a), the fractured surface was very smooth, showing a typical characteristic of brittle fracture. In comparison, it was observed on the fractured surface of the composite with 10 wt.% MWCNT (Fig. 5-19 (b)) was observed that many MWCNTs was well-distributed in the matrix and formed the electrical networks, but with some minor agglomerations, which would affect the mechanical and electrical properties. During extrusion process, a few minor agglomerations of MWCNTs were formed during the preparation of the 10 wt.% MWCNTs composite, thereby attenuating the tensile properties.

Comparing Fig. 5-19 (c) with (d) demonstrates that there are unobvious differences in the distribution and dispersion of the MWCNTs. Moreover, the compatibility between

MWCNTs and PLA was reasonable without pulling out the MWCNTs, and the MWCNTs were dispersed homogeneously without any agglomeration. Obviously, the incorporation of 3 wt.% MWCNTs was beneficial to display the outstanding properties of the MWCNT; the mechanical properties of the PLA was enhanced, and the good conductive networks were formed, subsequently improving the mechanical and electrical properties of the composites.

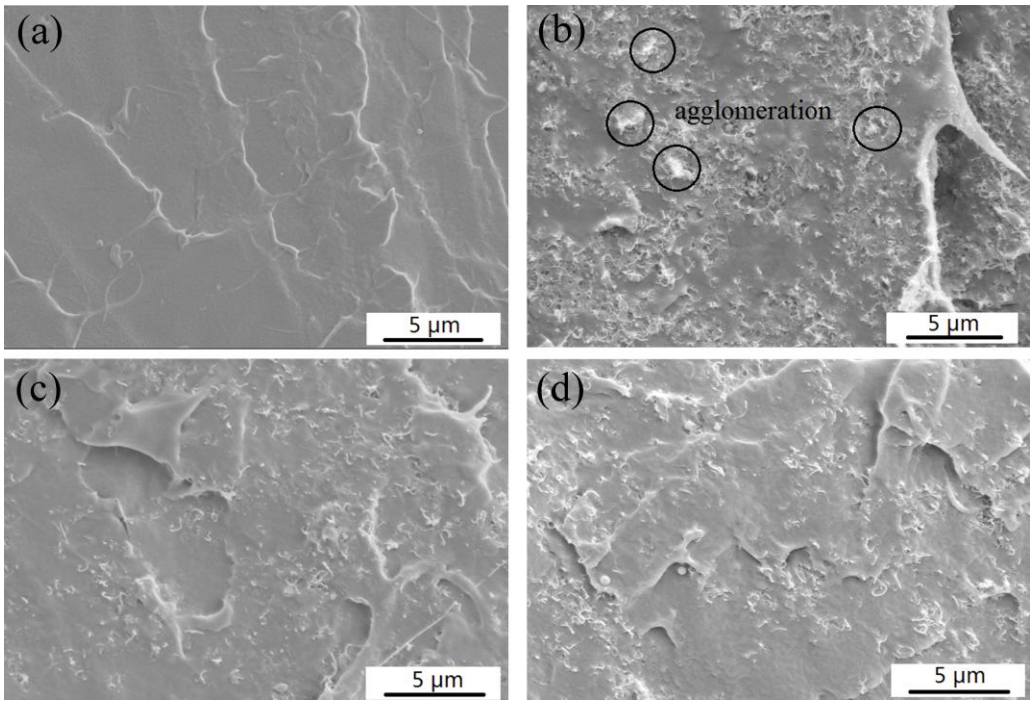

Fig. 5-19 SEM micrographs of tensile-fractured surfaces: (a) Pure PLA; (b) 10 wt.% MWCNT/PLA; (c) and (d) 3 wt.% MWCNT/PLA; (a), (b) and (c) parallel to the extrusion direction and (d) vertical to the extrusion direction.

To further prove that the variation of the internal microstructure during the rolling process, i.e., crystallinity and molecular orientation, would affect the mechanical properties of the polymers, tensile tests were carried out. The obtained results of pure PLA are shown in Fig. 5-20. Fig. 5-20 (a) exhibits the nominal stress-strain curves of the PLA with various rolling ratios (i.e., ξ = 0%, 40%, and 75%) parallel and vertical to the rolling directions. Obviously, the unrolled PLA was fractured within a strain of 10%,

regardless of whether parallel or vertical to the rolling direction. However, after being rolled, the yield stress and tensile strength were significantly enhanced compared to unrolled the PLA, especially in the parallel direction; the strains were suddenly increased to more than 70% at the rolling ratio of 40%, showing a high ductility. It was proved that the large microstructures of the heart part could not affect the mechanical property of the rolled PLA. Moreover, the specimens with the rolling ratios of 40% or 75% had an even plastic deformation during tensile testing; the middle of the specimens became thinner, and the transparency of the specimens increased. This result was consistent with the microhardness distribution in the longitudinal sections. It was confirmed that the internal microstructures of the specimens were greatly changed, and the PLA produced anisotropy during the rolling process, which coincided with the results of the dynamic mechanical analysis.

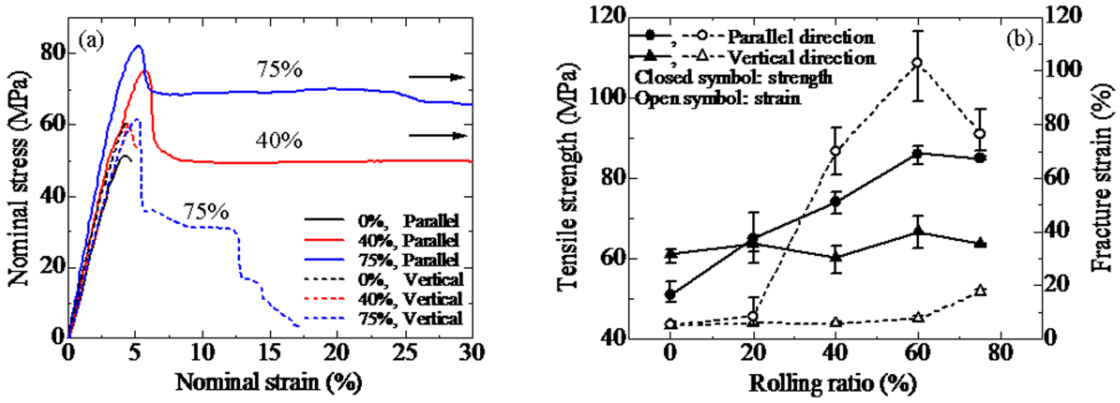

Fig. 5-20 Tensile properties of PLA: (a) Strain-stress curves and, (b) tensile strength and fracture strain.

In Fig. 5-20 (b), variations of the tensile strength and fracture strain were not obvious in the vertical direction. On the contrary, variations in the parallel direction were very notable; both the tensile strength and fracture strain were significantly increased with the increase of the rolling ratio up to 60%. When the rolling ratio reached 60%, the tensile strength and fracture strain increased from 51.1 MPa to 86.0 MPa and from 5.3% to 103.1%, respectively. It can be considered that the tensile property was

anisotropic, thus having a different value when measured in different directions. This result was similar to the DMA results mentioned above. The reinforcement of the tensile properties was very striking despite the fact that they were decreased slightly at the rolling ratio of 75%. This was related to the microhardness distribution of PLA at the 75% rolling ratio, and the decreased tensile properties at the 75% rolling ratio can be eventually ascribed to the decrease of the molecular orientation. Moreover, when the rolling ratio was 20%, the tensile strength of the parallel direction was the same as that of the vertical direction. This was one reason why the values of tan δ of 20% rolled PLA were similar regardless of the direction in the DMA analysis (as shown in Fig. 5-16). Overall, the tensile properties also proved that a anisotropy was generated during rolling process.

The data in Fig. 5-20 shows that the tensile properties of the rolled PLA in the parallel direction were affected by the rolling ratio greatly. Thus, representative tensile fractured specimens were observed via SEM, and the SEM micrographs are shown in Fig. 5-21. Fig. 5-21 (a), (c), and (e) show the whole fractured sections of the specimens with rolling ratios of 0%, 40%, and 75%, respectively, and it is found that the starting points of the fractures appeared near the specimen surfaces. From Fig. 5-21 (a), it can be clearly observed that the size of the fractured surfaces was not changed, and the high-magnification micrograph (Fig. 5-21 (b)) shows that the interior of the fractured surface was smooth. Hence, a typical brittle fracture was observed. This phenomenon can be related to the microhardness distribution of the unrolled PLA as mentioned above. However, Fig. 5-21 (c) and (e) obviously show that the fractured sizes of both specimens became smaller, indicating the typical characteristics of a ductile fracture. Due to the observation that the actual broken position was in the curved part of the specimen, the area of the fractured surface was larger than that of the parallel part. Furthermore, during the tensile test, a large amplitude recovery occurred in the specimen, resulting in the non-uniform of the size of the fractured surface (as shown in Fig. 5-21 (e)). Moreover, from the high-magnification micrographs of the interiors (Fig.

5-21 (d) and (f)), it is observed that there are many fibrillar PLA on the fractured surfaces, especially in the case of the 75% rolling ratio (Fig. 5-21 (f)). The increase of the fracture toughness with rolling ratio can be related to the increase of fibril formation. Although the surface crystals of PLA were destroyed during the rolling process, they were highly orientated in the interior along the rolling direction. Additionally, based on the microhardness distribution from previously, the PLA specimens were homogenized at a high rolling ratio; thus, the tensile properties of rolled PLA were reinforced.

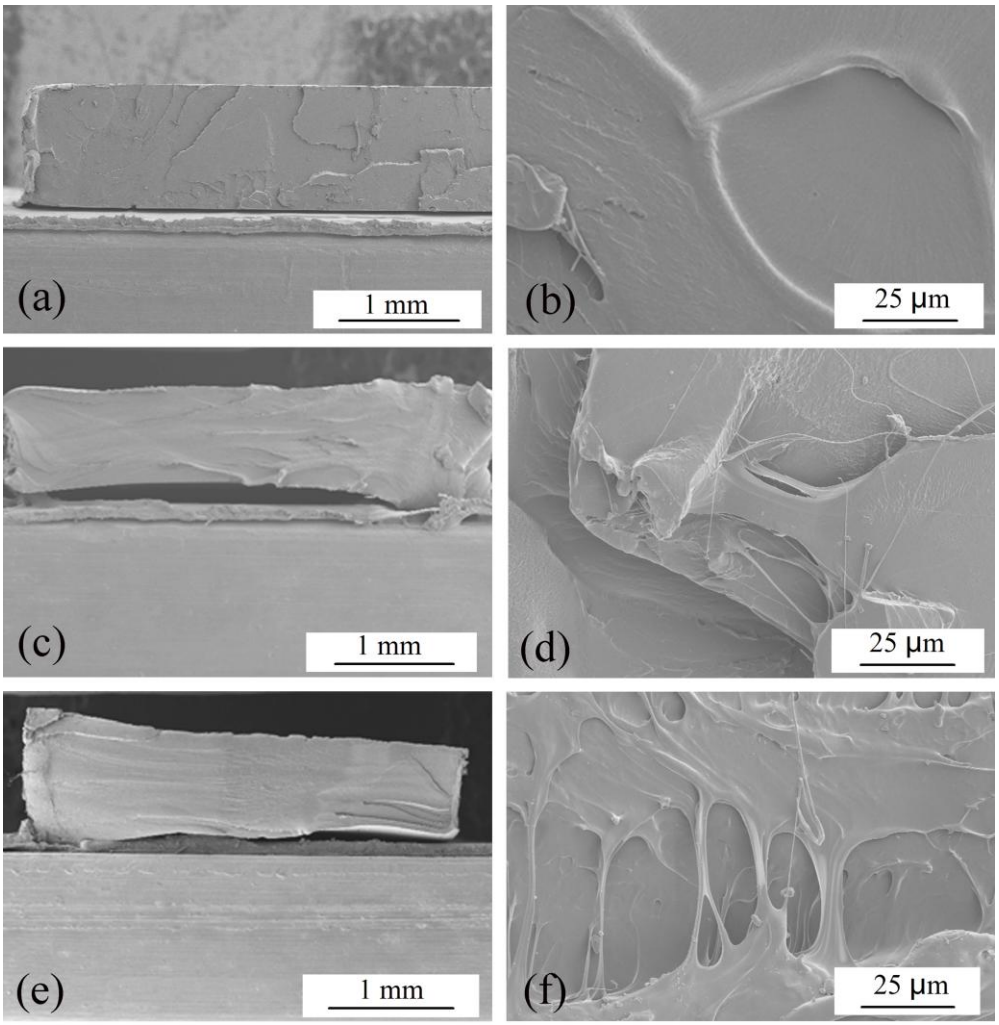

Fig. 5-21 SEM micrographs of tensile fractured surfaces: (a) ξ: 0%, (c) ξ: 40%, (e) ξ: 75%. (b), (d), and (f) are high-magnification micrographs of (a), (c) and (e), respectively.

The microhardness distribution of the rolled PLA with a high rolling ratio exhibited homogenization. The microhardness of the intermediate layer became lower during the rolling process, leading to smaller differences between the mechanical reactivity and the surrounding; thus, the local stress concentration was eased, and the specimens were not prone to cracking, resulting in the improvement of strength and the increase in the ductility of the PLA.

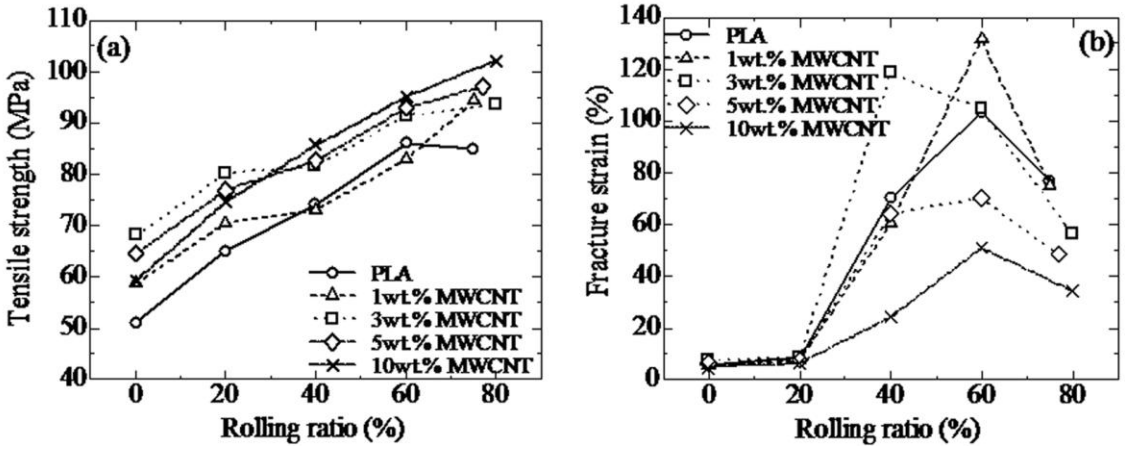

Fig. 5-22 Tensile properties under various rolling ratios: (a) Tensile strength and (b) fracture strain (parallel to the rolling direction).

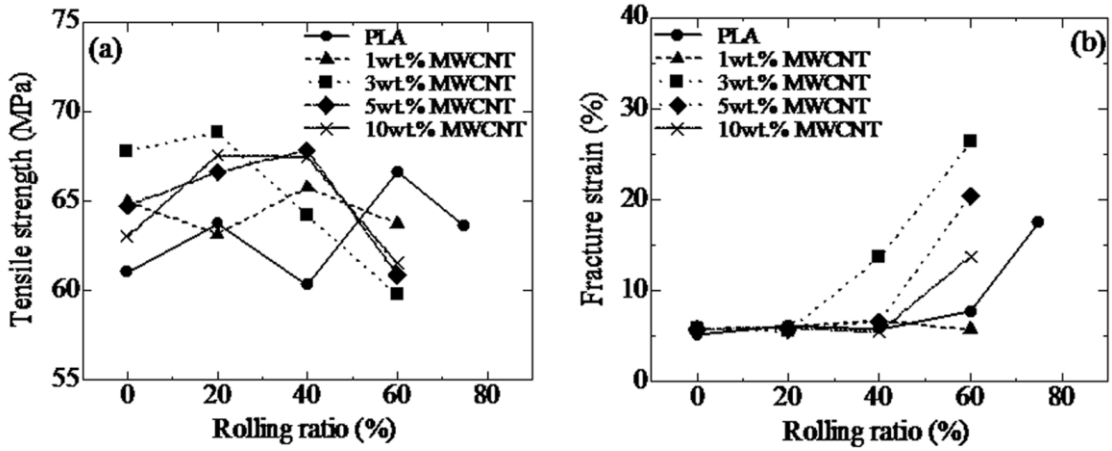

Fig. 5-23 Tensile properties under various rolling ratios: (a) Tensile strength and (b) fracture strain (vertical to the rolling direction).

Furthermore, Fig. 5-22 and Fig. 5-23 show the tensile properties of the MWCNT/PLA composites with different rolling ratios (in parallel and vertical to the rolling direction). It is known from Fig. 5-22 that regardless of MWCNT content the tensile strength of the composites was increased with the rolling ratio increasing. Even if the addition of 1 wt.% MWCNT, when the rolling ratio increased from 0% to 75%, the tensile strength was increased from the 58.6 MPa to 94.3 MPa, increased by 60.87%. However, for the fracture strain, the maximum values appeared at the 40% and 60% rolling ratios. Also, the fracture strain of the composites with 1 wt.% MWCNT was sharply increased to 131.48% under the rolling ratio of 60%, enhanced by approximately 23-fold than that of pure PLA. Nevertheless, in Fig. 5-23, it is clear that the effects of rolling ratio on tensile strength and fracture strain are not so much obvious. The tensile strength was in the range of 60–70 MPa, and even if the fracture strain was increased with the increase of the rolling ratio, but also not outstanding like the case of the parallel direction. It was also considered that this might because the anisotropy of tensile properties of the MWCNT/PLA composites, which resulting the obvious difference in the tensile properties.

5.3.9 Effect of rolling ratios on the electrical properties

The unrolled and rolled plates were cut to dumbbell-shaped specimens to measure the electrical resistivity. Because the surface resistivity and volume resistivity are the same trend, the surface resistivity is only discussed in this part. The surface resistivity of the composites with different MWCNT contents is exhibited in Fig. 5-24. These results showed that the surface resistivity of the MWCNT/PLA composites decreased exponentially with the increase of MWCNT content. As the MWCNT content was increased from 1 wt.% to 5 wt.%, the surface resistivity of the composites linearly decreased by 10 orders of magnitude (from $10^{11}\,\Omega$/sq decreased to $10^{1}\,\Omega$/sq). This case is better than the MWCNT/PC composites previously prepared by injection molding process. The surface resistivity of the MWCNT/PC composite with 5 wt.% MWCNT

was approximately 10^2 Ω/sq [53]. However, when the MWCNT content was from 5 wt.% increased to 10 wt.%, the magnitude of surface resistivity was not changed. It was considered that the percolation threshold was approximately 3 wt.% MWCNT content, which was the similar as our previous research on the MWCNT/PC composites [14, 53]; when the MWCNT content increased to 10 wt.%, the formation of agglomerations (observed in Fig. 5-19 (b)) would hide the electrical conductivity of MWCNTs, resulting in that the surface resistivity of the composites could not continuously fall.

Generally, the incorporation of MWCNT was conducive to improving the electrical conductivity of polymers [54]. However, when the MWCNT content exceeded a certain value, the effect of MWCNT content on the surface resistivity was not noticeable. Therefore, the effect of MWCNT content on the electrical conductivity was such that a proper increase in MWCNT content more easily promoted the formation of conductive networks.

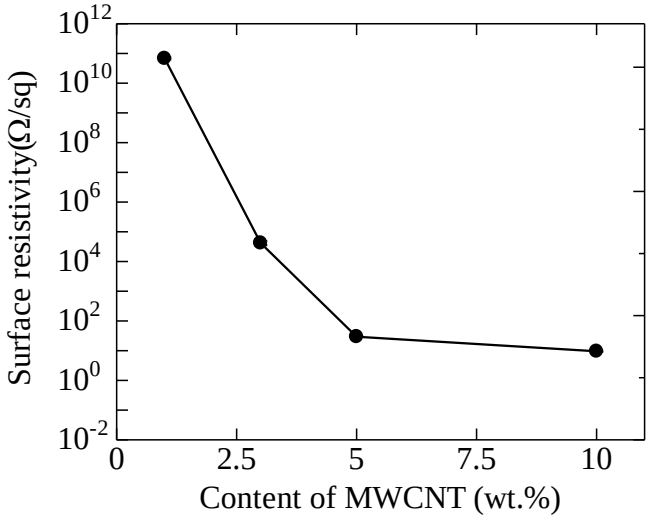

Fig. 5-24 Surface resistivity of unrolled MWCNT/PLA composites.

Besides, an SEM image of the tensile-fractured surface of the composites with 3 wt.% MWCNTs (parallel to the extrusion direction) is shown in Fig. 5-25. Obviously, even if the MWCNT content was increased to 3 wt.%, any obvious agglomeration of

MWCNTs was not observed, and the electrical conductive networks were distinctly observed. Moreover, the distribution of MWCNT was very uniform, and the dispersion of MWCNTs in PLA was very good. During the extrusion process, as the higher temperature molten polymers were cooled slowly, MWCNTs were not oriented along the extrusion direction, which contributed to the formation of conductive networks. As well, the conductive properties of the MWCNTs were the best observed, and the electrical resistivity of the composites was significantly improved with the increase of MWCNT content. Additionally, the good compatibility between MWCNTs and PLA was confirmed by the TGA. Therefore, it was considered that a proper incorporation of MWCNT could fully display its excellent electrical conductivity and form well conductive networks, resulting in the enhancement of the composite electrical properties.

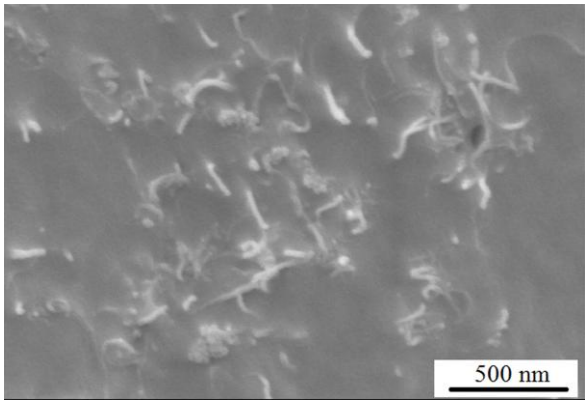

Fig. 5-25 SEM image of the tensile fractured surface of 3 wt.% MWCNT/PLA composite.

Moreover, the effect of rolling ratio on the surface resistivity is shown as plotted in Fig. 5-26. Obviously，the effect of rolling ratio on the electrical resistivity of the composites with 1, 3 wt.% MWCNTs was more evident, especially 1 wt.% MWCNT composites, when the rolling ratio was 20%, the surface resistivity was decreased by 2–3 orders of magnitude (irrespective of parallel or vertical to rolling direction). Nevertheless, when the MWCNT content was 5 wt.% or 10 wt.%, the surface resistivity

is 10^0–10^1 Ω/sq, the variation of the surface resistivity was within 1 order of magnitude, suggesting the unobvious effect. These results indicated that at the MWCNT content within 3 wt.% did not reach the percolation threshold, the surface resistivity affected by the rolling ratio was obvious; at the MWCNT content above 3 wt.%, the differences in the dispersion and sizes of agglomerates did not affect significantly the electrical resistivity. Overall, the effect of rolling ratio on the electrical resistivity was not obvious.

However, for mechanical tests, the differences in the dispersion may be higher importance since the MWCNT agglomerations are expected to act as imperfections and reduce the mechanical properties.

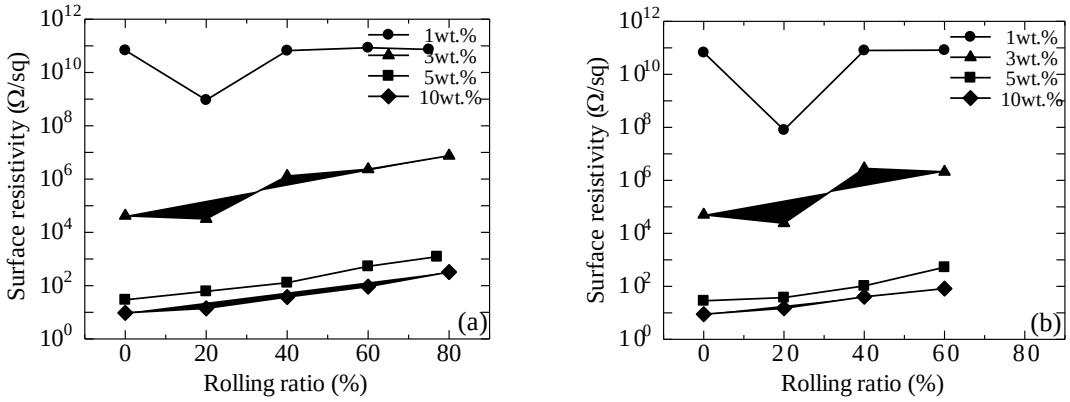

Fig. 5-26 Surface resistivity of the composites under various rolling ratios:
(a) Parallel to the rolling direction and, (b) vertical to the rolling direction.

5.4 Conclusions

Five different MWCNT/PLA composites were produced under variation of MWCNT contents. The crystal morphology, crystallinity, molecular orientation, mechanical properties and electrical properties of the rolled composites were investigated in detail. Based on the obtained results, the most important factors affecting plastic processing of MWCNT/PLA composites for industrial applications are listed as

follows.

(1) The distribution and dispersion of MWCNTs in the PLA were observed by optical microscope, and found that the size of MWCNT agglomeration was increased with the increase of MWCNT content.

(2) The compatibility between MWCNTs and PLA was good, and a proper incorporation of MWCNTs was a favorable method for maintaining good thermal properties of the PLA.

(3) The crystallinity of pure PLA was dropped as the rolling ratio increased. While the crystallinity was greatly increased by the incorporation of MWCNTs. MWCNT played a role as a nucleating agent in PLA. The density method also proved that the crystals were destroyed during rolling process, but the MWCNT could improve the crystallinity of the composites. Besides, the plastic deformation more easily occurred on the surface than the interior deformation of the PLA. The deformation layer was expanded with the increase of rolling ratio.

(4) The rolling processing was conducive to molecular orientation. Moreover, the composites orientation was slightly increased with the MWCNT content increasing.

(5) The microhardness distributions of the PLA with lower rolling ratios were divided into three regions, i.e., a rise, a decline, and a plateau. An appropriate rolling ratio (e.g., ξ = 40% and 60%) was necessary to produce a homogenized composite, which could improve the original mechanical properties of the PLA.

(6) The dynamic mechanical properties showed that the PLA composites were softened and produced an anisotropy during the rolling process. It was indicated that the easy mobility of molecular chains was enhanced during the rolling process.

(7) When the rolling ratio reached 60%, the tensile strength and fracture strain in the rolling direction increased from 51.1 MPa to 86.0 MPa and from 5.3% to 103.1%, respectively. Moreover, the tensile properties of the rolled composites in the rolling direction were mostly reinforced compared with that in the vertical direction, due to the high molecular orientation along the rolling direction.

(8) The incorporation of MWCNT was conducive to improving the electrical conductivity of PLA. The electrical properties exponentially increased as the MWCNT content increased. When the MWCNT content was 5 wt.%, the surface resistivity dropped to 10^1 Ω/sq. Moreover, the effect of the rolling ratio on the electrical resistivity was not outstanding.

References

[1] M. Jonoobi, J. Harun, A.P. Mathew and K. Oksman. Mechanical Properties of Cellulose Nanofiber (CNF) Reinforced Polylactic acid (PLA) Prepared by Twin Screw Extrusion. Compos. Sci. Technol. 70 (2010) 1742-1747.

[2] S. Gogolewski and A.J. Pennings. Resorbable Materials of Poly(L-lactide). II. Fibers Spun from Solutions of Poly (L-lactide) in Good Solvents. J. Appl. Poly. Sci. 28 (1983) 1045-1061.

[3] L. Yu, H. Liu, F. Xie, L. Chen and X. Li. Effect of Annealing and Orientation on Microstructures and Mechanical Properties of Polylactic Acid. Polymer Engineering & Science 48 (2008) 634-641.

[4] B. Eling, S. Gogolewski and A.J. Pennings. Biodegradable Materials of Poly (l-lactic acid): 1. Melt-Spun and Solution-Spun Fibres. Polymer 23 (1982) 1587-1593.

[5] V. Siracusa, P. Rocculi, S. Romani and M.D. Rosa. Biodegradable Polymers for Food Packaging: A Review. Trends in Food Science & Technology 19 (2008) 634-643.

[6] K. Oksman, M. Skrifvars and J.F. Selin. Natural Fibres as Reinforcement in Polylactic acid (PLA) Composites. Composites Science and Technology 63 (2003) 1317-1324.

[7] G. Koronis, A. Silva and M. Fontul. Green Composites: A Review of Adequate Materials for Automotive Applications. Composites: Part B: Engineering 44 (2013) 120-127.

[8] L. Yu, H. Liu, F. Xie, L. Chen and X. Li. Effect of Annealing and Orientation on Microstructures and Mechanical Properties of Polylactic acid. Polym. Eng. Sci. 48 (2008) 634-641.

[9] S. Ata, T. Mizuno, A. Nishizawa, C. Subramaniam, D.N. Futaba and K. Hata. Influence of Matching Solubility Parameter of Polymer Matrix and CNT on

Electrical Conductivity of CNT/Rubber Composite. Scientific reports (2014) DOI: 10.1038/srep07232.

[10] S.D. Bergin, Z. Sun, D. Rickard, P.V. Streich, J.P. Hamilton and J.N. Coleman. Multicomponent Solubility Parameters for Single-walled Carbon Nanotube-Solvent Mixtures. ACS Nano. 3 (2009) 2340-2350.

[11] H.T. Ham, Y.S. Choi and I.J. Chung. An Explanation of Dispersion States of Single-walled Carbon Nanotubes in Solvents and Aqueous Surfactant Solutions Using Solubility Parameters. J. Colloid. Interf. Sci. 286 (2005) 216-223.

[12] A. Agrawal, A.D. Saran, S.S. Rath and A. Khanna. Constrained Nonlinear Optimization for Solubility Parameters of Poly (lactic acid) and Poly(glycolic acid)—Validation and Comparison. Polymer 45 (2004) 8603-8612.

[13] J. Oliveira, G.S. Brichi, J.M. Marconcini, L.H. Capparelli Mattoso, G.M. Glenn and E.S. Medeiros. Effect of Solvent on The Physical and Morphological Properties of Poly(lactic acid) Nanofibers Obtained by Solution Blow Spinning. J. Eng. Fiber. Fabr. 9 (2014) 117-125.

[14] L. Wang, J. Qiu, E. Sakai and X. Wei. Effects of Multiwalled Carbon Nanotube Mass Fraction on Microstructures and Electrical Resistivity of Polycarbonate-Based Conductive Composites. Science and Engineering of Composite Materials (2015) DOI: 10.1515/secm-2015-0074.

[15] J. Qiu. Effects of Hot Roll Process on the Morphology and Tensile Properties of Injection-Molded Polypropylene (in Japanese). Kobunshi Ronbunshu 63 (2006) 397-403.

[16] J. Qiu, T. Murata, X. Wu, M. Kitagawa and M. Kudo. Plastic Deformation Mechanism of Crystalline Polymer Materials in the Equal Channel Angular Extrusion Process. Journal of Materials Processing Technology 212 (2012) 1528-1536.

[17] D. Younesi, R. Mehravaran, S. Akbarian and M. Younesi. Fabrication of the New Structure High Toughness PP/HA-PP Sandwich Nano-Composites by Rolling

Process. Materials and Design 43 (2013) 549-559.

[18] J. Qiu, T. Murata, X. Wu, M. Kudo and E. Sakai. Plastic Deformation Mechanism of Crystalline Polymer Materials during the Rolling Process. J. Mater. Sci. 48 (2013) 1920-1931.

[19] T. Murata, J. Qiu and X. Wu. Effect of Rolling Temperature on Microstructure and Tensile Properties of Polypropylene. Polymer Engineering and Science 53 (2013) 2573-2581.

[20] N. Chapleau, J. Mohanraj, A. Ajji and I.M. Ward. Roll-Drawing and Die-Drawing of Toughened Poly (ethylene terephthalate). Part 1. Structure and Mechanical Characterization. Polymer 46 (2005) 1956-1966.

[21] S.H. Lee, K. Nakayama and H.H. Cho. Fine Structure and Physical Properties of Poly(buthylene terephthalate) Sheets Prepared by Roller Drawing Method. Fiber. Polym. 9 (2008) 740-746.

[22] R. Bao, Z. Ding, G. Zhong, W. Yang, B. Xie and M. Yang. Deformation-Induced Morphology Evolution during Uniaxial Stretching of Isotactic Polypropylene: Effect of Temperature. Colloid Polym. Sci. 290 (2012) 261-274.

[23] J. Qiu, T. Murata, X. Wu, M. Kitagawa and M. Kudo. Plastic Deformation Mechanism of Crystalline Polymer Materials in the Equal Channel Angular Extrusion Process. J. Mater. Process. Tech. 212 (2012) 1528-1536.

[24] A.G. Gibson, I.M. Ward, B.N. Cole and B. Parsons. Hydrostatic Extrusion of Linear Polyethylene. J. Mater. Sci. 9 (1974) 1193-1196.

[25] J. Qiu, T. Murata, K. Takahashi and X. Wu. The Plastic Deformation Characteristics of Crystalline Polymer Materials via Rolling Process. Adv. Mater. Res. 391-392 (2012) 585-589.

[26] K. Nakayama, K. Qi and X. Hu. Dynamic Mechanical Properties of Rolled Polypropylene Sheets. Polym. Polym. Compos. 9 (2001) 151-156.

[27] M.D. Wang, E. Nakanishi and S. Hibi. Effect of Molecular Weight on Rolled High Density Polyethylene: 1. Structure, Morphology and Anisotropic Mechanical

Behaviour. Polymer 34 (1993) 2783-2791.

[28] J. Mohanraj, J. Morawiec, A. Pawlak, D.C. Barton, A. Galeski and I.M. Ward. Orientation of Polyoxymethylene by Rolling with Side Constraints. Polymer 49 (2008) 303-316.

[29] J. Qiu. Effect of the Stress Amplitude and the Test Temperature on the Fatigue Property of Cold Rolled PP (in Japanese). Trans. Jpn. Soc. Mech. Eng. A 68 (2002) 65-73.

[30] J. Qiu, M. Kawagoe, W. Mizuno and M. Morita. Effect on Fatigue Failure of Injection-Molded Polypropylene Sheets by Rolling Process (in Japanese). Kobunshi Ronbunshu 57 (2000) 255-262.

[31] T. Murata, J. Qiu, E. Sakai, X. Wu and M. Kudo. Morphology Change of Extrusion Molded Crystalline Polymer by Rolling Process. Adv. Mater. Res. 391-392 (2012) 595-599.

[32] J. Qiu, M. Kawagoe, W. Mizuno and M. Morita. Effect of Morphology and Tensile Properties of Polypropylene by the Rolling Process (in Japanese). Trans. Jpn. Soc. Mech. Eng. A. 66 (2000) 867-874.

[33] T. Miyata and T. Masuko. Morphology of Poly(l-lactide) Solution-Grown Crystals. Polymer 38 (1997) 4003-4009.

[34] J. Puiggali, Y. Ikada, H. Tsuji, L. Cartier, T. Okihara and B. Lotz. The Frustrated Structure of Poly(l-lactide). Polymer 41 (2000) 8921-8930.

[35] L. Yu, H. Liu, F. Xie, L. Chen and X. Li. Effect of Annealing and Orientation on Microstructures and Mechanical Properties of Polylactic Acid. Polymer Engineering & Science 48 (2008) 634-641.

[36] P.H. Nadella, E.J. Spruiell and L.J. White. Drawing and Annealing of Polypropylene Fibers: Structural Changes and Mechanical Properties. J. Appl. Polym. Sci. 18 (1978) 3121-3133.

[37] T. Villmow, P. Pötschke, S. Pegel, L. Häussler and B. Kretzschmar. Influence of Twin-Screw Extrusion Conditions on the Dispersion of Multi-walled Carbon

Nanotubes in a Poly (lactic acid) Matrix. Polymer 49 (2008) 3500-3509.

[38] Z. Jin, K.P. Pramoda, G. Xu and S.H. Goh. Dynamic Mechanical Behavior of Melt-Processed Multi-walled Carbon Nanotube/Poly(methyl methacrylate) composites. Chem. Phys. Lett. 337 (2001) 43-47.

[39] Q. Jiang, X. Wang, Y. Zhu, D. Hui and Y. Qiu. Mechanical, Electrical and Thermal Properties of Aligned Carbon Nanotube/Polyimide Composites. Composites Part B: Engineering 56 (2014) 408-412.

[40] J. Guo, Y. Liu, R. Prada-Silvy, Y. Tan, S. Azad, B. Krause, P. Pötschke and B.P. Grady. Aspect Ratio Effects of Multi-walled Carbon Nanotubes on Electrical, Mechanical, and Thermal Properties of Polycarbonate/MWCNT Composites. Journal of Polymer Science: Part B: Polymer Physics 52 (2014) 73-83.

[41] M. Yasuniwa, S. Tsubakihara, Y. Sugimoto, C. Nakafuku. Thermal Analysis of the Double-Melting Behavior of Poly(L-lactic acid). J. Polym. Sci. Polym. Phys. 42 (2004) 25-31.

[42] J. Jia, W. Mao and D. Raabe. Changes of Crystallinity and Spherulite Morphology in Isotactic Polypropylene after Rolling and Heat Treatment. Journal of University of Science and Technology Beijing, Mineral, Metallurgy, Material 15 (2008) 514-520.

[43] A.R. Bhattacharyya, T.V. Sreekumar, T. Liu, S. Kumar, L.M. Ericson, R.H. Hauge and R.E. Smalley. Crystallization and Orientation Studies in Polypropylene/Single Wall Carbon Nanotube Composite. Polymer 44 (2003) 2373-2377.

[44] K.P. Ryan, M. Cadek, V. Nicolosi, D. Blond, M. Ruether, G. Armstrong, H. Swan, A. Fonseca, J.B. Nagy, W.K. Maser, W.J. Blau and J.N. Coleman. Carbon Nanotubes for Reinforcement of Plastics? A Case Study with Poly(vinyl alcohol). Composites Science and Technology 67 (2007) 1640-1649.

[45] J.T. Yoon, Y.G. Jeong and S.C. Lee. Infuences of Poly (lactic acid)-Grafted Carbon Nanotube on Thermal, Mechanical, and Electrical Properties of Poly(lactic acid). Polym. Adv. Technol. 20 (2009) 631-638.

[46] Z. Li, X. Zhao, L. Ye, P. Coates, F. Caton-Rose and M. Martyn. Structure and Blood Compatibility of Highly Oriented PLA/MWNTs Composites Produced by Solid Hot Drawing. Journal of Biomaterials Applications 28 (2014) 978-989.

[47] H. Quan, S. Zhang, J. Qiao and L. Zhang. The Electrical Properties and Crystallization of Stereocomplex Poly(lactic acid) Filled with Carbon Nanotubes. Polymer 53 (2012) 4547-4552.

[48] S. Barrau, C. Vanmansart, M. Moreau, A. Addad, G. Stoclet, J.M. Lefebvre and R. Seguela. Crystallization Behavior of Carbon Nanotube–Polylactide Nanocomposites. Macromolecules 44 (2011) 6496-6502.

[49] K. Pielichowski and A. Leszczynska. Structure-Property Relationships in Polyoxymethylene/Thermoplastic Polyurethane Elastomer Blends. J. Polym. Eng. 25 (2005) 359-373.

[50] H. Marubayashi, S. Asai and M. Sumita. Complex Crystal Formation of Poly (l-lactide) with Solvent Molecules. Macromolecules 45 (2012) 1384-1397.

[51] J. Qiu. Effects of Flow Distance and Injection Speed on the Fatigue Property of Injection-Molded Polypropylene Sheets (in Japanese). Kobunshi Ronbunshu 62 (2005) 425-431.

[52] J. Qiu. Microstructure and Tensile Property of Cold Rolled PP/LCP Blends (in Japanese). Trans. Jpn. Soc. Mech. Eng. A 67 (2001) 1458-1463.

[53] J. Qiu, L. Wang, K. Uchiya and E. Sakai. Effects of Injection Molding Conditions on the Electrical Properties of Polycarbonate/Carbon Nanotube Nanocomposites. Polym. Compos. (2015) DOI: 10.1002/ pc.23523.

[54] C.F. Kuan, H.C. Kuan, C.C.M. Ma and C.H. Chen. Mechanical and Electrical Properties of Multi-Wall Carbon Nanotube/Poly(lactic acid) Composites. J. Phys. Chem. Solids. 69 (2008) 1395-1398.

Chapter 6 Conclusions

Conductive polymer composites are widely used in the electric, electronic, automobile and aeronautical industries because they meet requirements for miniaturized and light-weight industrial products. For actual applications, it is particularly necessary to control the electrical resistivity and hold good mechanical properties. Therefore, for the preparation of CPCs, the homogeneous dispersion of MWCNT in the polymer matrix and the strong interfacial interaction between the MWCNT and the polymer are two major challenges. Moreover, to expand the application range of CPCs, the second stage processing (e.g., plastic processing) was performed by proposed approaches.

In Chapter 1, the research backgrounds, research significance, and the construction of this thesis are described. The objectives of the research are to produce carbon nanotubes/polymer composites in industrial-scale and evaluate their properties.

In Chapter 2, the properties of MWCNT and polymers (i.e., PC and PLA) are presented. The main experimental and evaluation methods are also displayed in this chapter.

In Chapter 3, the multi-walled carbon nanotube/polycarbonate (MWCNT/PC) composites were successfully prepared by a two-step dispersion strategy (the twin-screw extrusion followed by injection molding process). As a result, the MWCNTs were well-dispersed in PC matrix. TGA showed that a small MWCNT content (i.e., 1 wt.%) was more propitious for improving thermal stability of the composites. Analysis of the mechanical properties demonstrated that the tensile properties of the composites with low MWCNT content could be comparable to that of PC, the tensile strength of the composites with 2.5 wt.% raw MWCNTs exhibited an increase of ~5 MPa (~8.6%) at a particular injection condition. However, as the MWCNT content increased to 10 wt.%, the tensile strength and bending strength decreased by 35% and 47%, respectively, from the values of PC. The impact strength and microhardness were improved with the

increase in MWCNT content. Results of dynamic mechanical analysis showed that the storage modulus of PC was increased after the incorporation of MWCNTs, particularly at high temperatures. Therefore, for different practical applications, the preparation of MWCNT/PC composites with different mechanical properties can be achieved by changing MWCNT content or injection conditions.

In Chapter 4, the effects of the MWCNT content and injection conditions on the electrical resistivity of the MWCNT/PC composites were investigated. As the CNT contents increased, the electrical resistivity of the composites almost decreased linearly. The electrical resistivity of the 5 wt.% raw MWCNTs composites was considerably decreased to $10^2\,\Omega$/sq, a value approximately 15 orders of magnitude lower than that of PC. And it was considered that the percolation threshold of the composites was within 3 wt.% MWCNTs. In addition, the electrical resistivity showed a variation tendency that the electrical resistivity was lower at higher injection temperature and lower injection speed and that was most evident in the case of the addition of 1 wt.% MWCNTs. More importantly, the distributions of the electrical resistivity had three stages of a rising distribution, a declining distribution and a constant distribution. Basically, the observed phenomena were attributed to the formation mechanism of the internal microstructures of the prepared nanocomposites during injection molding.

In Chapter 5, to expand the application of CPCs, the second stage processing was carried out to prepare the MWCNT/PLA composites with various MWCNT contents (0–10 wt.%) by extrusion molding followed by rolling process. It was demonstrated that how rolling conditions affect the microstructures, mechanical properties and electrical properties of PLA composites in cold rolling process, which is an industrially relevant plastic processing technique. A proper incorporation of MWCNTs was a favorable method for maintaining good thermal properties of the PLA. The crystallinity of pure PLA was dropped as the rolling ratio increased. However, the crystallinity was greatly increased by the incorporation of MWCNTs. MWCNT played a role as a nucleating agent in PLA. Irrespective of the MWCNT content, the orientation was raised by the

increase of rolling ratio, raised by approximately 1.5%–1.9%. When the rolling ratio reached 60%, the tensile strength and fracture strain in the rolling direction increased from 51.1 MPa to 86.0 MPa and from 5.3% to 103.1%, respectively. The incorporation of MWCNT was conducive to improving the electrical conductivity of PLA. When the carbon content was 5 wt.%, the electrical resistivity was dropped to 10^1 Ω/sq. It offers an alternative green and easy solution to produce conductive MWCNT/PLA bio-composites as an environmentally friendly CPC.

Publications

Ⅰ. Periodical papers

(1). **Lijun Wang**, Jianhui Qiu, Eiichi Sakai

The Relationship between Microstructure and Mechanical Properties of Carbon Nanotubes/Polylactic acid Nanocomposites by Twin-screw Extrusion

Composites Part A, DOI: 10.1016/ j.compositesa.2015.12.016.

(2). **Lijun Wang**, Jianhui Qiu, Eiichi Sakai

Microstructures and Mechanical Properties of Polylactic acid Prepared by a Cold Rolling Process

Journal of Materials Processing Technology 232 (2016) 184-194.

(3). **Lijun Wang**, Jianhui Qiu, Eiichi Sakai

Thermal Behaviors, Mechanical and Dynamic Mechanical Properties of Multi-walled Carbon Nanotube-reinforced Polycarbonate Nanocomposites

Polymer Composites, DOI: 10.1002/pc.23801.

(4). **Lijun Wang**, Jianhui Qiu, Eiichi Sakai, Xiaowei Wei

Effects of Multiwalled Carbon Nanotube Mass Fraction on Microstructures and Electrical Resistivity of Polycarbonate-based Conductive Composites

Science and Engineering of Composite Materials, DOI: 10.1515/secm-2015-0074.

(5). Jianhui Qiu, **Lijun Wang**, Kengo Uchiya, Eiichi Sakai

Effects of Injection Molding Conditions on the Electrical Conductivity of Carbon Nanotube/Polycarbonate Nanocomposites

Polymer Composites, DOI: 10.1002/pc.23523.

(6). **Lijun Wang**, Jianhui Qiu, Eiichi Sakai, Xiaowei Wei

Effect of Injection Conditions on the Electrical Conductivity of MWCNTs/ PC Conductive Composites

Advanced Materials Research, Vol. 983, (2014), pp.105-109.

(7). **Lijun Wang**, Jianhui Qiu, Eiichi Sakai

Influence of Injection Conditions on the Mechanical Property of MWCNTs/PC Nanocomposites

Advanced Materials Research, Vol. 983, (2014), pp.94-98.

(8). Jianhui Qiu, Limin Zang, Chao Yang, Kengo Uchiya, Eiichi Sakai, **Lijun Wang**

Preparation and Volume Resistivity of CNT/Polycarbonate Nanocomposites with Different Injection Molding Temperatures

Applied Mechanics and Materials, Vol.543-547, (2014), pp.3878-3881.

Ⅱ. International conference paper

(1). **Lijun Wang**, Jianhui Qiu, Eiichi Sakai

The Relationship between Microstructure and Mechanical Properties Carbon Nanotubes/Polylactic acid Nanocomposites by Twin-screw Extrusion

2nd China International Congress on Composite Materials (CCCM -2), Zhenjiang, China, September 21-23, (2015).

(2). Jianhui Qiu, **Lijun Wang**, Limin Zang, Genki Watanabe and Eiichi Sakai

The Relationship of Welding Strength and Interfacial Structure of PC-PMMA Joined by Injection of Interposed Material

2nd China International Congress on Composite Materials (CCCM -2), Zhenjiang, China, September 21-23, (2015).

(3). **Lijun Wang**, Jianhui Qiu, Eiichi Sakai

Preparation and Evaluation of the Mechanical Property of MWCNTs/PC Conductive Composites

11th Japan-China Joint Conference on Composites (CJJCC-11), Chongqing, China, October 18-23, (2014).

(4). **Lijun Wang**, Jianhui Qiu, Eiichi Sakai, Xiaowei Wei

Characterization of the Injection Conditions on the Electrical Conductivity of

MWCNTs/PC Nanocomposites

11th Japan-China Joint Conference on Composites (CJJCC-11), Chongqing, China, October 18-23, (2014).

(5) Jianhui Qiu, **Lijun Wang**, Eiichi Sakai

Creation of CNT/PC Nanocomposite and Electrical Conductivity Evaluation

11th Japan-China Joint Conference on Composites (CJJCC-11), Chongqing, China, October 18-23, (2014).

(6) **Lijun Wang**, Jianhui Qiu, Eiichi Sakai

Influence of Injection Conditions on the Mechanical Property of MWCNTs/PC Nanocomposites

Annual Int. Conf. on Intelligence Materials and Nanomaterials (AIMN14), Seoul, South Korea, April 18-19, (2014).

(7) **Lijun Wang**, Jianhui Qiu, Eiichi Sakai, Xiaowei Wei

Effect of Injection Conditions on the Electrical Conductivity of MWCNTs/PC Conductive Composites

Annual Int. Conf. on Intelligence Materials and Nanomaterials (AIMN14), Seoul, South Korea, April 18-19, (2014).

(8) Jianhui Qiu, Limin Zang, Kengo Uchiya, Eiichi Sakai, **Lijun Wang**

Preparation and Volume Resistivity of CNT/Polycarbonate Nanocomposites with Different Injection Molding Temperatures

2nd International Conference on Materials and Manufacturing Research (ICMMR), Guilin, China, March 29-30, (2014).

Ⅲ. Domestic conference paper

(1). **Lijun Wang**, Jianhui Qiu, Eiichi Sakai, Makoto Kudo, Rie Nobe

Microstructure and Tensile Properties of Polylactic acid by Colded Rolling Process

Proceedings of 51th Autumn Meeting of the Japan Society of Mechanical Engineers Tohoku Branch, Electronic file USB memory, Lecture number No.

202, Iwaki, Fukushima, Japan, September 26, (2014).

(2). **Lijun Wang**, Jianhui Qiu, Eiichi Sakai

A Study of the Influence of Injection Conditions on the Mechanical Property and Electrical Conductivity of MWCNTs/ PC Nanocomposites

Proceedings of the 39th Symposium on Composite Materials, pp.215-216, Akita, Japan, September 18-19, (2014).

(3). **Lijun Wang**, Wei Xiaowei, Jianhui Qiu, Eiichi Sakai

Effect of Injection Speed and Temperature on the Electrical Conductivity of MWCNTs/ PC Conductive Composites

Proceedings of 49th Autumn Meeting of the Japan Society of Mechanical Engineers Tohoku Branch, pp.59-60, Morioka, Japan, September 20, (2013).

(4). Yuta Nakamura, Suguru Murakami, Jianhui Qiu, Eiichi Sakai, **Lijun Wang**

Effect of Surface Treatment on the Bonding Strength of PPS-Al Assembly

Proceedings of 49th Autumn Meeting of the Japan Society of Mechanical Engineers Tohoku Branch, pp.47-48, Morioka, Japan, September 20, (2013).

Acknowledgements

I would firstly like to acknowledge the guidance and support of my advisor Professor Jianhui Qiu, who works at Department of Machine Intelligence and Systems Engineering, Faculty of Systems Science and Technology of Akita Prefectural University. He imparted the knowledge of material science and technology to me, and his elaborated guidance, considerable encouragement and invaluable discussion make my research of great achievement and my study life unforgettable. Also, thank you for the financial support and the opportunities that were provided to me.

My deepest appreciation goes to the professors in Department of Machine Intelligence and Systems Engineering, Faculty of Systems Science and Technology at Akita Prefectural University, Dr. Mamoru Mizuno and Dr. Teruo Bitoh, and professor in Department of Urban and Civil Engineering at Ibaraki University, Dr. Zhishen Wu for the comments and suggestions, whose advices have inestimable value for my research.

In addition, I would like to express my sincere thanks to Assistant Eiichi Sakai (Department of Machine Intelligence and Systems Engineering, Faculty of Systems Science and Technology of Akita Prefectural University), who supported me a lot in my study that helped facilitate me completing this thesis easily.

I also appreciate the technical support from Dr. Takao Komiyama in Akita Prefectural University, Dr. Makoto Kudo in Akita Industrial Technology Center, Prof. Qingqing Ni in Shinshu University and Prof. Ning Hu in Chiba University. Thanks for Mrs. Qiu who has taken good care of me in last three years; the professor at Xihua University, Dr. Xiaowei Wei; the professor at Chinese Academy of Sciences, Dr. Shaoyun Fu; the professor at Southwest Jiaotong University, Dr. Zuowan Zhou. And thanks also go to my peer research group members including Guohong Zhang, Yang Zhao, Lin Lei, Takuya Murata, Xueli Wu, Wenjuan Zhang, Limin Zang, Bin Wang, Liqiang Gu, Baiyi Chen, Longxiang Zhu, Jiao Chen, Yanling Yu, Yukiko Takeuchi,

Yoshie Sugiura, Rie Nobe, Kengo Uchiya, Suguru Murakami, Yuki Iwase, Yuya Matsumura, Kazuki Nishitoba, Tatsuya Onogaki, Fumiya Saitou, Taiyou Sasaki, for assisting with my research as well as providing friendship and support.

Gratitude is due to my Japanese teachers, Eiko Kamata, Minako Kudo, Chika Furukawa, Eiko Fujishima and for their support, patience and understanding throughout this endeavor.

A giant thank you also goes to my family for their moral support, warm encouragement and patience throughout the course of this PhD and indeed for my entire life.

Lijun Wang

2016. 03